Late Quaternary paleoseismic history of the Te Puninga Fault, Hauraki Plains, northern New Zealand

A thesis

submitted in partial fulfilment

of the requirements for the degree

of

MSc (Research) in Earth Sciences

at

The University of Waikato
(Hamilton)

by

Joshua William Hughes

THE UNIVERSITY OF
WAIKATO
Te Whare Wānanga o Waikato

2023

Abstract

The Te Puninga Fault is a newly discovered active fault on the western side of the Hauraki Plains, northern North Island, New Zealand. Preliminary evidence in a 2016 study suggests that it may generate earthquakes Mw>6.8. Therefore, the fault presents a hazard and risk to the population and infrastructure of the Hauraki Plains region, including the population centres of Morrinsville and Te Aroha, and beyond. Several consequences from rupture of the Te Puninga Fault are likely: strong ground motion from earthquakes (possibly amplified by basin effect in the Hamilton Basin and Hauraki Plains); permanent surface deformation by fault surface rupture; and secondary effects such as liquefaction and landslides. Thus, it is important to better understand the seismicity of this fault to better understand the hazard and risk to the wider region.

Paleoseismic trenching was undertaken in February 2021 along two fault traces at Ryland Trench and Arnold Trench. Exposures in the trenches enabled a stratigraphy to be established of the near-surface deposits (within 3 m) that were deformed by the fault. The deposits were described, and samples of organic material and tephra were collected. The organic material was submitted to the Waikato Radiocarbon Dating Laboratory for radiocarbon (^{14}C) dating, and major element analysis of volcanic glass was undertaken at the electron probe microanalysis (EPMA) facility, Victoria University of Wellington. The bulk of the deposits exposed in each trench comprised secondary volcaniclastic sediments of the Hinuera Formation. An additional alluvial unit, deposited after 11,000 cal yr BP, was identified in the Ryland trench and correlated with the Waitoa Formation. The ^{14}C dating indicated that the Hinuera Surface at each trench site was abandoned at approximately 24,000 cal yr BP. At both trenches, the Hinuera Surface was overlain by a cover bed of composite tephras deposited incrementally whilst being transformed pedologically (via pedogenic upbuilding) to form Allophanic Soils on well to moderately well drained higher landscape positions. Major element analysis of glass shards isolated from the base of the composite tephra column suggests that the Okareka (23,500 cal yr BP) or Rerewhakaaitu (17,600 cal yr BP), or both, (crypto)tephras were present, generally supporting the age ascribed to the Hinuera Surface (c. 24.0 cal ka) based on the ^{14}C age modelling. The Taupo (1718 ± 10 cal yr BP) and Kaharoa (636 ± 12 cal yr BP) tephras occurred in the upper parts of both trenches as visible, thin, discontinuous deposits. They were identified by their stratigraphic superpositioning and physical properties, confirmed by their diagnostic ferromagnesian minerals and glass-shard major element compositions.

A site near Quine Road where the fault scarp dipped westwards, in the opposite direction to the eastward slope of the general land surface, and intersected stream terraces, was identified using high resolution LiDAR data. Using a digital elevation model, a hillshade model, and field work including geomorphic mapping, the terraces formed by the streams were identified and labelled from 1 (youngest) to 8 (oldest). Because terraces became progressively younger as they descended from the c. 24 cal ka Hinuera Surface, they can be used as chronological markers for fault activity. If the scarps formed by fault surface ruptures represent different surface displacement of different terraces, an analysis can be done to assess numbers and timing of fault ruptures. Elevation profiles were drawn parallel and perpendicular to the fault and it was found that the vertical fault displacement decreased as the terraces got younger. By comparing two models for incision rates, terrace ages were modelled and thus possible ages of displacement were obtained. The oldest terraces had an average vertical displacement of 2.6 ± 0.15 m, whereas Terrace 3 had a vertical displacement of 1.0 ± 0.15 m, and the youngest two had no vertical displacement. Therefore, it is likely that the penultimate earthquake that generated the displacement occurred between the formation of Terrace 4 (19,500 ± 1,400 yrs BP) and Terrace 3 (18,600 ± 600 yrs BP), and the most recent earthquake occurred between the formation of Terraces 3 (18,600 ± 600 yrs BP) and 2 (15,000 ± 1,900 yrs BP). Using the age of the youngest terrace that was displaced in two events (19,500 yrs BP), and the average vertical displacement of the other terraces displaced twice (2.64 ± 0.15 m), a slip rate of 0.135 ± 0.01 mm/yr was calculated. As this is one of at least nine strands of the Te Puninga Fault at this latitude, is a possible the 2016 published slip rate of 0.160 ± 0.03 mm/yr is understated.

A trial investigation of ground penetrating radar (GPR) at three locations on the Te Puninga Fault was conducted. The first two applications were at each of the two paleoseismic trench sites (Arnold and Ryland trenches), and hence the reflectors could be compared to the known stratigraphy, and the third at the Quine Road study site. The Quine Road site is a possible future trench location. The GPR investigation found: a) that a suitable depth of stratigraphy (<2.5 m) could be obtained; b) the displaced surfaces at all three sites were formed by seismic deformation rather than fluvial erosional processes because the reflectors in the radargrams ran parallel to the land surface, reflecting folding; and c) at Quine Road, in contrast, the sediments potentially show clear faulting rather than folding which could provide key information if trenching were to be undertaken at the site.

Acknowledgements

Firstly, I want to express my upmost gratitude to my supervisors, Professor David Lowe and Dr. Vicki Moon at the University of Waikato, Hamilton and Dr. Pilar Villamor at GNS Science, Lower Hutt. Your technical support and advice have been instrumental to the completion of this thesis. As a wealth of information, David, you have been a fantastic help in every step of this thesis, especially in the writing portion. I also have really appreciated meeting and getting to know Maria and the rest of your lovely family. I will never forget Vicki's enthusiasm for the field work, and your motivation has really helped progress this thesis along. And Pilar those days in the field and meetings (zoom and in person) have been huge learning curves, and invaluable for what this work has become.

Thank you to the very large Te Puninga trenching team in February 2021, Dr. Kelvin Berryman, Dr. Kate Clark, Dr. Genevieve Coffey, Yaas Shah, Philippa Morris, George McQuillan, Dr Robert Langridge, Dr. Alan G. Hogg, Dr. Brent Alloway, and Olivia Mark. It was a whirlwind of two weeks that was an exciting introduction to research.

I would also express special thanks to the rest of the Tephra Seismites team, Dr. Max Kluger, Dr. Tehnuka Ilanko, Richard Melchert and Danche Chaneva for help and advice, along with creating a great social group, whether that is the Lunch Buddies or Eurovision. Thanks so much to Dr. Marlena Prentice for the moral support and advice on so many things, in the office.

I would like to thank the following for allowing us access to their properties for field work: Bruce Arnold, Laurie Torr and Alex and Rebecca Newland. Thank you to Ngati Haua for supporting the trenching in 2021. Obviously, this research could not have been done without that support from landowners. On the topic of field work, thanks to Seager Ray for providing assistance at Newland Farm.

The technicians have also been huge help. Thank you to Kirsty Vincent and Holly Harvey-Wishart for help and guidance in their respective laboratories and to Annette Rogers and Ben Roche for helping with field equipment and providing motivation over the past few months. At Victoria University of Wellington, Dr. Ian Schipper is thanked for the time on the probe and assistance while operating the electron microprobe.

I couldn't have done this without my friends: the quizzers and trampers. In no particular order, thank you to Sinead, Adam, Abbie, Calum, Aidan, Aimee, Nicola, Shay, Hannah, Matthew and Lev. You all kept me sane over the last two years, whether that has been on mountains or in the pub (or both!). But I especially want to highlight Flavian,

Matt and Esther, for being my closest friends over this time. I would also like to mention my Sunday league football team, Zig Zag, for one win, one draw and 28 losses over the course of this thesis. As impressive as those 28 losses in a row (and counting) in the 4th Division of the Waikato Sunday Soccer League is, I hope we break that streak sometime soon!

Lastly, thanks to the family: Grandma and Grandpa for the Sunday evening chats on the phone, and Beth, I am still surprised three years later that you followed me into geoscience. Good luck with your own thesis. And most of all, Mum and Dad. Thank you for the conversations about football with Dad and watching comedy shows and murder mysteries with Mum. But more seriously, words cannot express how much it has helped to have a stable roof over my head and hot meals these past five years of university. I cannot have done this thesis without you.

Note: Funding support for this project by Toka Tū Ake EQC, Te Pūtea Rangahua a Marsden Marsden Fund, and MBIE's Endeavour Fund, is acknowledged in section 1.4.

Table of Contents

List of figures

List of tables

Chapter 1
Introduction

1.1 Introduction

Active faults produce a hazard and a risk to communities. By definition, faults are considered "active" in New Zealand if they have ruptured or deformed the Earth's surface in the past 125,000 years. All known active faults in New Zealand are collated into central databases, the New Zealand Active Fault Database (Langridge et al., 2016) and Community Fault Model, which can be used to better understand seismic hazard and risk (Seebeck et al., 2023).

The Waikato region has been designated as having low to moderate seismic risk (based on the historic record of seismicity and what was perceived to be a limited number of active faults) (Downes, 2005; Stirling et al., 2012). Until recently, the only active fault recorded in the region is the Kerepehi Fault, an 80 km-long segmented normal fault which runs essentially north-south through the middle to eastern part of the Hauraki Plains. The Hauraki Plains are located within the Hauraki Rift, a c. 250-km-long half graben extending from Matamata in the south to the Hauraki Gulf in the north (Villamor et al., 2023). This fault produces occasional small earthquake swarms, the largest recorded in modern history being the 1972 Te Aroha Earthquake which measured M_w = 5.2 and caused minor damage to property (Adams et al., 1972; Persaud et al., 2016). A topical (at the time of writing) example of how earthquakes are uncommon in this region was the occurrence of two earthquakes associated with the Kerepehi fault of M_w = 5.1 and M_w = 4.8 in the summer of 2022–23. Although these are relatively small compared those experienced in other regions of New Zealand in the past decade, they caused some media attention due to the rarity of earthquakes of this magnitude in the region (Geonet, 2023). The Te Puninga Fault was revealed in 2016 on western margin of the Hauraki Plains using LiDAR. Preliminary evidence suggests it may generate earthquakes of Mw>6.8 (Persaud et al., 2016). This possibility presents a risk to the infrastructure and population of Morrinsville and Te Aroha, and the wider Hauraki Plains. The basin effect in the Hamilton Basin could cause an amplification of these seismic waves. Such amplification could possibly cause liquefaction in the Hamilton Basin and present a hazard and risk in the Hamilton region (Dempsey et al., 2021). Recent spatial and temporal analysis of soft-sediment deformation structures within tephra layers in modern lakes in the Hamilton Basin (a study related to that on Te Puninga Fault) has provided some evidence that

liquefaction of a sequence of tephras deposited between c. 17,500 and c. 14,000 cal yr BP was triggered by a seismic source to the northeast, namely Te Puninga and/or Kerepehi faults (Kluger et al., 2023).

1.1.1 Research aim and objectives

This study aims to provide a chronology and assessment of past seismicity for earthquakes on the Te Puninga Fault during the late Quaternary. Such an aim can be used to better understand the hazard and risk this fault poses to the region. To achieve this aim, the following objectives were identified:

a) Establish a stratigraphy and chronology for deposits exposed in two paleoseismic trenches athwart the Te Puninga Fault using radiocarbon (^{14}C) dating and tephrochronology, to define the stratigraphic framework for paleoseismic studies along the fault.
b) Use LiDAR to closely measure how a scarp that dips in the opposite direction to the land surface interacts with offset stream terraces straddling a segment of the fault (in a geomorphological case study at Quine Rd). This LiDAR-based case study can provide further evidence of surface displacement and help model ages of earthquakes on the segment.
c) A trial study of the application of ground penetrating radar (GPR) on the Te Puninga Fault to assist with future paleoseismic studies.

1.2 Study Area

The Hauraki Plains lie within the Hauraki Rift in the northern North Island of New Zealand, bounded by the Coromandel and Kaimai ranges to the east, and the Mamaku Plateau to the south. The Hapuakohe Range and Kiwitahi Volcanic Group divide the Hauraki Basin with the neighbouring Hamilton Basin (Figure 1.1). The plains extend to the Firth of Thames in the north, where the shoreline has migrated on a scale of 10s to 100s of kilometres with sea level changes since the Last Glacial Maximum (LGM) (Newnham et al., 1995; Williams, 2017; Lowe and Green, 2023). The basin was formed because of rifting that began in the late Neogene and has since been infilled by sediments, until the present day, where the modern rivers include the Waihou and Piako rivers. The two active faults in the basin, the Te Puninga and Kerepehi faults, strike in NNW direction broadly on the west and east of the basin. The nomenclature, Hauraki Plains and Hauraki Basin, are often used almost interchangeably, the former (a landform term) will be favoured in this study. However, “basin” will be occasionally used when discussing larger

scale tectonism. More comprehensive information on the geological setting is in Chapter 2.1.

Understanding the seismic risk for the region as is important as the Hauraki Plains are an important region economically for New Zealand. The plains, home to over 55,000 people (Stats NZ, 2018) and an important dairy farming hub, are situated between the major population centres of Auckland, Hamilton, and Tauranga, where over 40% of the country's population live within 40 km of the Hauraki Rift (Nicolin, 2019). The Te Puninga Fault Zone intersects key infrastructure of the region such State Highways 26 and 27 and the East Trunk Main Trunk railway. State Highways 26 and 27 cross fault traces studied in this study at 37°31'49"S, 175°35'14"E and 37°33'43"S, 175°32'51"E respectively. An earthquake large enough to cause deformation may disrupt these transport links.

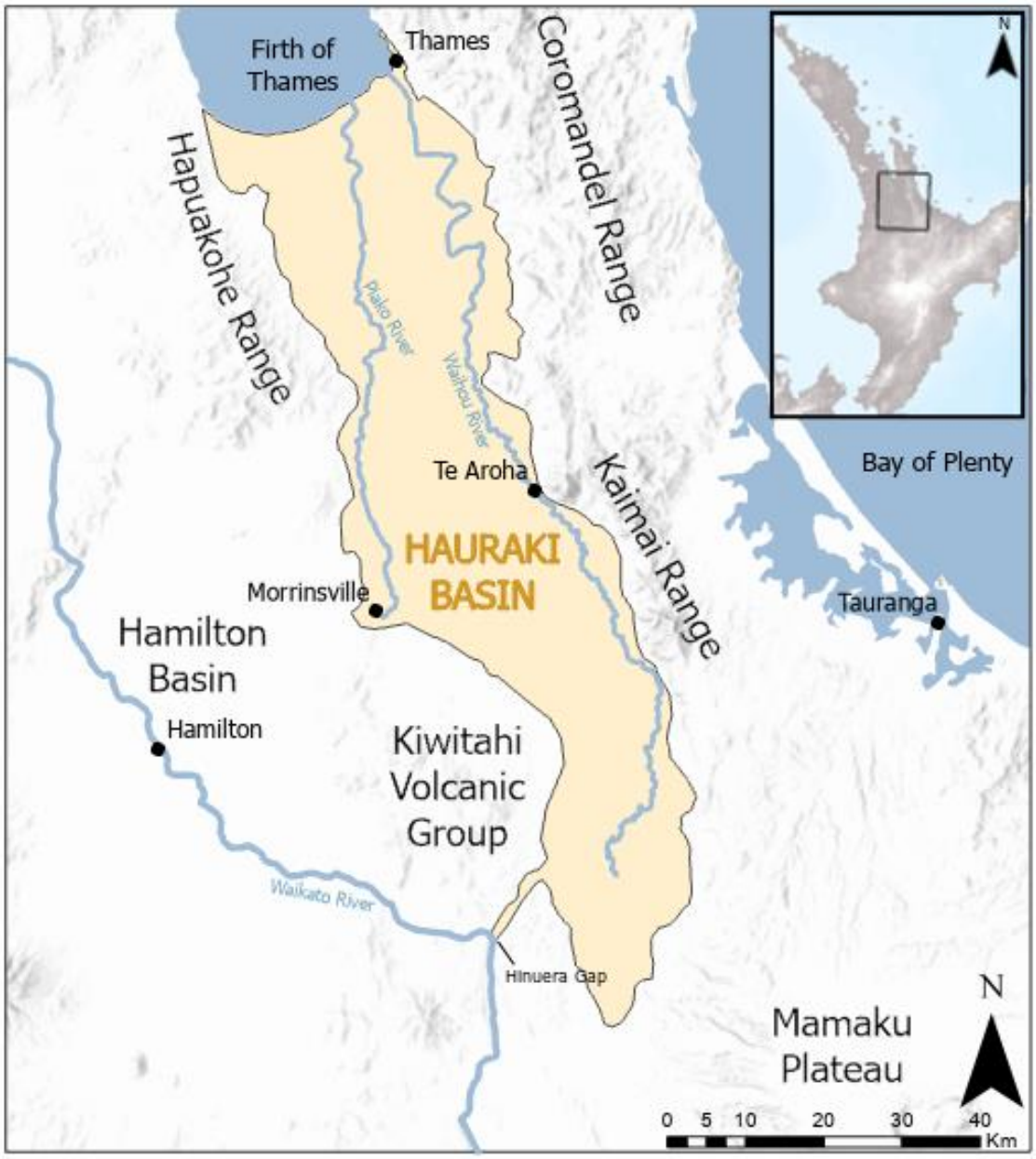

Figure 1.1: Map of the onshore extent of the Hauraki Basin, and associated landscape features, based on Cuthbertson (1981) and Houghton and Cuthbertson (1989). Hillshade model courtesy of R. Melchert. Inset shows the region's location in North Island.

1.3 Thesis structure

Chapter 2 is a literature review of the geological setting of the study area and the wider tectonic setting, along with background information of all the techniques used in this study, including tephrochronology and GPR.

In Chapter 3, I describe the deposits exposed in two paleoseismic trenches dug across two traces of the Te Puninga Fault. Radiocarbon (^{14}C) and tephrochronology are used to date the deposits exposed. This chapter establishes the stratigraphic framework

for paleoseismic studies on the Te Puninga Fault (e.g., Villamor et al., 2023) and it is used in Chapter 4.

Chapter 4 is primarily a geomorphological analysis of the relationship between a scarp to the northwest of the fault zone and the formation of terraces adjacent to a trace of the Te Puninga Fault and their offset. This work produced models that provide ranges of ages of earthquakes on the fault trace. In the last section of this chapter, I present slip rates calculated from these findings.

Chapter 5 is a trial using GPR on transects across the scarp to investigate: 1) the viability of using GPR for paleoseismic investigations in the Hauraki Plains, with challenging geology and high water table, 2) that the scarp is indeed a product of seismically-induced displacement and not formed by fluvial processes, and 3) how different geological units in the area and deformation are exhibited in the GPR data.

In Chapter 6, I summarise of the main findings of the study.

1.4 Funding support for study

In this study on Te Puninga Fault, I was supported by a masterate scholarship provided by the Marsden Fund (see below). This support is gratefully acknowledged. The study formed part of a wider project on the Te Puninga Fault that was supported partly by funding from Toka Tū Ake Earthquake Commission (EQC), led by Dr Pilar Villamor, entitled "Paleoseismology of the newly discovered Te Puninga Fault, Hauraki Plains" (contract BIG 012 2020), and partly by funding from Te Pūtea Rangahua a Marsden Marsden Fund (administered by the Royal Society of New Zealand) for a project led by Professor David Lowe entitled "Earth-shaking insight from liquefied volcanic-ash (tephra) layers in lakes: using geotechnical experiments, CT-scanned lake sediment cores, and tephrochronology to map and date prehistoric earthquakes" (contract UOW1902). Both the EQC and Marsden projects were carried out in conjunction with a parallel project, supported by the MBIE Endeavour Fund (Smart Ideas) (led by Lowe), "Evaluating earthquake risk using liquefied volcanic-ash layers in lakes" (contract UOWX1903).

Chapter 2

Literature Review

2.1 Geological setting

The present-day Hauraki Plains are located within the Hauraki Rift. The Hauraki Rift is a half graben, situated in the back-arc of the Hikurangi Subduction margin. Consisting of three sections, the Hauraki Gulf, the Firth of Thames, and the Hauraki Depression, the Hauraki Rift runs in an NNE direction for >200 km although the full length is not known as the southern end is infilled by volcanogenic sediments and buried by pyroclastic flow deposits (ignimbrites), such as the Mamaku Ignimbrite (Ballance, 2017). The Hauraki Rift is situated between the Jurassic greywacke (of Waipapa Terrane) to the southwest and the Miocene to Pliocene Coromandel Volcanic Zone to the northeast (Persaud et al., 2016). Block faulting in the late Miocene caused the uplift and formation of ranges such as the Hunua and Hapuakohe Ranges to the west of the Hauraki Basin, consisting largely of the aforementioned Waipapa Terrane (Singleton, 1981). The greywacke ranges are strongly weathered and show high degrees of argillisation (Wilson, 1980). Also on the western edge of the Hauraki Basin are the volcanic rocks of the Kiwitahi Lineament. This is a >100 km-long lineament of andesitic volcanoes with an age progression from 14 Ma* in the north on Waiheke Island to 6 Ma near Cambridge (Ballance, 2017).

The Hauraki Rift is filled by 2.5–3 km of Cenozoic sediments, the youngest and most voluminous being the Late Pleistocene aged Hinuera Formation. The Hinuera Formation is secondary volcaniclastic alluvium deposited by the ancestral Waikato River (Hume et al., 1975), derived mainly from reworked deposits of the Oruanui super-eruption (Manville and Wilson, 2004). Its emplacement in the Hauraki Basin was before the avulsion of the ancestral Waikato River into the Hamilton Basin between c. 23,500 cal yr BP* (Peti et al., 2021) and c. 24,000 cal yr BP (Lowe and Green, 2023).

**Note*: Throughout this thesis, most ages are reported in calibrated/calendar (cal) years (yr) before present (BP), "present" being 1950 AD on the radiocarbon time scale. As well, ages are reported in abbreviated form for convenience as cal ka BP, 'ka' meaning thousands of calendar years. 'Ma' means millions of years ago.

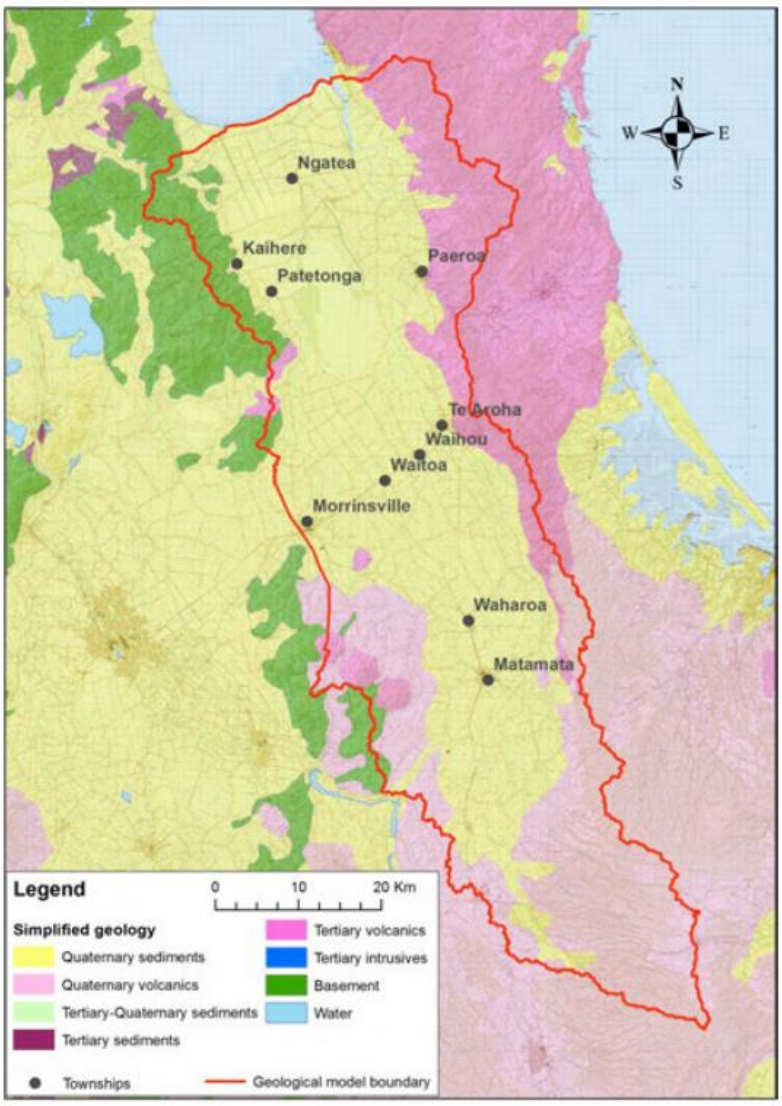

Figure 2.1: Simplified geological map of the Hauraki Plains (WRC, 2016; after Edbrooke, 2005, and Leonard et al., 2010).

In the north of the Hauraki Plains, deltaic and estuarine sediments are also present, deposited during a rising sea level in the early Holocene transgression at c. 7,500 cal yr BP (Newnham et al., 1995; Clement et al., 2010). In the Late Pleistocene and Holocene some alluvium has also been deposited from the Waihou, Waitoa and Piako Rivers, while extensive wetlands formed. The largest wetland is the Kopoutai bog (known also as peat dome), presently extending over 10,000 ha, that began forming c. 15,600 cal yr BP (Lowe and Green, 2023). Many rhyolitic and andesitic tephras from the Late Pleistocene and Holocene also mantle this and adjacent landscapes. They predominantly erupted from the rhyolitic centres of Taupo and Okataina in the central Taupo Volcanic Zone, as well as from Tuhua Volcanic Centre (Mayor Island), and andesitic centres Taranaki Maunga and Tongariro Volcanic Centre (Lowe, 1988; Newnham et al., 1995; Hopkins et al., 2021a).

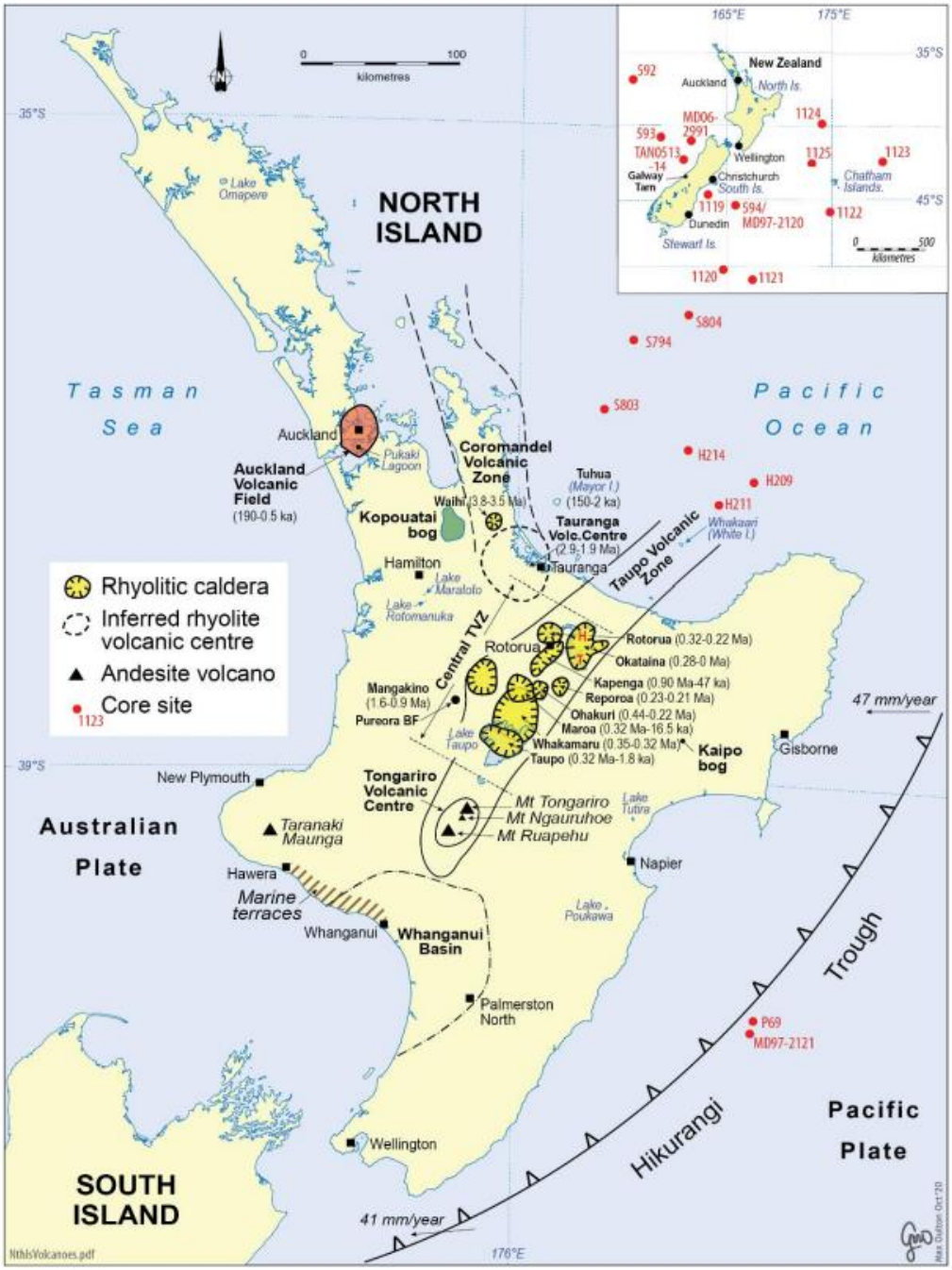

Figure 2.2: Map of the North Island with the sources of tephra in the Quaternary or shortly before (Hopkins et al., 2021a). The study area for my thesis is approximately 10 km south of Kopuatai bog.

2.1.1 Hinuera Formation

The Hinuera Formation consists of Pleistocene-aged, volcaniclastic alluvium deposited by the ancestral Waikato River (Schofield, 1965; Hume et al., 1975; Kear and Schofield, 1978; Manville and Wilson, 2004; Edbrooke, 2005; Leonard et al., 2010). It is distributed through the basins of Reporoa, Hauraki, and Hamilton, forming plains (Figure 2.3). The

flow of the Waikato River varied over this period due to volcanic activity in the headwaters (currently Lake Taupo) and climatic and vegetational variations, and local geomorphic conditions. As a result, the spatial distribution varies due to changes in the river's course, most notably the switch in diection (avulsion) at Piarere from the Hauraki Basin and the Hamilton Basin. Due to variations in the flow and sediment deposition, the formation's lithology is heterogenous. Hume et al. (1975) developed seven lithofacies of sediment types (Table 1.1).

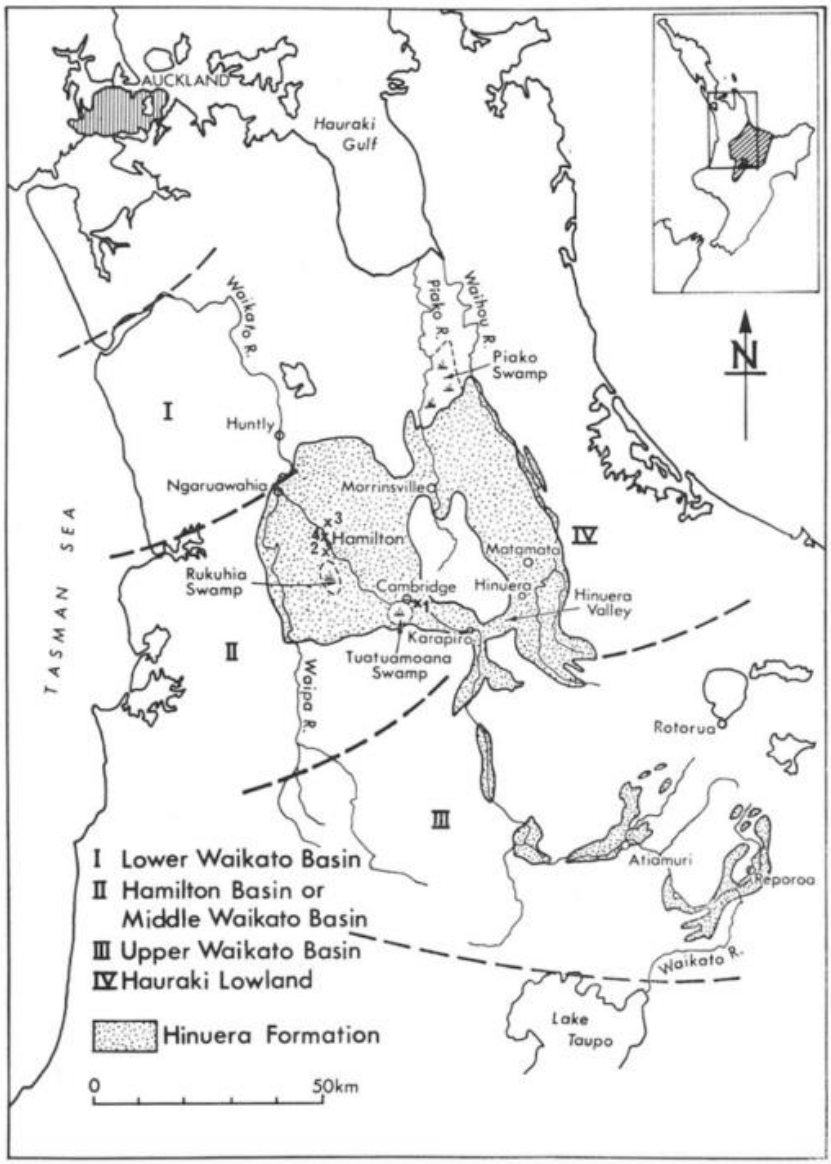

Figure 2.3: Distribution of the Hinuera Formation in the broad basins associated with the Waikato River (McGlone et al., 1978).

Table 1.1: Characteristics and depositional interpretation of the Hinuera Formation lithofacies (from Hume et al., 1975).

Lithofacies	Occurrence	Dominant Composition	Dominant Texture	Sedimentary Structures	Flow Regime	Bed Forms	Depositional Environment	Stratigraphic Position
A1	Extremely common	Quartz-feldspar-rhyolitic rock fragments-pumice	Gravelly sand	Rhc cross-stratification	Upper part of lower to lower part of upper	Dunes on longitudinal bars or longitudinal bar migration	Active braided channel	Channel
A2	Rare		Gravelly sand	Epsilon cross-stratification	Upper or lower			
B	Fairly common	Quartz-feldspar-pumice	Sand	Nu cross-stratification	Lower part of lower	Ripples on transverse bars		
C1	Uncommon	Quartz-feldspar-rhyolitic rock fragments	Sandy gravel	Type 1 horizontal stratification or massive	Upper	Plane-bed on longitudinal bars		
C2	Rare	Quartz-feldspar-pumice	Gravelly sand	Type 2a horizontal stratification	Transitional			
D	Moderately common	Glass shards-pumice	Silt	Type 2b horizontal stratification or massive	Suspension deposits	-	Abandoned braided channel	Overbank
E	Uncommon	Carbonaceous material-glass shards-pumice	Silt	Type 2b horizontal stratification	*In situ* and suspension deposits	-	Floodbasin	

Manville and Wilson, (2004) grouped the sediments of the Hinuera Formation into four subunits (A, B, C and D), primarily based on the age of deposition. The Hinuera Formation underlies most of the field area for this thesis, and hence dating the Hinuera Surface (Schofield, 1965) is a key task. I will outline each of the four subunits here. Figure 2.4 provides a visual representation of the sedimentation of the Hinuera Formation and the avulsion of the Waikato River.

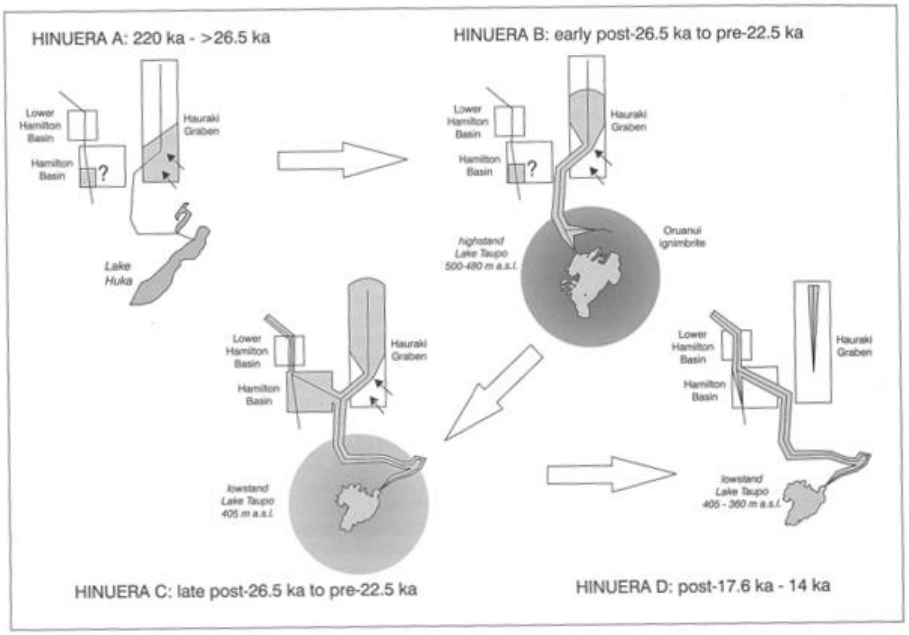

Figure 2.4: Depositional history of the Hinuera Formation, post-Oruanui eruption, showing changes of drainage basins and flow paths of the ancestral Waikato River (from Manville and Wilson, 2004).

2.1.2 Hinuera A

These sediments are only at the present land surface in the south Hauraki Plains. They are deposits of post-Mamaku (c. 220 ka BP) to pre-Rotoehu (c. 45 ka BP) eruption, high level steep alluvial fans. Some buried sediments in the Hamilton Basin are also classed in this subunit.

2.1.3 Hinuera B

The c. 25.4 cal ka BP Oruanui super-eruption caused enormous changes to the landscape of the central North Island (Wilson, 2001; Manville and Wilson, 2004). The eruption destroyed (paleo)Lake Huka, but the formation of the Oruanui caldera during the eruption led to the creation of a new, Lake Taupo (Lowe and Green, 2023). This was initially stable, before a catastrophic breakout flood occurred around 25 cal ka BP after the rising lake waters breached the caldera rim. The Hinuera B deposits represent the small quantity of deposition of alluvium in the Hauraki Plains during this c. 400 yr period. Like the Hinuera A sediments, these materials are only exposed at the present surface to the south of the Hauraki Plains.

2.1.4 Hinuera C

The breakout flood c. 25 ka cal BP caused Waikato River to re-establish its past route past Reporoa and towards Piarere and the Hauraki Plains. Over the next approximately 1000 years, the ancestral Waikato River deposited volcanogenic alluvium in a low angle (<1 °) fan over the entirety of the Hauraki Basin. While Hinuera C was being deposited, sediments piled up from the breakout flood event due to Oruanui-derived pyroclastic materials in a period of colder climate (the LGM) and related scrubland-grassland materials. This build-up of sediment eventually caused the river to spill into the Maungatautari gap, where it was captured by a tributary of the Waipa River, into the Hamilton Basin (Manville and Wilson, 2004; Williams, 2017). Several dates have been proposed for this avulsion of the Waikato River's course. The oldest tephra layer found in the old riverine blocked-valley lakes of the Hamilton Basin (which were formed by deposition of alluvium of the Waikato River) is the Okareka Tephra. So, the age of the tephra (23.5 cal ka BP: Peti et al., 2021) has been suggested as the latest this avulsion could have occurred. However, a few centimetres of lake sediments lie stratigraphically below the Okareka Tephra in Lake Rotomanuka (Lowe, 1988) and hence Lowe and Green (2023) suggested the lake was aged at least c. 24,000 cal yr BP. Consequenly, the ancestral Waikato River must have entered the Hamilton Basin at or a little before this

date. In addition, a suite of ^{14}C dates obtained on Hinuera Formation sediments in the Hamilton Basin (from Grant-Taylor and Rafter, 1963; Schofield, 1965; Hume et al., 1975; McGlone et al., 1984; Hogg et al., 1987), summarised in Appendix 1 of Lowe (2023), essentially supports this age.

The sediments deposited by the Waikato River in the Hamilton Basin after c. 24,000 cal yr BP are classed as Hinuera C (of Manville and Wilson, 2004). As a result, the surface that formed by the low angle alluvial fan of Hinuera C, became the dominant land surface of both the Hauraki and Hamilton basins.

2.1.5 Hinuera D

The Waikato River proceeded to deposit alluvium in the Hamilton Basin as a braided river system until c. 17.6 cal ka BP, when the climate began to warm, causing vegetation growth and a stabilisation of the landscape. These changes caused the Waikato River to entrench into its current course after a number of failed attempts recognised today in the landscape as shallow paleochannels (McCraw, 2011; Lowe and Green, 2023). This age (c. 17.6 cal ka BP) coincides with the deposition of the Rerewhakaaitiu Tephra, commonly used in North Island as a marker bed for these climatic changes (Newnham et al., 2003; Lowe et al., 2013). The entrenching river in the Hamilton Basin formed a series of degradational terraces, and in the Hauraki Basin rivers such as the Waihou, Waitoa and Piako also cut into the antecedent alluvium, generally until c. 14 cal ka BP but probably as late as c. 12 to 10 cal ka BP. These deposits are referred to as Hinuera D by Manville and Wilson (2004).

2.2 Seismic history in the Hauraki Rift

The Hauraki Rift has been active since the late Neogene (Hochstein and Nixon, 1979), before rifting then shifted to the Taupo rift ca. 2–3 Ma. Despite this, there is still evidence rifting is still occurring in the Hauraki Rift on a smaller scale than the Taupo Rift. The evidence includes shallow (<12 km) seismic activity, hot springs indicating upper mantle swell, and a recorded subsistence of 1.5 mm/yr (Riffault et al., 2017). Previously it was believed that there were two NNE-SSW faults in the Hauraki Rift, the inactive Hauraki Fault and the active Kerepehi Fault (Figure 2.5) (Houghton and Cuthbertson, 1989). The former is situated in the eastern margins of the rift along the Kaimai Range and is responsible for the formation of the range. The latter is towards the eastern margin of the rift.

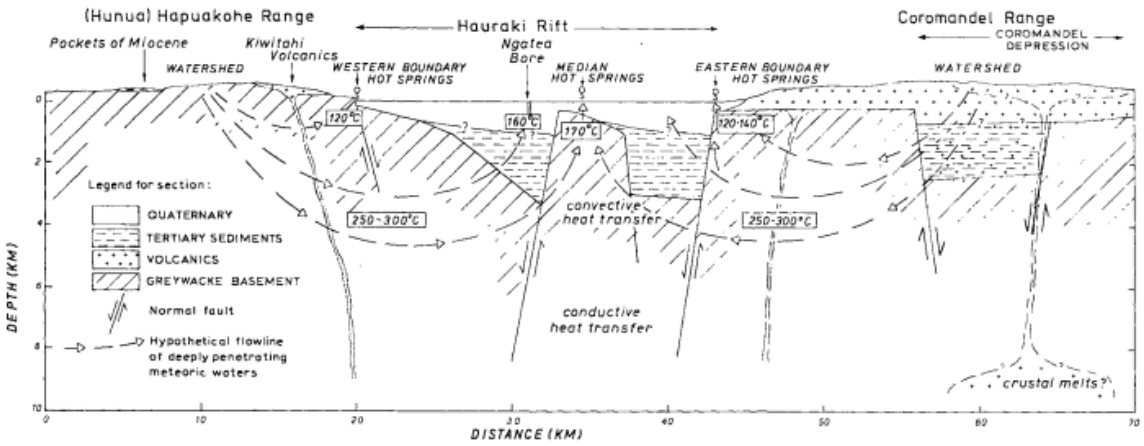

Figure 2.5: Simplified cross section of the Hauraki Rift with faults and hot springs labelled (Hochstein and Nixon, 1975).

The Kerepehi Fault is a normal fault, mostly dipping to the west and running in a NNE-SSW direction. Persaud et al. (2016) divided the on-shore traces into six segments, while four segments have been identified offshore (Chick, 2001). The largest earthquake on the Kerepehi Fault of recent times occurred in 1972, with a $M_w = 5.2$ (Persaud et al., 2016).

Recent LiDAR evaluation of the Hauraki Plains revealed a zone of fault scarps in the western margin of the plains (Figure 2.6). These scarps were estimated to be distributed over a length of 22 km and width of 5 km. Based on the LiDAR data, the scarp height was estimated to be 2.0–3.7 m. This displacement of the Hinuera Surface suggests that the fault was active in the last c. 24 ka BP (the assumed age of the surface). The fault was named the Te Puninga Fault and is the main topic of this thesis.

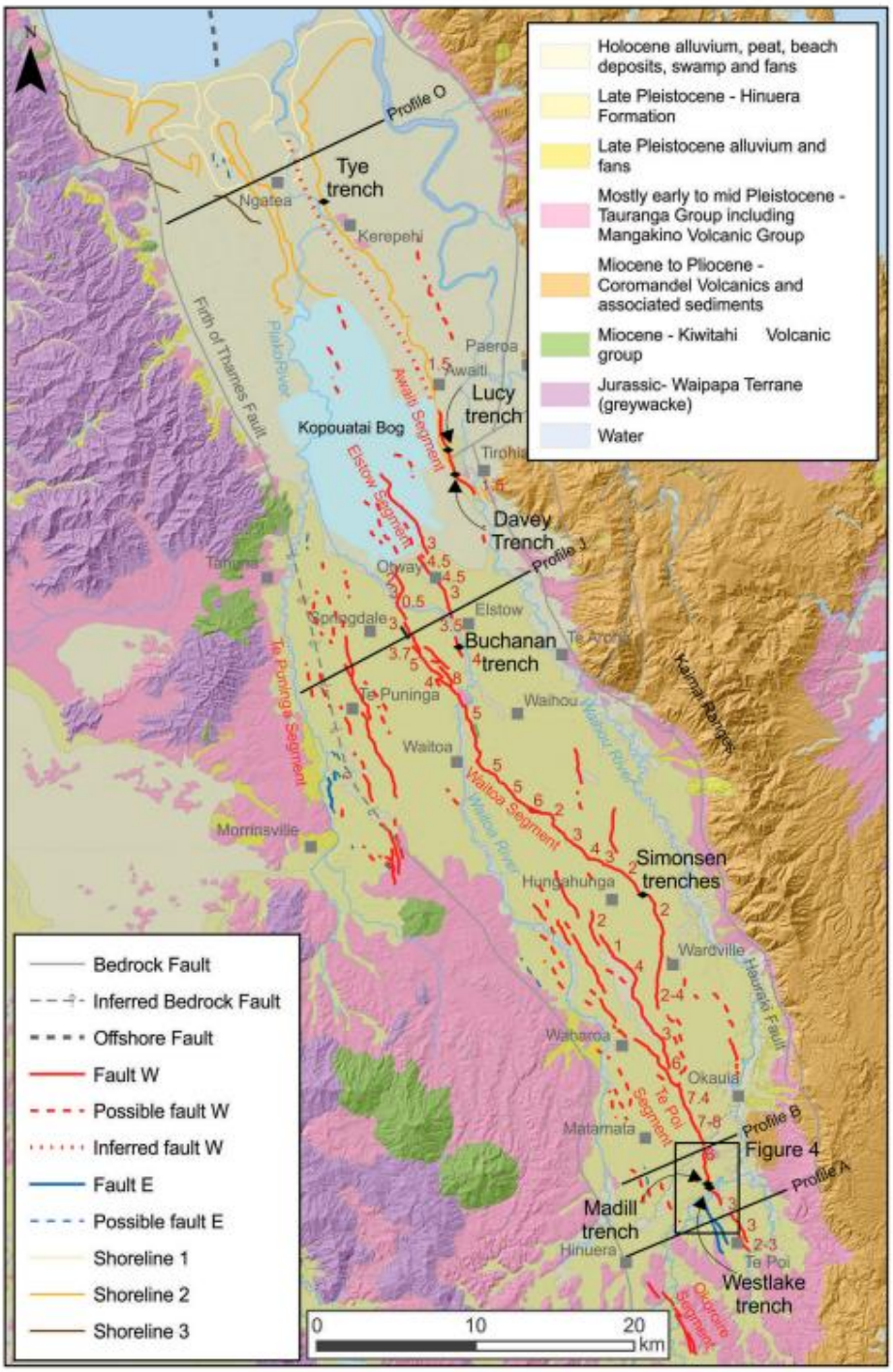

Figure 2.6: Active fault traces in the Hauraki Rift mapped from DEM, overlaid on a geological map (from Persaud et al., 2016). Note the Te Puninga Fault labelled to the west, near Morrinsville.

2.3 Tephrochronology

Tephras consist of all explosively erupted, unconsolidated pyroclastic products of volcanic eruptions. The pyroclasts can comprise crystals, glass (including shards, pumice

and/or scoria), and lithics. Tephras are deposited effectively instantaneously (from a geological timescale perspective) and over a wide area, and the deposits thus provide an isochron that can be used as a widely occurring stratigraphic connecting (correlational) and dating tool (Lowe, 2011). Tephrochronology (sensu stricto) is an age-equivalent dating method using tephra layers as isochrons to synchronise sequences and transfer relative or numerical ages using stratigraphy and other tools. Sensu lato, tephrochronology is used for all aspects of tephra studies and their application (Lowe, 2011).

Tephra characterisation is undertaken on visible and cryptotephra deposits using a range of analytical methods. These methods can be conducted on mineral assemblages, or on individual glass shards, crystals or phenocrystals (Table 1.2). This characterisation is then used in conjunction with other techniques such as stratigraphic positioning, paleoenvironmental data, and chronological criteria to identify a specific deposit (Lowe, 2011).

Table 1.2: Summary of analytical methods used to characterise glass or crystals in tephras (Lowe, 2011)*.

Tephra components and properties	Methods of analysis
Glass shards or selvedges	
Major elements	Electron microprobe
Rare-earth and trace elements	LA- or SN-ICPMS, INAA, SSMS, SIMS[a]
Shard morphology	Optical microscope, SEM[a]
Fe–Ti oxides	
Major and minor elements in crystals	Electron microprobe, Mössbauer spectroscopy
Eruption temperatures and oxygen fugacities	Electron microprobe
Ferromagnesian minerals	
Assemblages	Petrographic microscope[b]
Pyroxenes, amphiboles, olivine, biotite crystals	Electron microprobe
Feldspars	
Anorthite (An) content of plagioclase crystals	Electron microprobe

[a] LA- or SN-ICPMS, laser-ablation or solution nebulisation inductively-coupled plasma mass spectrometry; INAA, instrumental neutron activation analysis; SSMS, spark source mass spectrometry (now uncommon); SIMS, secondary ionization mass spectrometry (known also as ion probe/microprobe); SEM, scanning electron microscopy. Measurements of the refractive index (RI) of glass shards and also free crystals were widely used prior to the advent of the electron microprobe; high-precision RI methods for glass and crystals (e.g., cummingtonite) remain in limited use (e.g., Danhara et al., 1992; Soles et al., 1995; Nakamura et al., 2002; Enache and Cumming, 2006; Matsu'ura et al., submitted for publication).

[b] Where crystal quantities are abundant, ferromagnesian minerals may be identified using X-ray diffraction.

* See Lowe (2011) for the references cited in the footnotes

Cryptotephra is a term coined by Lowe and Hunt (2001) describing preserved distal tephra deposits of sparse glass shards and/or crystals insufficiently numerous to be visible as a layer to the naked eye (Lowe, 2011). These can be preserved in sediments, such as lacustrine sediments or peat, along with ice or soils or paleosols (Hopkins et al., 2021a). The indivdual grains can be detected, isolated (separated), and analysed using the techniques listed in Table 1.1.

2.3.1 Electron probe microanalysis of tephra

Electron probe microanalysis (EPMA**)** is a single grain technique used for determining the major element composition of minerals (crystals) and glass shards via the electron probe. Grains are separated from sediment using a variety of methods and sieved into size fractions. Then the individual grains are mounted in a suitable resin and polished to expose a fresh surface, before coating with carbon (Froggatt and Gosson, 1982; Froggatt, 1992; Hopkins et al., 2021b). The electron probe directs a focused beam of electrons, generating X-rays. The individual elements in the sample then produce X-rays of different wavelengths, with the intensity proportional to the abundance (Shane, 2000). Analysis of the major elements of the samples – tephra fingerprinting – can allow for the identification of the tephra through comparison with previously published analyses (along with essential stratigraphic and chronological information). Regarding glass, the major element data, once normalised, are able to be compared with data of known eruptives using, for example, binary or tertiary plots of key elements usually expressed as oxides, or statistical methods such as discriminant function analysis (Lowe, 2011; Lowe et al., 2017).

2.4 Formation of river terraces

Over time, the erosion and deposition of sediments by waterways form terraces. These can be classed into two types, aggradational (formed from deposition of sediments) and degradational (formed from erosion of sediments). Deposition of the Hinuera Formation as a series of very low-angle fans in both the Hauraki and Hamilton basins generated in effect an aggradational surface (Schofield, 1965; Kear and Schofield, 1978; Edbrooke, 2005). The entrenchment of the Waikato River into its antecedent sediments was marked by still stands in downcutting that resulted in degradational terraces (such as evident in the Maungatautari gorge/Karapiro area as well as in the Hamilton area). In Chapter 4 of

this thesis, I use incision rates and the resulting formation of terraces to potentially provide age ranges for earthquakes on the Te Puninga Fault.

In general, a variety of factors can affect fluvial incision. These include lithology, such as how easily erodible the underlying units are, and structural constraints (Duvall et al., 2019), vegetation cover, climatic changes, and resulting streamflow relative to sediment inputs (Clement and Fuller, 2007), and the base level that the waterways ultimately erode down to (sea level change can influence that: Schumm, 1993). The controls on fluvial incision also depend on the time scale. Given New Zealand's maritime location, generally abundant rainfall, generally steep catchments, and some lithologies prone to fast erosion (e.g. mudstones), rivers can be highly responsive to climate change (Clement and Fuller, 2007). Other factors can control incision in New Zealand, especially increased sediment inputs due to active volcanism in the North Island (Jauregui and Brierley, 2007; Manville and Wilson, 2004) and structural constraints due to faulting and uplift in more tectonically active areas in New Zealand such as the upper South Island (Duvall et al., 2019).

2.4.1 Trends of terrace development in northern North Island

Some studies have attempted to correlate riverine terraces across multiple catchments to produce regional scale comparisons of terrace formation. To achieve this, methods such as the correlation of loess and paleosols along with tephrostratigraphy, OSL dating and radiocarbon dating are used (Litchfield and Berryman, 2006). After the LGM, when the trend of rivers in the North Island was aggradational terrace formation, the warming climate in the late Pleistocene to Holocene led rivers to transition to degradational terrace formation (Clement and Fuller, 2007).

The terraces formed after the LGM by Waihou River in the Hauraki Basin, 17 km east of Quine Road, have been dated (Persaud et al., 2016). The terraces were formed within the Hinuera C surface (Manville and Wilson, 2004). Downcutting after the formation of the surface was rapid from 20 ± 2.5 cal ka BP to ca. 16 cal ka BP (using the age on the Hinuera Surface adopted by Manville and Wilson, 2004, of 20 ± 2.5 cal ka BP), before slowing down (Figure 2.7). Degradation terrace formation in the Waihou River catchment was largely completed by 12–10 ka BP (Persaud et al., 2016).

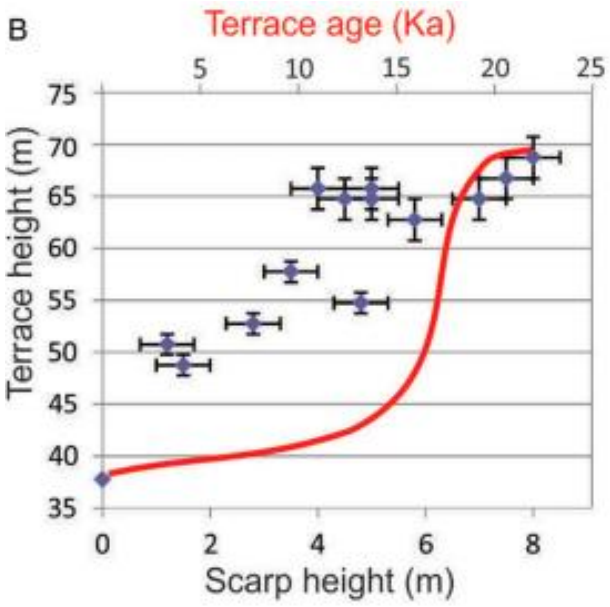

Figure 2.7: Plot of terrace height (asl) versus fault throw of the hanging wall of the Kerepehi Fault. An estimated terrace age vs terrace height curve is also graphed (Persaud et al., 2016).

This pattern is consistent to others in the adjacent Hamilton Basin, the Waikato River transitioned from an aggregational, braided river system to a degradational, entrenched river from c. 17 cal ka BP. This occurred due to the reduction of volcanic sediment inputs post-Oruanui eruption along with the climate change causing higher flow and a stabilisation of the landscape due to an increased forest cover (Newnham et al., 1999, 2003). This trend rivers beginning to entrench and form degradational terraces post-LGM is seen in similar rivers in the region.

2.5 Ground penetrating radar (GPR)

GPR is a technique used to identify underground features in situ. Originally developed for engineering purposes such as maintaining pipes or foundations, it is now used in geosciences for many purposes such as mapping tephra, faults, lake sediments, and soils (Lowe, 1985; Annan, 2002). In addition to in situ analysis, another advantage of the technique is that it can be used for continuous (not point source) data, which can be used in conjunction with ground truthing with soil pits or coring to develop a model of the geology of a field area.

GPR emits short high frequency electromagnetic pulses (25–1000 MHz) from one antenna through the ground material, measuring the time of these to be reflected back to

the receiver antenna (Lowe, 1985; Busby et al., 2004) (Figure 2.8). The time taken for the pulses to reflect depends on the dielectric constant of the material. The dielectric constant is a material's ability to store electric energy in electric field. It is a function of primarily mineralogy, porosity, saturation, geometry, and frequency of the antenna used in a survey among other properties (Knight and Endres, 1990; Martinez and Bynes, 2001). As the dielectric constant determines how the electromagnetic pulses propagate through the material, differences in the dielectric constant cause the time of reflection to change and thus, a reflector is produced. The amplitudes of these reflectors decrease with depth, as the wave propagates through more material, so these reflectors need to be amplified in the processing stage. The GPR is moved across the surface in a transect, producing a 2D cross-section. And many of these cross-sections, if sufficiently numerous, can be used to develop a 3D model.

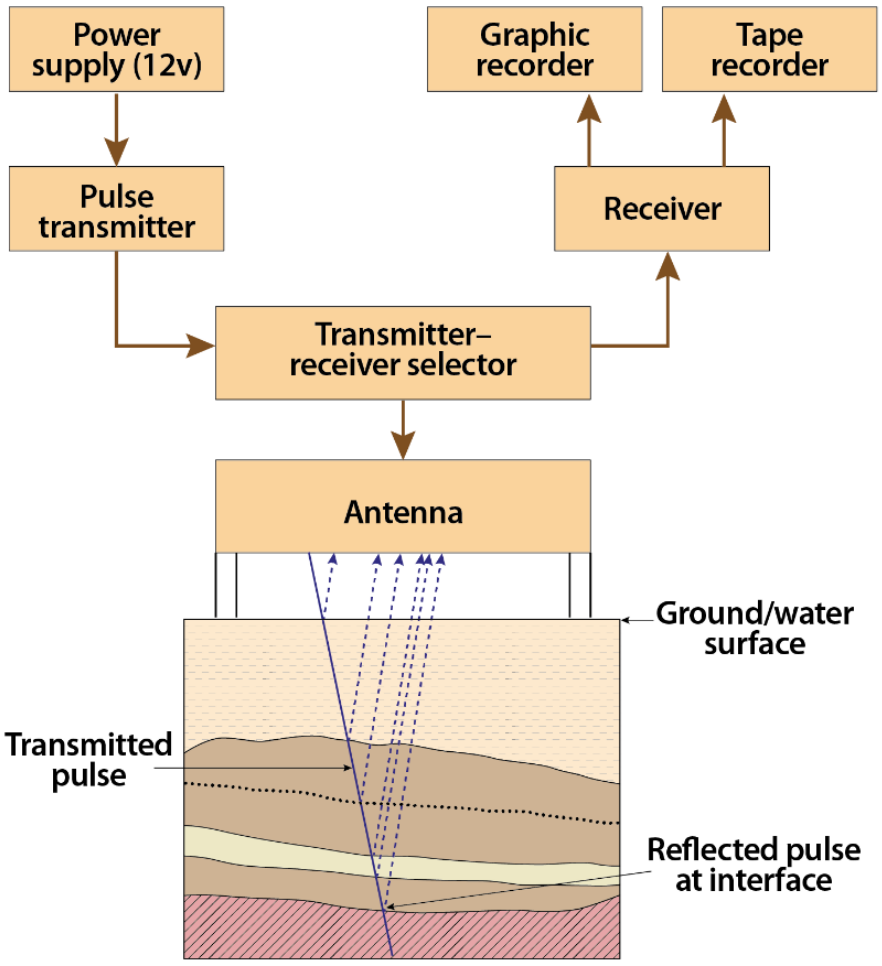

Figure 2.8: Schematic diagram of the GPR system with materials of different dielectric constants shown in lowermost diagram (after Lowe, 1985).

Chapter 3

Stratigraphy and chronology of Late Quaternary deposits exposed in paleoseismic trenches

3.1 Introduction

Paleoseismic trenching was undertaken on two sites, on two different fault strands, to define the ages of the sediments and other deposits offset by the Te Puninga Fault. These two sites are referred to as the Arnold and Ryland sites (Fig. 1). The trenching was undertaken for several reasons: 1) to date the sediments and other deposits and soils displaced by the fault, 2) to refine the age of the surface of the Hinuera Formation in the Te Puninga Fault area, and 3) to compare the offset of the stratigraphy to the displacement at the surface.

The purpose of this chapter is to establish the stratigraphy of the sediments and other deposits, and soils, exposed in the trenches, using tephrochronology and radiocarbon (^{14}C) dating to determine a chronology of the deposits. This information can then be used to inform the research undertaken for Chapters 4 and 5.

3.2 Methods

Over nine days, fieldwork was undertaken at the two sites (Arnold and Ryland, Figure 3.1). These trenches were excavated perpendicular to the scarps. The Arnold trench was 41 m long and 3 m deep across a 2 to 2.5 m high scarp, and the Ryland trench was 38 m long and 2.4 m deep across a 3.3 m high scarp (Villamor, 2022).

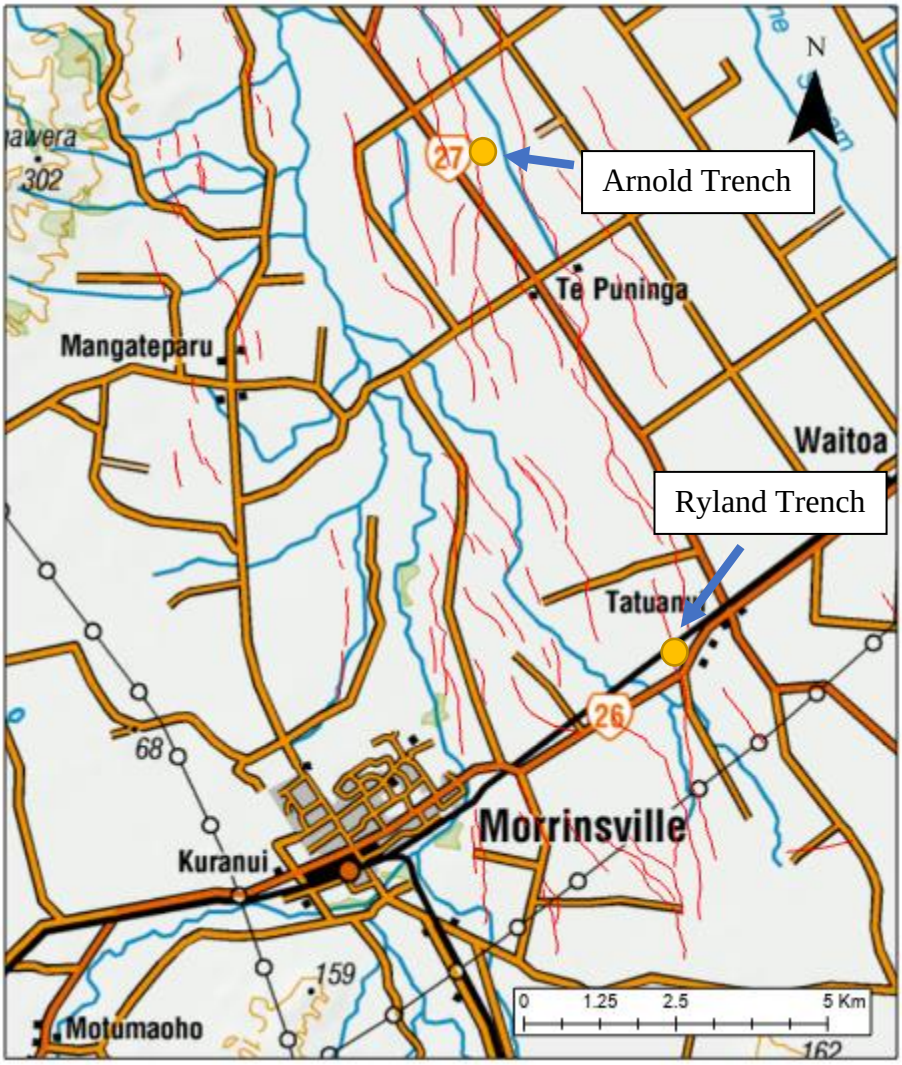

Figure 3.1: Location of the two paleoseismic trenches excavated across traces of the Te Puninga Fault. Map from NZ Map Series 260.

To describe all the exposed units, stratigraphic units were identified at specific sites within the trenches. Then geological and pedological descriptions were made for each of the units. A number of ^{14}C samples were extracted from the trench exposures and submitted for dating at the Waikato Radiocarbon Dating Laboratory. Ages were calibrated using OxCal v.4.4.4 (Chris

Bronk Ramsey: https://c14.arch.ox.ac.uk/oxcal/OxCal.html) and the SHCal20 atmospheric calibration curve of Hogg et al. (2020).

In situ descriptions were made of tephra deposits before sampling. Laboratory work was undertaken to characterise the tephra deposits as follows. Using an Astrason ultrasonic cleaner, tephra samples were separated from encasing soil material and then wet sieved into the following size fractions: 64−256 μm, 256 μm−1 mm and > 1 mm. Once dried, the materials were separated into constituent mineral and glass fractions using a Frantz isodynamic magnetic separator (Froggatt and Gosson, 1982; Froggart, 1992). Major element analysis of araldite-mounted and polished glass shards was undertaken at the electron probe microanalysis (EPMA) facility at Victoria University of Wellington. The EPMA was conducted using the JEOL JXA-8230 SuperProbe, with a beam diameter of 10 μm, beam voltage of 15 kV and a probe current of 8 Å (following recommendations of Hopkins et al., 2021b). The standards used were ATHO-G (Jochum et al., 2014) and VG-568 rhyolitic glass (Jarosewich et al., 1980). The major elements were analysed as oxides and Microsoft Excel was used to tabulate and graph the resulting analyses. All glass analyses were normalised to facilitate valid comparison between samples and to meet requirements for classifying them on an anhydrous basis using Le Maitre et al. (2002) (Lowe et al., 2017).

3.3 Results

3.3.1 Stratigraphy and chronology of units exposed in the Arnold trench

At the base of the trench, the unit was identified as the Hinuera Formation. This comprises volcanogenic alluvium (which can also be described as secondary volcaniclastic sediments: (Di Capua et al. 2022), deposited as a series of low-angle fans forming a plain, by a high energy, braided river system (the ancestral Waikato River) approximately 25 ka cal yr BP (following the 25.4 ka cal yr BP Oruanui supereruption: Wilson, 2001; Vandergoes et al., 2013). Up to 90 m thick, the Hinuera Formation comprise heterogeneous rhyolitic quartzofeldspathic, ignimbritic, and pumiceous sandy gravels, gravelly sands, and sands, commonly with current bedding, and silts and occasional peat lenses (Schofield, 1965; Hume et al., 1975; Kear and Schofield, 1978; Manville and Wilson, 2004; Edbrooke, 2005; Leonard et al., 2010). The surface of the plain is called the Hinuera Surface (Schofield, 1965). This alluvium has been overlain by distal rhyolitic tephras, deposited incrementally since the abandonment of the Hinuera Surface, and has undergone modification by soil forming processes.

Based on previous work on the Hinuera Formation and tephras and other deposits in the Hauraki and Hamilton basins (e.g., Hume et al., 1975; Hogg et al., 1987; Houghton and Cuthbertson, 1989; Newnham et al., 1995; Manville and Wilson, 2004), the radiocarbon dates obtained were as expected. Radiocarbon dates on the early deposition of the Hinuera Formation in the Hamilton Basin, plus ages on blocked-valley riverine lakes formed by its deposition, have been estimated recently at c. 24 ka cal yr BP (Lowe and Green, 2023) (Figuare 3.2).

A peat lens extending over 10 m horizontally across the lower part (near base) of the exposed deposits in the Arnold trench provided an isochron. Three samples, Wk52552, Wk52554, and Wk52555, including leaf material, from this lens provided ages from 23,485 ± 55 cal yr BP to 24,900 ± 220 cal yr BP (Fig. 3). By undertaking Bayesian modelling of these dates, Vilamor et al. (2023) determined that the Waikato River abandoned the Hauraki Plains between c. 22,000 and c. 24,000 cal yr BP (median age 23,385 cal yr BP). This age is consistent with two previously published dates on (deep) peat samples from the Hinuera Formation in the Matamata area of 23,781 ± 200 cal yr BP (Wk216) and 22,863 ± 200 cal yr BP (Wk217) (Hogg et al., 1987; Houghton and Cuthbertson, 1989). Thus, the date at which the Hinuera Surface in the study area (Hauraki Plains) was abandoned by the avulsion of the Waikato River at Piarere (Williams, 2017) is c. 23,400 cal yr BP, which approximately matches that of the river's entry to the Hamilton Basin estimated at c. 23,500 cal yr BP (Peti et al., 2021) and c. 24,000 cal yr BP (Lowe and Green, 2023) (Fig. 3.2A, B). I adopt here an age of avulsion of c. 24,000 ca yr

BP following Lowe and Green (2023), and hence an age of c. 24,000 cal yr BP for the Hinuera Surface at both trench sites.

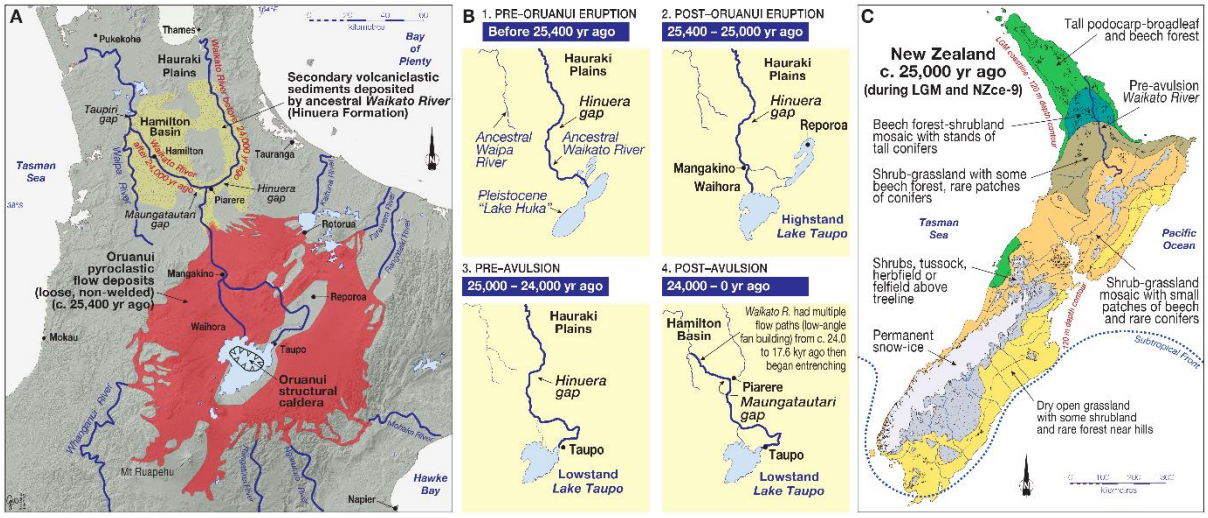

Figure 3.2: Maps showing the avulsion, or switch in flow direction, of the ancestral Waikato River at c. 24,000 cal yr BP into the Hamilton Basin (away from the Hauraki Plains) at a time of cold and dry climate and lowered sea level (figure after Lowe and Green, 2023). **A**. Map showing the distribution of the non-welded Ōruanui ignimbrite (red) erupted c. 25,400 cal yr BP, and secondary volcaniclastic sediments (Hinuera Formation) in the Hamilton, part Lower Waikato, and Hauraki basins (yellow). Waikato River flow paths before (notional) and after the avulsion are shown. Map after Manville (2001). **B**. Waikato River flow paths before and after the Ōruanui eruption (maps 1, 2), and before and after the avulsion at Piarere (maps 3, 4). Maps after Manville (2001). **C**. New Zealand c. 25,000 cal yr BP during the Last Glacial Maximum (LGM). NZce-9 = New Zealand Climate Event 9 of Barrell et al. (2013). Map after McGlone (1988), Manville and Wilson (2004), and Newnham et al. (2013).

A feature of the Arnold trench with unknown origins was a bowl-shaped feature roughly halfway down the trench wall (Appendix 1.4). As it crosscut the sediments of the Hinuera Formation, it must have been formed after their deposition (hence is younger than c. 23.4 cal yr BP). Two ^{14}C samples were taken from the within the feature, a stump at the base, was dated at c. 7,500 cal yr BP and a peat layer based at c. 7,000 cal yr BP (Fig. 3). The Taupo (1718 ± 10 cal yr BP) and Kaharoa (636 ± 12 cal yr BP) tephras (ages from Hogg et al., 2003, 2012, 2019) were identified as the only visible tephra layers exposed in the Arnold trench (Figure 3.3).

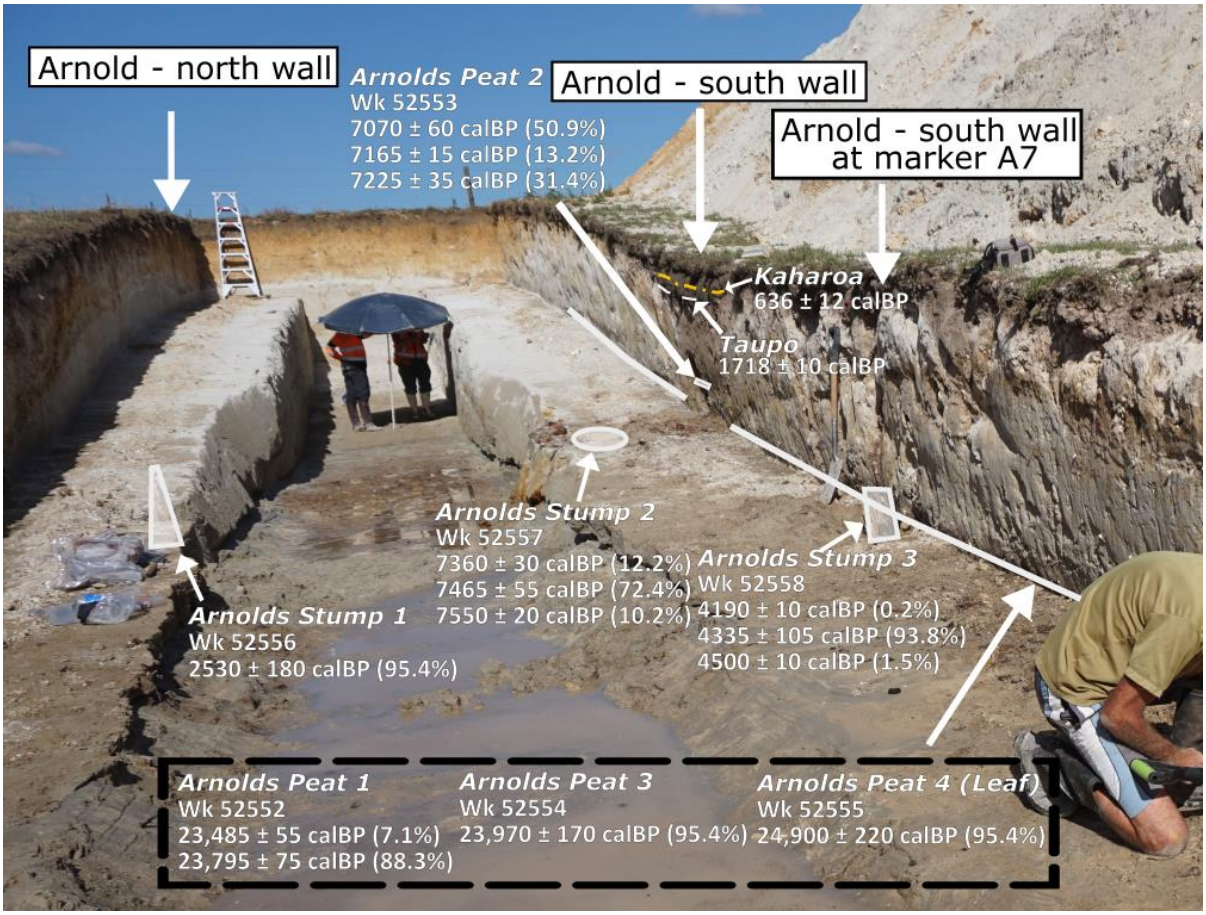

Figure 3.3: Synthesis of calibrated radiocarbon ages of wood and peat and dates of visible tephra layers observed in the Arnold trench. Photo: D.J. Lowe.

3.3.2 Stratigraphy and chronology of units exposed in the Ryland trench

As for the Arnold trench, the deposits in the bottom of the trench comprised alluvium of the Hinuera Formation and the uppermost unit, a composite of mainly rhyolitic tephra (see Chapter 3.3.1).

However, in the hanging wall side of the fault, a peat layer at 1.5 m depth is aged at c. 11,000 cal yr BP. This age indicated deposition of ~1.5 m of post-Hinuera Formation, fine to coarse sandy alluvium. This is thought to be alluvium from an ancestral path of the nearby Piako River and is here proposed to correlate with the Waitoa Formation (Houghton and Cutherbertson, 1989; Brathwaite and Christie, 1996; Hughes et al., 2022).

The Ryland Trench has post-Hinuera Formation deposition, stratigraphically positioned above the peat lens radiocarbon dated at c. 11,000 cal yr BP (Fig. 3.4).

The other radiocarbon dates from Ryland trench were dated post-human arrival, with a tree root aged 695 ± cal yr BP (95.4%) and peat 40 ± 20 cal yr BP (95.4%). The Ryland trench

sequence includes two tephra layers, Taupo and Kaharoa tephras, that could be identified in the field on the basis of their stratigraphic positions and field properties, and they were more extensive than in the Arnold Trench. The 1718 ± 10 cal yr BP Taupo Tephra was visible as fine pumice lapilli and was identified in the field in part because of their cream colour and because they were easy to crush between the fingernails (Lowe, 2006). The 636 ± 12 cal yr BP Kaharoa Tephra was present as an intermittent silty deposit. It was identified due to the presence of biotite, a key marker mineral found in the tephra (Lowe et al., 1998), and its near surface stratigraphic position overlying Taupo Tephra. As recorded below, both tephra correlations (identifications) were confirmed by major element analysis of glass shards from each (Chapter 3.4.3)

Figure 3.4: Synthesis of radiocarbon dates of wood and peat, and (tephrochronological) dates of visible tephra layers, observed in the Arnold trench. Photo: D.J. Lowe.

3.4 Discussion

The units exposed in the Arnold trench where mostly as expected, based on previous studies in the Hauraki Basin by Hume et al. (1975) and Houghton and Cuthbertson (1989). Three main units were erected: (i) Late Pleistocene alluvium of the Hinuera Formation, (ii) a post-Hinuera Formation rhyolitic tephra mantle, and, in the Ryland trench only, (iii) Holocene alluvium of the Waitoa Formation (Figure 3.5).

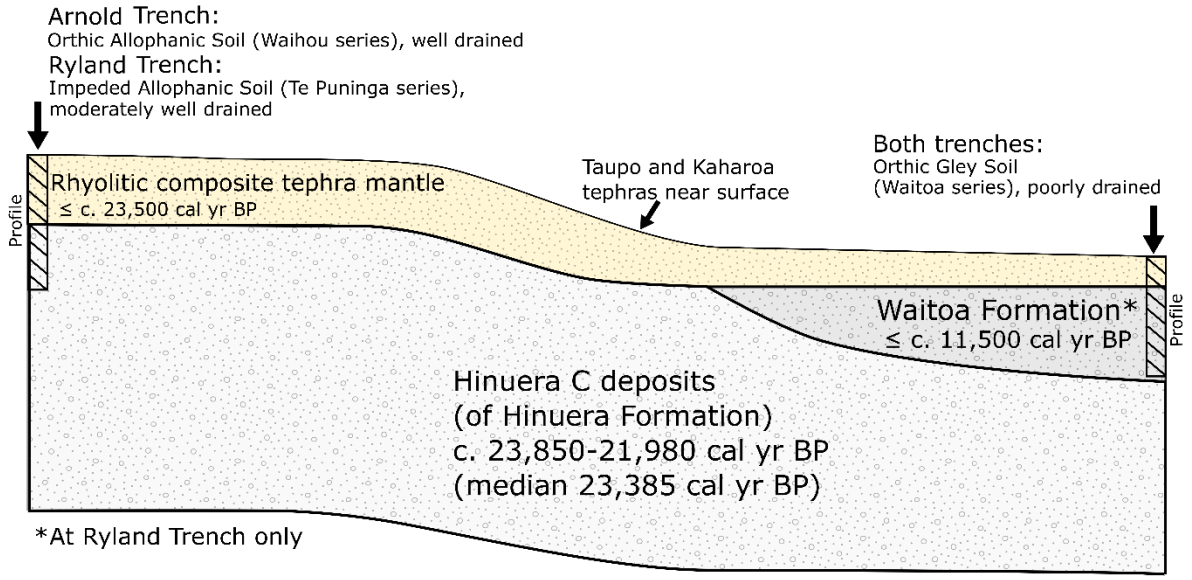

Figure 3.5: Simplified stratigraphy of deposits exposed in the Ryland and Arnold trenches. Ages on Hinuera C deposits of Manville and Wilson (2004) are from analyses of the dates reported above for Arnold Trench by Villamor et al. (2023). I adopt an age of c. 24,000 cal yr BP for the abandonment of the Hinuera Surface.

3.4.1 The Hinuera and Waitoa formations

The bulk of the deposits forming the modern plains in both the southern Hauraki Plains and the Hamilton Basin is known as Hinuera C, the top of which is designated Hinuera-C surface (Manville and Wilson, 2004). A wedge of marine sediments covers the surface of the northern part of the Hauraki Plains. These were deposited in the high stand of the Holocene transgression around 8,000 cal yr BP (Newnham et al., 1995; Clement et al., 2016; Hopkins et al., 2021a). These marine sediments were not observed in the trenches, and the ancestral shoreline was

likely to have been c. 10–15 km north of the Arnold Trench (Newnham et al., 1995; Lowe and Green, 2023).

As the Hinuera Formation is the product of deposition from a braided river system, with sandy to gravely textured channel deposits and silty overbank deposits, the deposits exposed in the trench could be expected to vary. Hume et al. (1975) characterised the deposits of the Hinuera Formation into 7 lithofacies (A to E) (Table 1). Without a detailed study on the sedimentary structures (which is the main way of distinguishing the lithofacies), at least four of the lithofacies (A1 or A2, B, D and E) were represented in the Ryland and Arnold trenches. Either A1 or A2 was represented in both Ryland and Arnold trenches. These lithofacies are quartzofeldspathic cross-bedded, gravelly sand with fragments of rhyolitic rock and pumice. Lithofacies B (sand) was also present in both trenches, with quartz, feldspar and pumice. Both overbank lithofacies (D and E) were present in the trenches. Lithofacies D was present extensively in the Ryland Trench and in the footwall of the Arnold Trench, as massive, silty deposits with quartz and plagioclase. Lithofacies E is characterised by carbonaceous material (sampled for ^{14}C dating as noted above) with silty glass shards/pumice.

In the Ryland Trench, as a result of the ^{14}C dating (Chapter 3.3.2), it was revealed that 1.5 m of alluvium had been deposited after the Waikato River had abandoned the Hauraki Plains. This alluvium is referred to as post-Hinuera Formation because Manville and Wilson, (2004) described the last deposition of Hinuera Formation-like sediments in the Hauraki Basin as unit Hinuera D, being deposited between the 17.6 cal yr BP Rerewhakaaitu Tephra (Newnham et al., 2003; Lowe et al., 2013) and 14 cal yr BP in entrenched degradational river terraces. Rather than the source of the sediments coming from the Waikato River, which had now avulsed into the Hamilton Basin and subsequently entrenched, these sediments are from the rivers of the Hauraki Plains (Waihou, Waitoa and Piako rivers) and likely include reworked (cannibalised) deposits of the Hinuera Formation (Manville and Wilson, 2004).

Based on the ages of these sediments, younger than c.11 ka, and the characteristics, fine to medium sandy alluvium, these belong to the Waitoa Formation (defined by Houghton and Cuthbertson, 1989; applied by Brathwaite and Christie, 1996; Hughes et al., 2022). One possible source of this alluvium is from a past channel of the nearby (now entrenched) Piako River.

Table 3.1: Sedimentology of the lithofacies of the Hinuera Formation (from Hume et al., 1975)

Lithofacies	**Occurrence**	**Dominant composition**	**Dominant texture**	**Sedimentary structures**	**Flow regime**	**Bed forms**	**Depositional environment**	**Stratigraphic position**
A1	Extremely common	Quartz-feldspar-volcanic rock-fragments-pumice	Gravelly sand	Rho cross-stratification	Upper part of lower to lower part of upper	Dunes on longitudinal bars or longitudinal bar migration		
A2	Rare		Gravelly sand	Epsilon cross-stratification	Upper or lower			
B	Fairly common	Quartz-feldspar-pumice	Sand	Nu cross-stratification	Lower part of lower	Ripples on transverse bars	Active braided channel	Channel
C1	Uncommon	Quartz-feldspar-volcanic rock-fragments	Sandy gravel	Type 1 horizontal stratification or massive	Upper	Plane-bed on longitudinal bars		
C2	Rare	Quartz-feldspar-pumice	Gravelly sand	Type 2a horizontal stratification or massive	Transitional			
D	Moderately common	Glass shards-pumice	Silt	Type 2b horizontal stratification or massive	Suspension particles	-	Abandoned braided channel	Overbank
E	Uncommon	Carbonaceous material-glass shards-pumice	Silt	Type 2b horizontal stratification or massive	In situ and suspension particles	-	Floodbasin	

3.4.2 Tephra cover beds and soil development

Since the end of deposition of alluvium c. 24,000 cal yr BP, a cover bed of numerous thin mainly rhyolitic tephra layers has been deposited on the Hinuera Surface. The source of these tephras were volcanoes of the Taupo Volcanic Zone (mainly Okataina and Taupo Volcanic Centres, likely with minor amounts from Tongariro Volcanic Centre), Taranaki Maunga, and Tuhua Volcanic Centre (Mayor Island). The tephras were deposited incrementally, millimetre by millimetre, by fallout (e.g., Wilson, 1980; Lowe, 1988). As the deposition was incremental, the tephra deposits were subject to pedological modification (soil horizon development) at the same time as accumulation, a process called developmental upbuilding pedogenesis (e.g., see Hewitt et al., 2021; Hopkins et al., 2021a).

The tephra thickness in total amounted to ~30 cm in Ryland Trench and ~65 cm in Arnold Trench on the elevated profiles of the scarp (footwall), and ~37 cm on the hanging wall of the Ryland Trench and ~27 cm on the Arnold Trench. In soil notation, the tephra deposits of the footwall sites represented Ap and Bw horizons (Clayden and Hewitt, 1989). These horizons returned a weak positive NaF test, indicting the presence of allophane, a clay mineral that is the product of the weathering of volcanic glass under good drainage (Churchman and Lowe, 2012). Samples of the base of the composite tephra accumulation were taken in the Arnold Trench for cyptotephra analysis (Section 3.4.3). The tephra (Ap horizon) in the hanging wall did not return a positive NaF test.

Due to the earthquake-causing movement altering the elevation of the landscape, different soil profiles have formed on the footwall and hanging wall on both trench locations. The footwall sits higher in the landscape, and the resulting soil is formed in a thicker composite tephra deposit than that of the hanging wall. Thus, the soils are formed effectively on different parent materials: that on the lower land surfaces, is formed on relatively thin tephra on (poorly drained) alluvium, and that on the higher land surfaces, is formed on relatively thick tephra overlying (well drained) alluvium. The change in elevation causes the water table to sit relatively higher in the soil profile on the hanging wall of the fault. For the Arnold Trench, the soils on the lower landscape position on thin tephra over alluvium, with poor drainage, are Orthic Gley Soils (Hewitt 2010), representative of the Waitoa (soil) series as defined by Wilson (1980). The soils on the higher landscape position on thick tephras over alluvium, with good drainage, are Orthic Allophanic Soils (Hewitt 2010), representative of the Waihou series (Wilson, 1980). In the Ryland Trench, the upper land surface has a total tephra cover of 30 cm and evidence

of redox reactions (MnO_2 concretions and mottling) in the subsoil and so the soil, moderately well drained, is an Impeded Allophanic Soil (Hewitt 2010), hence correlates with the Te Puninga series (Wilson, 1980). The complex of Waitoa-Te Puninga-Waihou series soils normally exists in the Hauraki Basin on ridges and swales of abandoned paleochannels that represent a range of well drained to poorly drained positions (Wilson, 1980).

3.4.3 Glass shard chemistry of tephras exposed in the trenches

The major element compositions were expressed as oxides and compared with published compositions of glass shards from possible correlative tephras. Samples R1–1 and R1–2 from the Ryland Trench were identified as Taupo and Kaharoa tephras, respectively, in the field from stratigraphic positions and field properties (Chapter 1.3). Samples T2a and T2b (Appendix 6) were taken at the same depth (60 cm) at the base of the tephra cover beds (i.e. at the top of the now-buried Hinuera Surface) at the uppermost wall of the Arnold Trench (Appendix 1.3). The major element analyses of SiO_2 and the sum of the alkali elements, Na_2O and K_2O, were superimposed onto a graph with the equivalent compositions of glass representing tephras derived from five active volcanic centres (Hopkins et al., 2021a) (Figure 3.6). All the datapoints sat within the expected values for glass from tephras derived from the centres in the central Taupo Volcanic Zone, as rhyolite, except for two datapoints from the basal tephra (T2a) with have a lower SiO_2 value and which are classed as dacite. These dacitic shards are not unexpected, as the basal tephra is an homogenised-looking composite of numerous deposits (not a distinct layer) and it is possible that some dacitic shards from Tongariro Volcanic Centre were deposited.

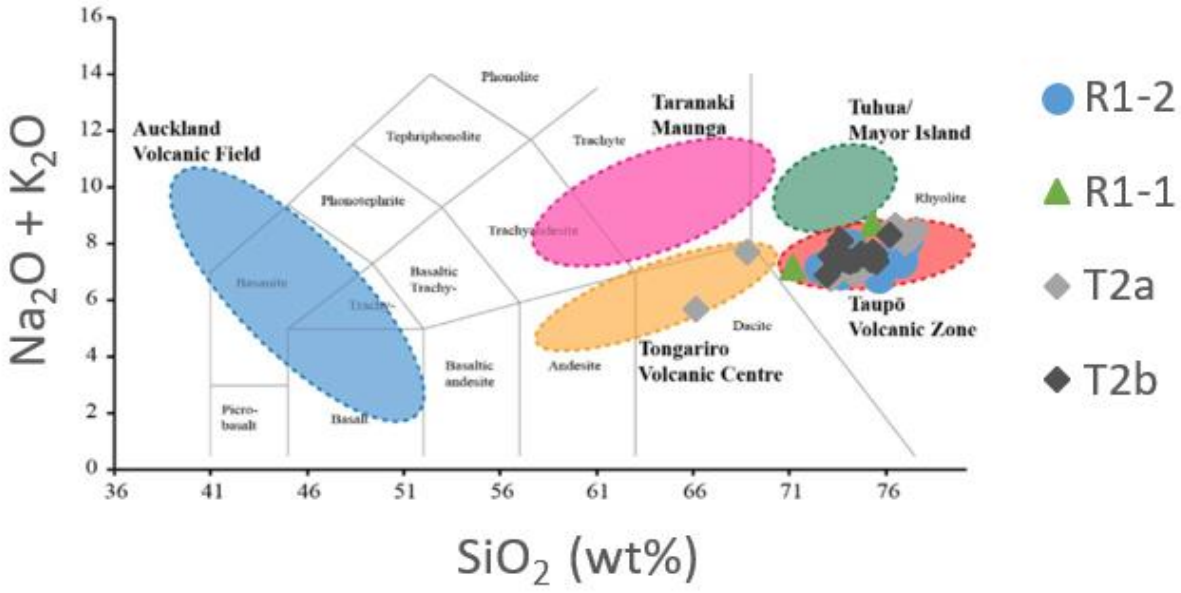

Figure 3.6: Biplot of SiO_2 and total alkali ($Na_2O + K_2O$) contents in glass (normalised) of four samples (R1–1 and R1–2; T2–a and T2–b) with classification of igneous rocks (based on Le Maitre et al., 2002) and ranges of glass compositional data (normalised) for five volcanic centres (from Hopkins et al., 2021a).

The CaO and K_2O contents of glass from both sets of samples were plotted and compared with those for glass from Taupo and Kaharoa tephras that were sampled mostly from the central Waikato region (Figure 3.7). Although the Taupo Tephra glass analyses (sample R1–1, green triangles) closely match those for the published data (within error), thus confirming the correlation with Taupo Tephra, the Kaharoa glass analyses (sample R1–2, brown dots) are somewhat scattered. Some analyses match those for the Kaharoa reference glasses presented here but others show somewhat low K_2O and somewhat high CaO contents. These analyses may reflect natural variability because data for Kaharoa glass in Hopkins et al. (2021b) show moderate to large standard deviations for these elements: K_2O content is 3.99 ± 0.39 wt % and CaO content is 0.62 ± 0.18 wt %. Or they may suggest there is a small 'drift' attributable to some other factor. However, other oxides generally match those for Kaharoa and the definitive field properties and biotite-dominated mineralogy (data not shown), and stratigraphic position, confirming the sample as Kaharoa Tephra.

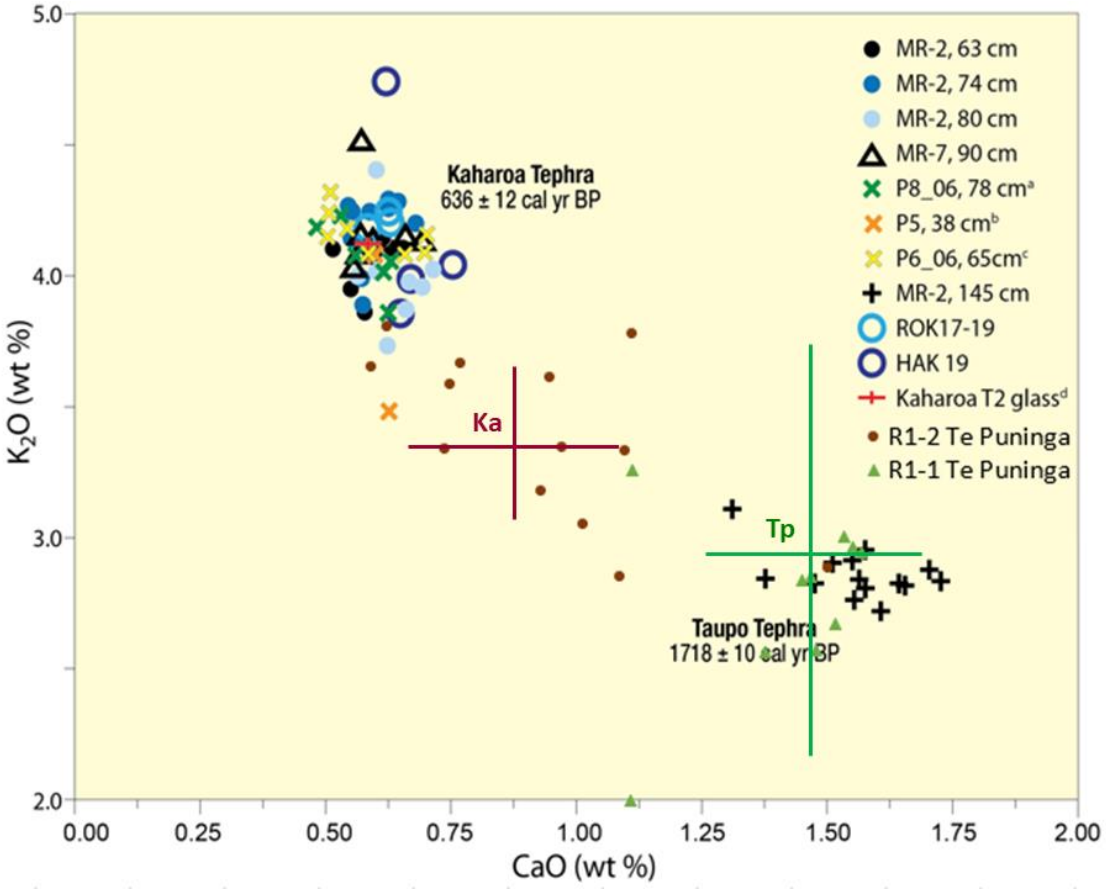

Figure 3.7: Biplot of CaO and K2O contents in glass shards (normalised) from the two Ryland Trench samples: brown dots = R1-1 (Kaharoa tephra, Ka); green triangles = R1-2 (Taupo tephra, Tp). These analyses are superimposed on reference analyses of glass (normalised) for Kaharoa and Taupo tephras (derived from Gehrels, 2009, and from D.J. Lowe, unpublished data, from lakes Rotokauri and Hakanoa; Kaharoa T2 glass analyses after Lowe et al., 2008). As well as the individual shard analyses, mean analyses of Ka (n = 13) and Tp (n = 10) for our Ryland trench samples are shown ± 1 standard deviation.

To try to identify the basal (oldest) tephra in the basal composite cover beds, and thus the minimum age for the immediately underlying Hinuera Surface, analyses of glass from composite samples T2a and T2b were compared with published analyses of glass from Okareka (c. 23.5 cal ka BP) and Rerewhakaaitu (c. 17.6 cal ka BP) tephras. (Note that I attempted to extract biotite from these samples as well as glass because biotite from these two tephras is compositionally different, enabling the tephras to be distinguished, as shown by Shane et al. (2003). However, I could not find sufficient biotite in my samples to undertake EPMA analyses.)

A number of major element glass analyses from the basal tephra samples (combined as a single sample as they are from stratigraphically identical positions at the base of the tephra cover bed) were plotted against published glass analyses for the Okareka Tephra

(based on Smith et al., 2005; Hopkins et al., 2021b) and for the Rerewhakaaitu Tephra (based on Newnham et al., 2003; Hopkins et al., 2021b) (Figure 3.8). The graphs show a distribution of values, which is expected as the sample was a bulk of composite ('homogenised') tephra deposits (rather than a distinct tephra layer). The presence of some analytical data points within the standard deviation of the published glass analyses for Okareka Tephra (Figure 3.8 A and B) suggests that it is possible that Okareka Tephra is represented at the base of the tephra cover bed column. However, the analyses for glass from Rerewhakaaitu Tephra (green triangles) are very similar to those of Okareka Tephra for the elements plotted in Figure 8. Consequently, that some shards may represent Rerewhakaaitu Tephra instead (or in addition to) Okareka Tephra cannot be ruled out.

However, in another plot of glass analyses of K_2O vs CaO (Figure 3.9), the analyses for samples T2a and T2b combined (blue dots) seem to fall into two populations that, with a small offset, seem to closely mirror the bimodal distribution of glass analyses for Okareka Tephra as reported by Lowe et al. (2008 and others). If the glass analyses in Figure 3.9 therefore represent Okareka Tephra, the age on the Hinuera C surface would be c. 23.5 ka cal yr BP (the age on Okareka Tephra: Peti et al., 2021) or older, consistent with the age of c. 24.0 cal yr BP estimated elsewhere in this chapter for the surface.

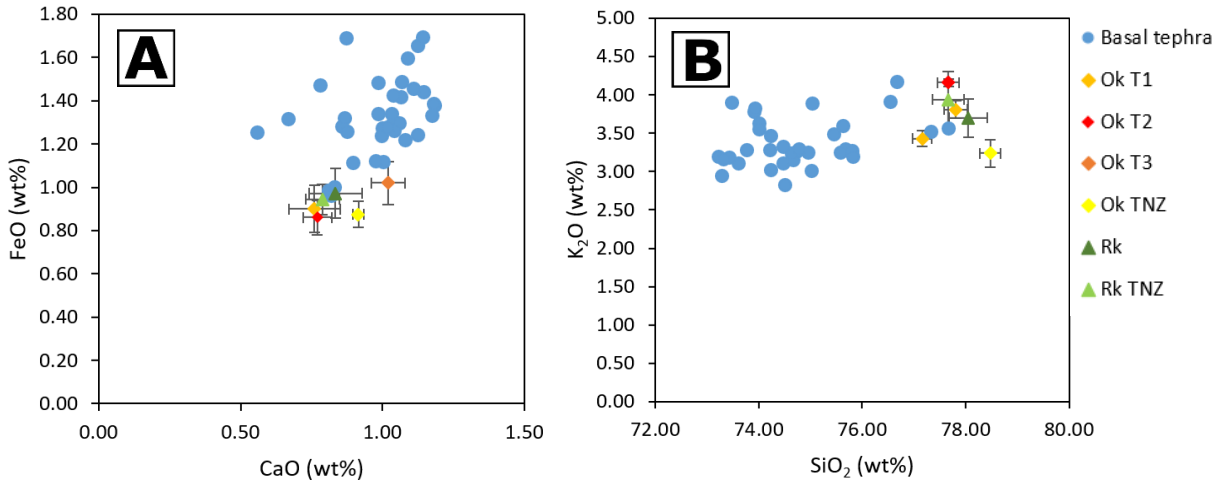

Figure 3.8: Biplots of glass analyses (normalised) from the basal tephra samples shown as large blue dots (T2a and T2b combined) for (A) FeO vs CaO and (B) K2O vs SiO2. Total iron is expressed as FeO. Comparative glass analyses (normalised) are shown as mean ± standard deviation plots for Okareka Tephra as follows: Ok T1–3 (Smith et al., 2005); Ok TNZ (Hopkins et al., 2021b). Glass analyses for Rerewhakaaitu Tephra as follows: Rk, Newnham et al. (2003); Rk TNZ, Hopkins et al. (2021b).

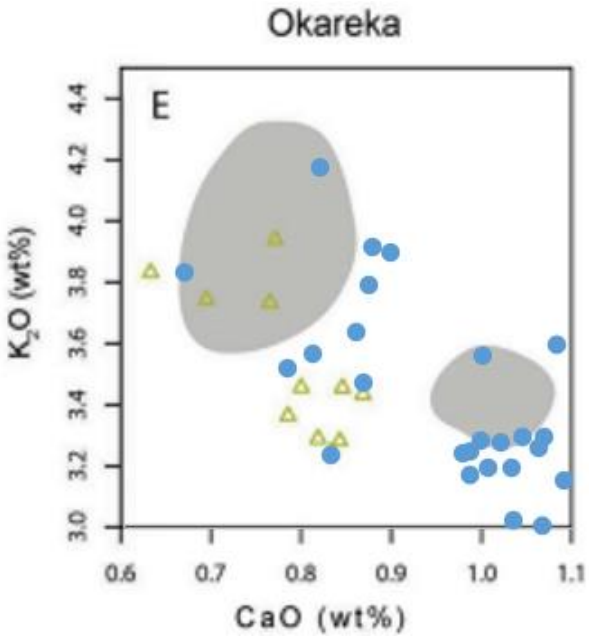

Figure 3.9: Biplot of glass analyses (normalised) for K2O and CaO from the basal tephra samples shown as large blue dots (T2a and T2b combined). The yellow triangles represent analyses (normalised) of glass shards from Okareka Tephra identified in Meade trench in Ngakuru Graben near Rotorua by Loame et al. (2019); the grey polygons show the range of analyses (normalised) for Okareka Tephra as bimodal plots (different magma types) as reported by Lowe et al. (2008) after Smith et al. (2005) (from Loame et al., 2019).

3.4.4 Tephra cover beds and relation to faulting

Soils representative of the Waitoa series are analogous to the Te Kowahi series in the Hamilton Basin. Both are Gley Soils formed on the Hinuera Formation, in swales of the landscape. Tephra is not readily observed in the soil profile of either series, when it should be expected, since tephras have blanketed the landscape (Hewitt et al., 2021; Hopkins et al., 2021a). The reasons for this "absence" are uncertain. However, recently a pit exposing a Te Kowhai soil in the Hamilton Basin was found to have an inconspicuous but definite tephra cover bed (Lowe, 2023), and so the tephra deposits may be unrecognisable because of their transformation by strong and prolonged reducing and redox conditions. Such conditions also favour the formation of halloysitic clays rather than allophanic clays (Parfitt et al., 1984; Lowe, 1986; Singleton et al., 1989; Churchman and Lowe, 2012), and the soil morphology is therefore not easily recognisable as being developed from tephra deposits. An analogous situation has been described by Lowe (2019a) for the halloysite-rich Kainui soils developed from tephras (with impeded drainage) mantling hills in the northern Hamilton Basin (classed as Ultic Soils) that contrast markedly with the allophane-rich Otorohanga soils formed in the same tephra deposits (but well drained) on hills in the southern Hamilton Basin (classed as Allophanic Soils). Lowe (2019b)

referred to Kainui soil as ‘the leopard that changed its spots’, meaning that two different soil series can be formed from the same tephra materials with contrasting morphologies and classifications.

The land surface of both trenches would have originally been at the same height, so tephra would have been deposited before the surface level changed in an earthquake. All the exposed sediments in the hanging wall of the Ryland Trench were younger than c. 11,000 cal yr BP, after faulting occurred, so any tephra (that had not been eroded in the deposition of the of the Waitoa Formation sediments) would still be buried. The Arnold Trench, however, has fine sand unit (Unit A) that could actually represent the tephra cover beds that were deposited before faulting. This unit sits lower in the landscape, but has the same thickness as the tephra cover beds on the upper surface. Reduction from the relatively higher water table could have caused lower chroma colours and concretions to form, and halloysite to form rather than allophane, as noted above (see Churchman and Lowe, 2012; Lowe, 2019a). Further explanation of the mechanisms of the “missing” tephra and study of the differences of thickness of tephra beds could possibly be used to estimate the timing of the earthquakes.

3.5 Summary

Two paleoseismic trenches were excavated across the scarps of two different traces of the Te Puninga Fault. These trenches exposed alluvial sediments, cover beds of tephras, and organic material. The stratigraphy was established in the field, while samples of tephra and organic material were taken for dating by laboratory techniques including ^{14}C dating, and EPMA.

Both trenches (Ryland and Arnold) had similar stratigraphies, with the oldest sediments exposed being the Late Pleistocene Hinuera Formation. The Hinuera Formation was exhibited in the trenches as sandy to gravelly, cross-bedded quartzofeldspathic and pumice alluvium, with peat lenses. It was deposited in the Hauraki Basin between 25,000 cal yr BP and 24,000 cal yr BP, from when the sediments of the 25,400 cal yr BP Oruanui super-eruption were bought down the Hauraki Basin by the high-energy, braided ancestral Waikato River until the river avulsed into the Hamilton Basin approximately 24,000 cal yr BP. Radiocarbon dates of peat lenses within these sediments in the trenches are consistent with these dates.

Ryland Trench had an alluvial unit on the footwall of the trench, deposited after c. 11,000 cal yr BP, which is best correlated to the Holocene Waitoa Formation. The unit was exhibited as fine to coarse sand, and in contrast to the Hinuera Formation, did not contain any distinct cross-bedding.

The alluvium at both sites was overlaid by a cover bed of composite tephra deposits that had been deposited incrementally since the alluvial surface (Hinuera C) was abandoned c. 24,000 cal yr BP. These tephra deposits are mainly rhyolitic, largely from the distant volcanoes of Okataina and Taupo centres in the central Taupo Volcanic Zone (Lowe, 1988; see also Figure 3.6). Two of the tephra layers were visible, Taupo (1718 cal yr BP) and Kaharoa (636 cal yr BP), and were identified by field techniques, ferromagnesian mineralogy (data not shown), and (largely) confirmed by analyses of glass by EPMA. EPMA analyses of glass shards taken from samples at the base of the tephra cover bed on the footwall of the Arnold Trench matched in part those for Okareka Tephra and Rerewhakaaitu Tephra (which are similar to each other) (Figure 3.8), but the bimodality of the analyses from the basal tephra deposits with respect to their K_2O vs CaO content was mirrored (with slight offset for some data) by glass analyses for these oxides from the literature for Okareka Tephra (Figure 3.9). If the base of the tephra cover bed is indeed dominated by glass of Okareka Tephra, the implication is that the Hinuera C surface is aged c. 23.5 ka cal ka BP or older, which is consistent with other age estimates

in this chapter including the age of c. 24.0 cal ka BP I have adopted as the most likely age for the surface.

The thickness of the tephra cover bed was greater on the upper land surface (footwall) than on the lower land surface (hanging wall), mirroring the relationship of tephra on alluvium on ridges and swales, respectively, on the Hinuera Formation. The tephras have undergone soil forming processes during their deposition (via developmental upbuilding pedogenesis) and, as a result, different soils have eventuated. Due to the relatively higher water table, the soil on the lower land surface is a Gley Soil representative of the Waitoa series. On the higher land surface (footwall), a thicker tephra cover bed and free to moderate drainage in the underlying alluvium resulted in an Allophanic Soil (Arnold trench) and an Impeded Allophanic Soil (Ryland trench), respectively. In the Arnold Trench, the tephra was sufficiently thick (65 cm) and the soil was allophanic and hence it was classed as representative of the Waihou series, while in the Ryland Trench, the tephra was thinner (30 cm) and the lower profile showed redox features because of slower drainage, and so would be classed as a representative of the Te Puninga series. It is possible that some (<40 cm) tephra is present in the hanging wall of the Arnold Trench, deposited while in an elevated position in the landscape before faulting.

Chapter 4

Geomorphology of a scarp of the Te Puninga Fault at Quine Road, and interpretation of past seismicity

4.1 Introduction

In this chapter I present a localised study on a particular fault scarp in the northwest part of the Te Puninga fault zone. This field site is located near Quine Road, off the Morrinsville-Tahuna Road (Figure 4.1). A geomorphological analysis of the scarp and surroundings was undertaken by mapping in the field and using GIS. The mapping was undertaken to focus on the relationship between the scarp and the terraces formed by some stream systems with the aim of assessing whether the fault scarps represent several earthquakes and timing can be assess through terrace ages (Persaud et al., 2016). Radiocarbon (^{14}C) samples were also collected to provide an age of a terrace.

4.1.1 Localised geological setting

A fault scarp at Quine Road was chosen because the fault crossed several streams, leading to the possibility of different terraces being offset by the fault. The site sits on two adjacent farms near the intersection of the Morrinsville-Tahuna Road and Quine Rd (37°33'47.11"S; 175°30'7.95"E), towards the western margin of the Hauraki Plains, which is marked by a range of hills >40 m in elevation approximately 1 km west of the site. The landscape pattern is low rolling hills, around 20 m in elevation, situated between steeper hills of the Hangawera Hills and flat plains near the Piako River. The two farms are relatively flat compared to the surrounding rolling hills, likely due to erosion from the numerous stream valleys that run in a west-east direction.

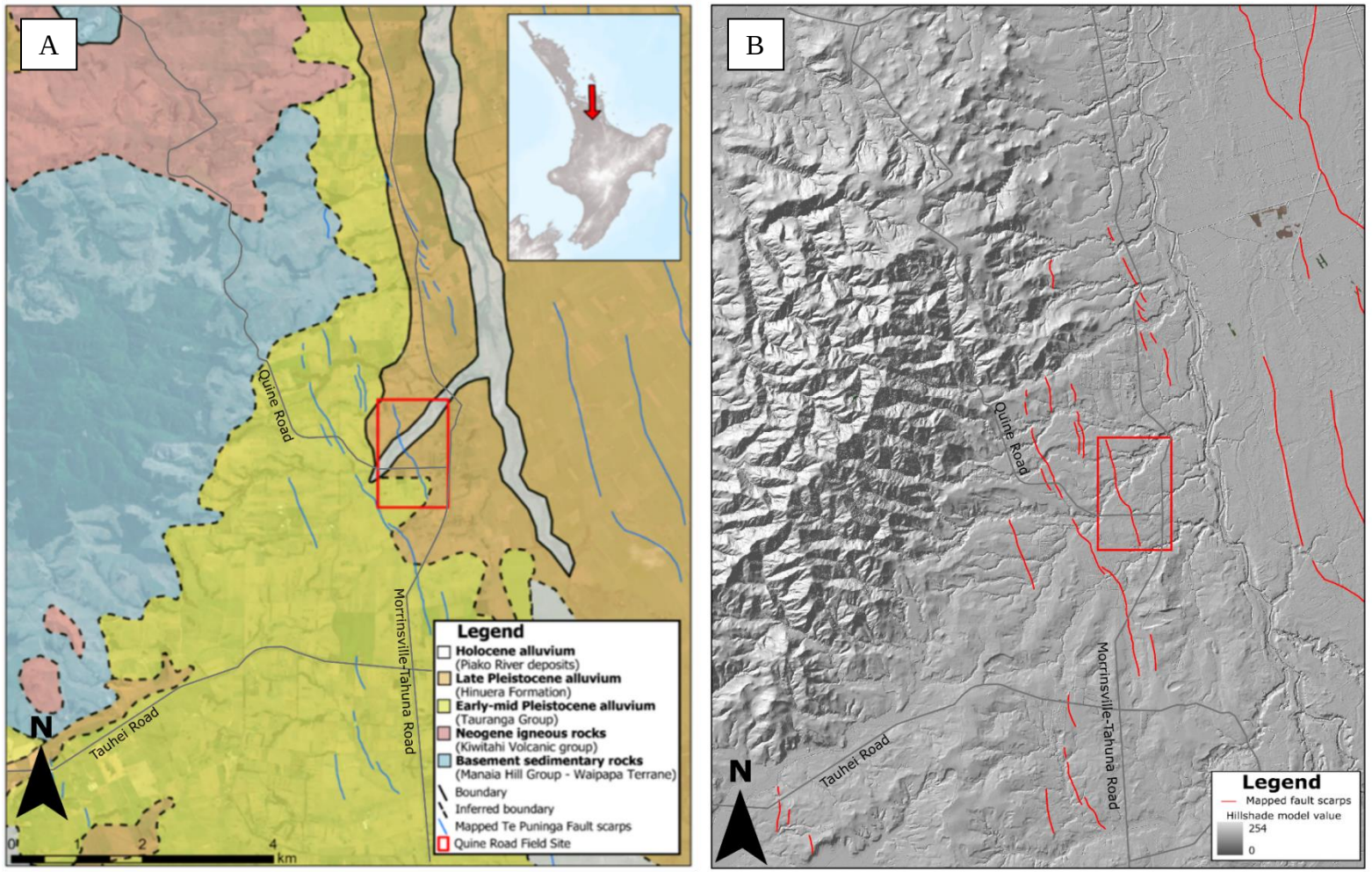

Figure 4.1: A: Geological map of the Quine Road area from QMap (Edbrooke, 2001; Leonard et al., 2010). Te Puninga Fault scarps (Villamor, 2022) are overlain (blue lines) and the Quine Road field site is highlighted. B: Hillshade model of the same area, to the same scale, showing the geomorphology of the field site.

4.2 Methodology

4.2.1 LiDAR

Digital elevation models (DEMs) used here are the product of LiDAR surveys and are the basis of geographic information system (GIS) analyses. These provide a "bare earth" view of the Earth's surface without vegetation or human-made infrastructure obscuring the view. DEMs colour the terrain based on the elevation. From the DEM, a hillshade model can be produced. Hillshade models shade regions of slope, rather than elevation. DEMs produced by GNS Science from LiDAR surveys by Waikato Regional Council (WRC) in 2007/2008 were used in this chapter. The vertical error of these datasets was 0.15 m (WRC, 2008) and this value will be used as the uncertainty for vertical measurements in this chapter.

The 2007/2008 WRC data were used to produce a map of the traces of the Te Puninga (Villamor, 2022). Further, using GIS software, ArcGIS Pro and ArcMap, maps were produced of the Te Puninga Fault and then analysed.

4.2.2 Geomorphological analysis

Locations where the fault scarps crossed streams and terraces where extensively surveyed on LiDAR. The aim of this was to find a site where the footwall of the fault sits upstream from the hanging wall, creating a difference in relative terrace heights on each side of the fault. After visiting areas of interest in person, and gaining for permission from landowners, a section of fault scarp near Quine Rd was chosen.

4.2.3 Field methods

Auguring was undertaken across the field site to ground truth the geological deposits and soils. The (pedological) soils on the different landscape positions differed, reflecting mainly the age of the parent materials. There was also a focus to try and find material that could be used to date the terraces, such as organic material, or tephra layers. When suitable organic material was found by auger, a soil pit was dug using a spade. This allowed for sampling of the materials for ^{14}C dating with less chance of contamination and a more accurate depth than from an auger.

Field mapping also complemented the LiDAR desktop study. Where unusual patterns were noticed in the LiDAR data, ground truthing this area proved useful to identify where

artificial structures crossed ArcGIS elevation profiles, especially small farm fences and drains that may be difficult to identify on satellite imagery.

4.3 Results

4.3.1 Fault scarp mapping

The Quine Road scarp was originally mapped by Villamor (2022). Based on my geomorphological mapping, the mapped fault traces were revised (Figure 4.2). The main scarp was straightened around the streams wheras two other branches of the fault were mapped: one short section just south of the Awaroa Stream that partitions the offset over the two strands to the point where it appears negligibly visible to the eye in the field; and one ~160 m further south, which appears to affect the drainage of a tributary to the Mangakahika Stream. These two additional strands were based on evidence from elevation profiles constructed perpendicular to the fault (Chapter 4.3.3)

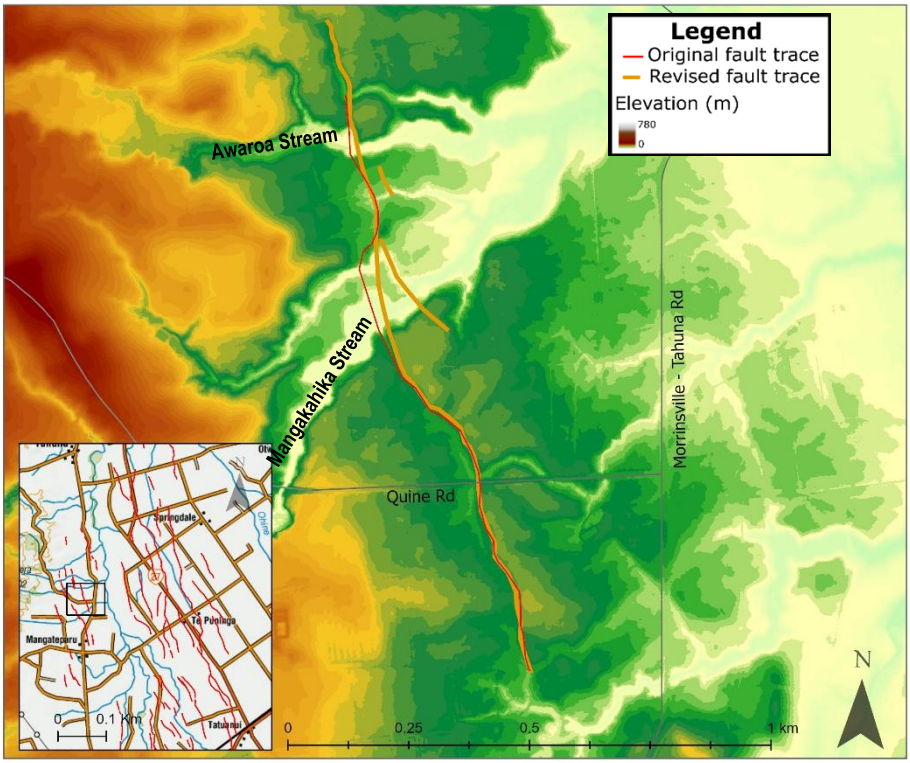

Figure 4.2: DEM of the Quine Road area, showing the original and revised fault trace.

4.3.2 Terrace mapping

Streams in the field site flow in an approximate southwest to northeast direction from the Mangawera Hill to the Piako River; these have incised gullies in the landscape. Elevation profiles were produced on ArcMap parallel to the fault scarp on the footwall and hangwall sides. These profiles show a general trend of erosion as the streams incised, with the formation

of terraces. These terraces were then defined based on elevation and correlated across the fault scarp, with care taken to account for the slope of the surface. This was due to the land surface being on the Hinuera Formation, a low-angle alluvial fan that slopes at a mean gradient of 1.8 m/km towards the north (Manville and Wilson, 2004). The correlated terraces were then numbered from youngest (1) to oldest (8) (Figure 4.3).

The first terrace (1) was the current floodplain of the two streams through the field site. This is the youngest surface of the site and is comprised of alluvium from the stream. At the field site, this sits at 11 m above sea level (asl). Terrace 2 is a low-angle surface around 15 m asl that forms a small bluff between two streams. Terrace 3 sits between 17 m and 18 m asl and is roughly 200 m across. With the exception of a scarp, 40 m across, situated to the north of the streams belonging to Terrace 7, Terraces 4, 5, 6, 7, and 8, are all present south of the two streams. Terraces 4–7 are formed on Hinuera Formation, based on the geomorphology and the characteristics of the lithological units observed in augers which were those expected in the Hinuera Formation, based on Hume et al. (1975) and the deposits seen in the paleoseismic trenches (Chapter 3): alluvium with the overlying tephra cover beds. Terrace heights at the site on the footwall were 19.8–20.0 m, 20.0–20.2 m, and 20.3–20.4 m asl. The two highest points of the landscape were assigned to the oldest terrace (Terrace 8; with 20.9–21 m asl terrace height at the site), and the assumption was made that these were remnants of the original Hinuera Surface as they are the highest, and subsequently likely least eroded points in the landscape, and have a measured slope of <1° (0.2 m per 550 m) (Manville and Wilson, 2004). This dip was then used subsequently for correlating the points of Terraces 4–7.

On the hanging wall, there are three unlabelled terraces at the northernmost portion of the fault. These do not correspond with terraces on the footwall. Therefore, they have been excluded from this study because they were not formed in the Hinuera Formation. However, the fault trace intersects (older) Tauranga Group alluvium suggesting that the age of these surfaces is much older (Early to Mid-Pleistocene) (Leonard et al., 2020), and hence they may have been subject to additional erosion compared with the younger Late Pleistocene Hinuera Formation and a different number of earthquake displacements.

.

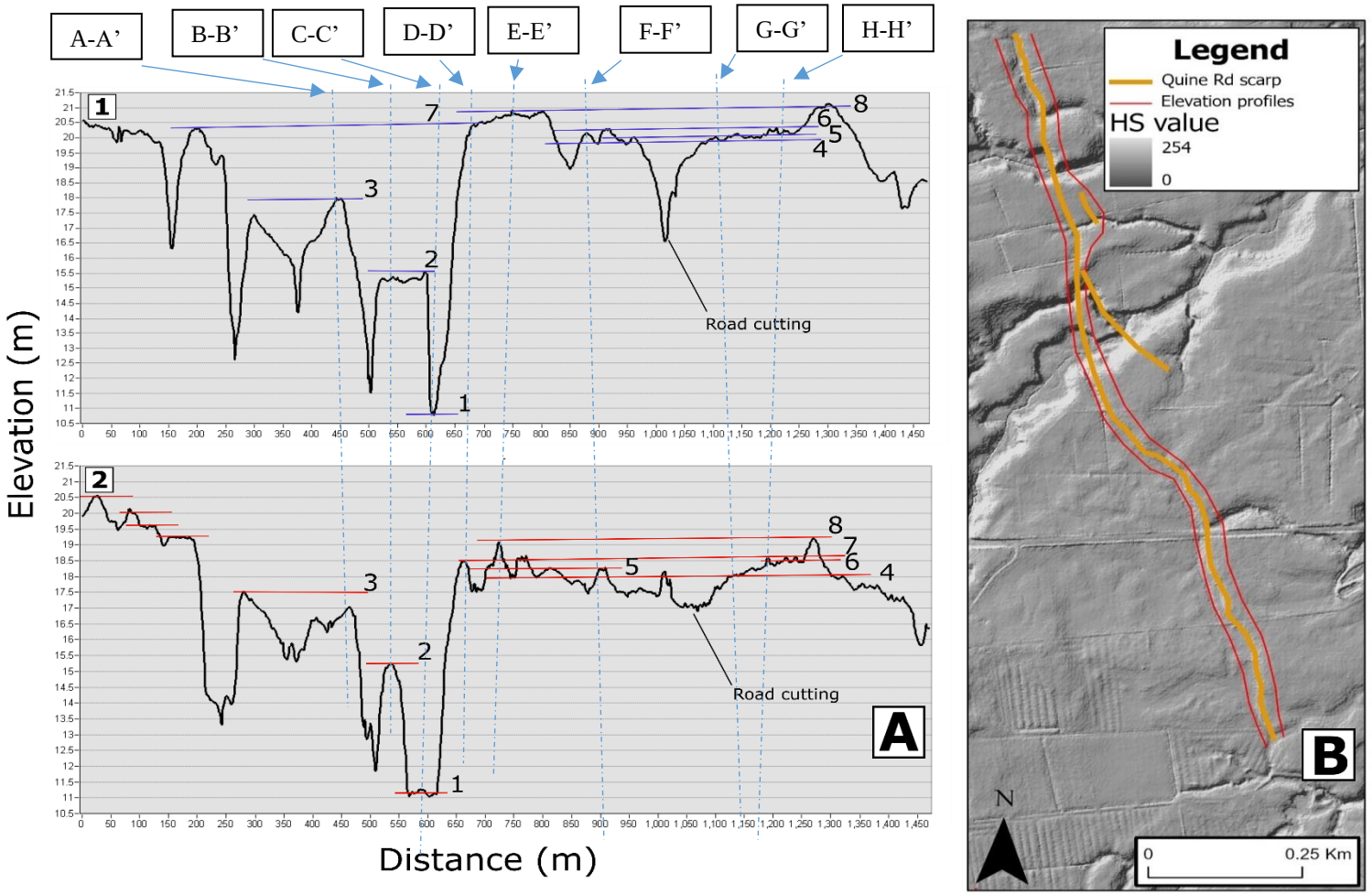

Figure 4.3: A: Elevation profiles generated on ArcMap of footwall (1) and hanging wall (2) sides of the scarp. Terraces were identified, labelled and correlated with blue lines (footwall) and red lines (hanging wall). Note the slight slope angle (<1°) towards the north, accounting for the low angle of the surface of the Hinuera Formation (unit Hinuera C) alluvial fan (Manville and Wilson, 2004). The dashed lines indicate where the profiles in Chapter 4.3.3 where drawn. B: Hillshade model of the Quine Rd scarp with the transects used to produce Figure 4.3A labelled.

4.3.3 Surface displacement of the faults

Elevation profiles that were made using ArcMap perpendicular to the fault (Figure 4.4) were used to better define the fault location and calculate displacements across the scarp (Figure 4.5). These profiles were drawn as perpendicular as possible to the scarp and correlated to terraces identified in Figure 4.3. They were drawn long enough to get a suitable average slope of the land surface of the terrace on each side of the fault but needed to avoid crossing other terraces. Then a line was drawn across the surface on each side of the fault, following the highest elevation of the surfaces (as the surface is eroded downwards). Care was taken to avoid artificial alterations to the surface, primarily farm drains and road cuttings.

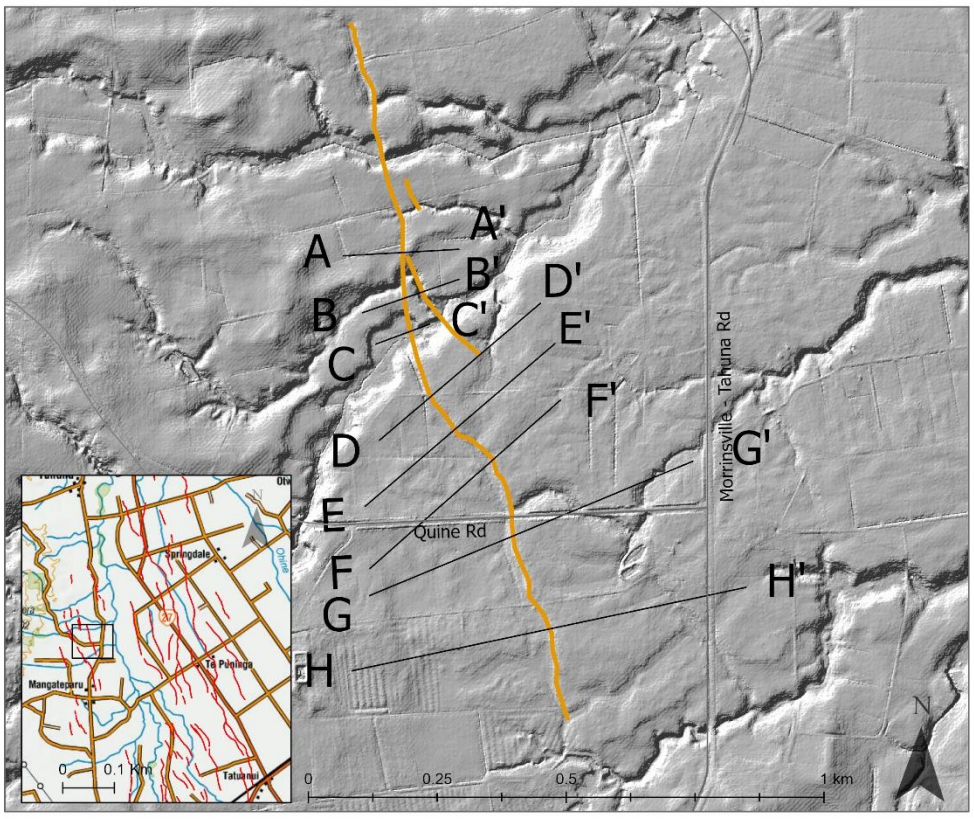

Figure 4.4: Map of the transects used to produce elevation profiles perpendicular to the scarp.

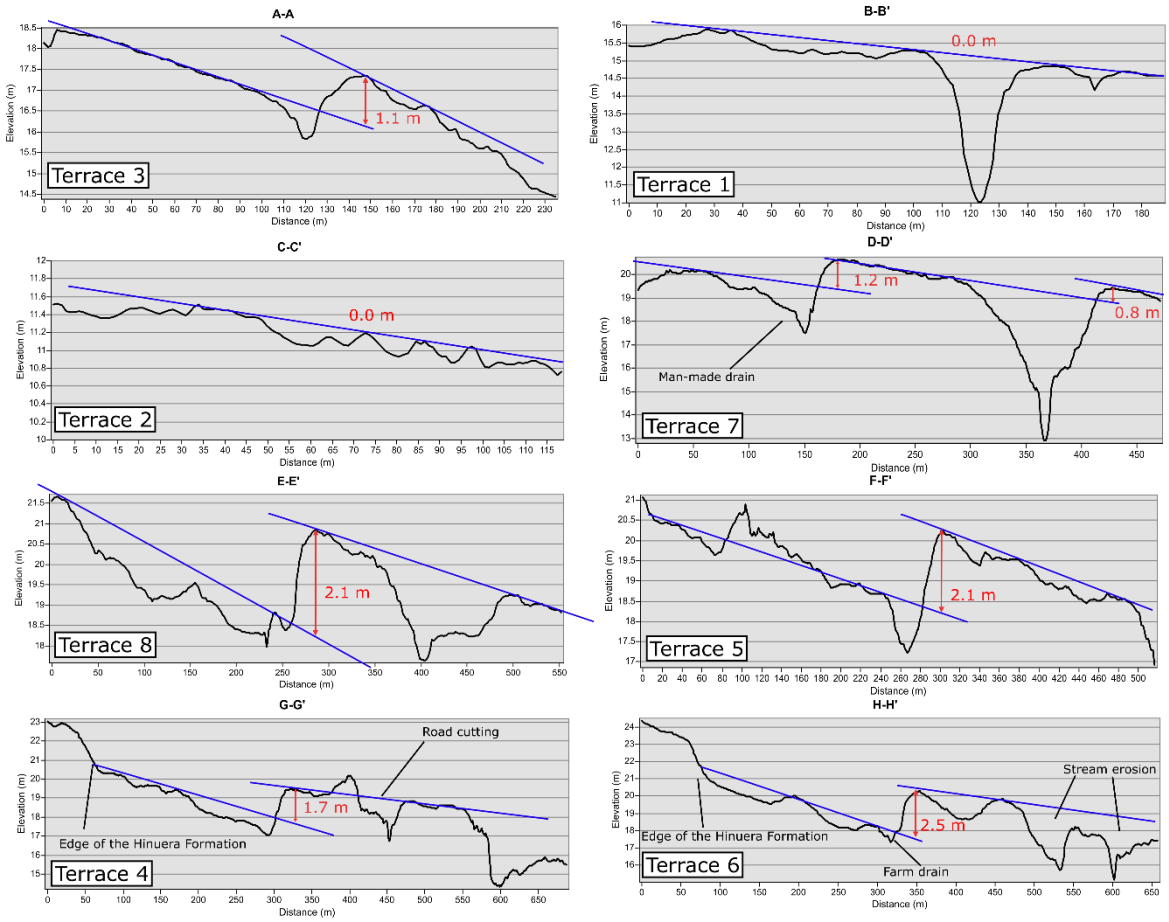

Figure 4.5: Surface elevation profiles of the transects perpendicular to the fault. The transects are those labelled in Figure 4.4.

Terraces 1 and 2 (B-B’ and C-C’) did not have any measurable displacement across the fault trace. Terrace 3 had 1.0 m vertical fault displacement (A-A’) and vertical fault displacement on Terraces 4–7 (D-D’, E-E’, F-F’, G-G’ and H-H’) ranged from 1.7 m (Terrace 4) to 2.5 m (Terrace 6). There is a wider range of values in the Terraces 4–8; this is likely due to uncertainty in drawing the lines along the surfaces as the site is eroded and modified, with visible stream erosion and human alterations evident on the surface, so the values calculated from the parallel transects will be used for this study.

The profiles of the terrace displacements on each of the profiles perpendicular to the scarp (Figure 4.5), and the offsets of the terraces from the profiles parallel to the scarp (Figure 4.3) (with and without adjusting for the slope), are displayed in Table 4.1. When calculating the displacement for the parallel profiles, the slope of the terrain towards the east was considered. The parallel profiles were drawn roughly north to south and were approximately 50 m apart. Hence, ignoring the relative movement of the fault, the eastern

profile (footwall) would be lower than the western profile (hanging wall). Since the fault dipped to the west, opposite to the slope of the surface, the fault displacement between the terraces in the parallel profiles would be undermeasured (Figure 4.6). To account for this undermeasurement, the slope was calculated from the transects perpendicular to the fault and this was added to the vertical offset calculated from the profiles. The difference in average slope of Terraces 4–8 was minimal, so the slope for all of these terraces was calculated at 1.5 m/100 m (0.86°) on the Terraces 4–8, 1/100 m (0.57°) on Terrace 3, and negligible on Terraces 1 and 2.

Table 4.1: Displacements on each terrace calculated from the parallel profiles (Figure 4.3) and the perpendicular profiles (Figure 4.5). For the offsets calculated from the parallel profiles, the slope of the land surface to the east was also taken into account.

	Calculated from Figure 4.3		**Calculated from Figure 4.5**
Terrace number	**Vertical offset before adjusting for slope (m) (± 0.15)**	**Vertical offset after adjusting for slope (m) (± 0.15)**	**Offset (m) (± 0.15)**
1	0.1	0.0	0.0
2	0.3	0.0	0.0
3	0.5	1.0	1.0
4	1.8	2.6	1.7
5	1.7	2.5	2.1
6	1.9	2.7	2.5
7	2.0	2.8	2.0*
8	1.8	2.6	2.1

* Sum of two offsets from fault branching in two

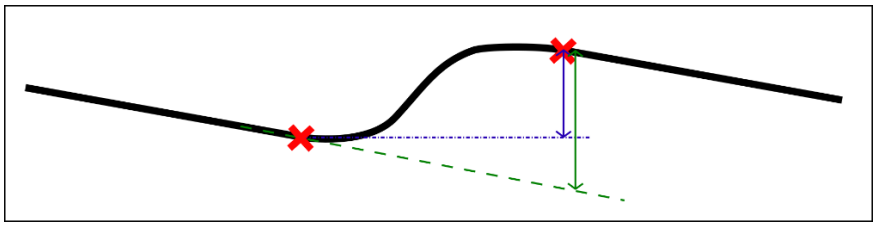

Figure 4.6: Simplified schematic diagram of the cross section of a fault scarp on a slope, showing how the vertical offset measured between two points (red crosses) from the profiles parallel to the fault (vertical offset in blue) undermeasures the true vertical offset caused by faulting (green).

4.3.4 Dating Terrace 1 using ^{14}C dating and soil properties/profiles

Samples of buried charcoal material were collected at four locations along the lowermost terrace (Terrace 1) (Figure 4.7). This terrace was not offset by the fault, indicating that there has not been an earthquake since the formation of this terrace, and this knowledge can then be used to constrain the age of the last event. The samples were collected from pits dug by spade until reaching the water table (Figure 4.8). The (pedological) soil exposed on Terrace 1 is a Gley Soil (Hewitt, 2010). Reduction and oxidation features are present, with dominant low chroma colours in the subsoil and orange mottles, suggesting a high water table much of the year. Some peat lenses were present in the profile at c. 50 cm depth. The high water table was confirmed from field observations, as some areas of Terrace 1 had surface ponding and few pits had a water table deeper than 50 cm during a site visit in late autumn.

The oldest (deepest) organic samples in these pits were sampled; these were charcoal. To maximise the chances of finding organic material, the pits were dug in depressions in the terrace, presumably in the most recent former stream channel (Figure 4.9).

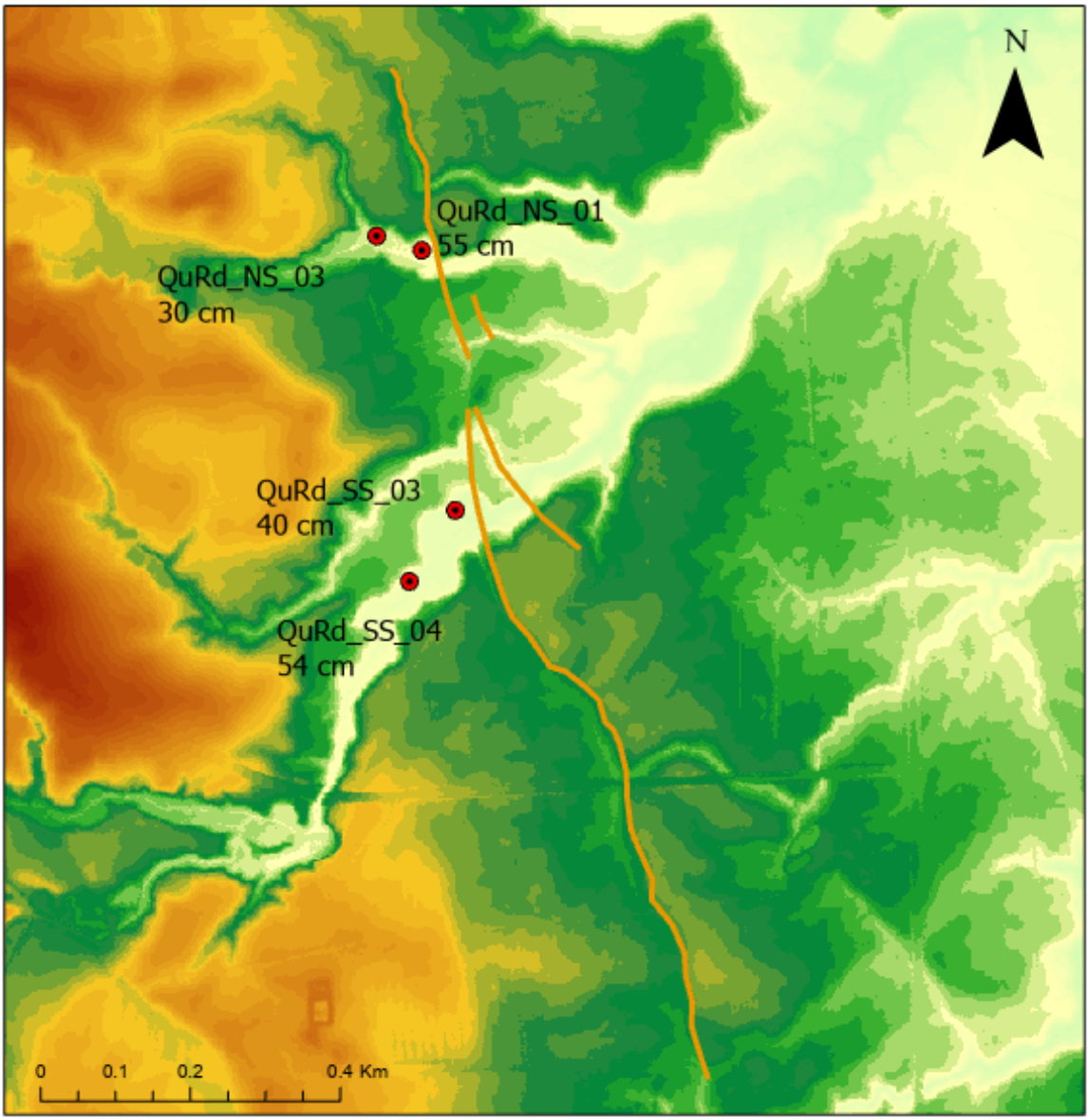

Figure 4.7: Locations of ^{14}C samples (red and black dots) with depths from which the sample was taken.

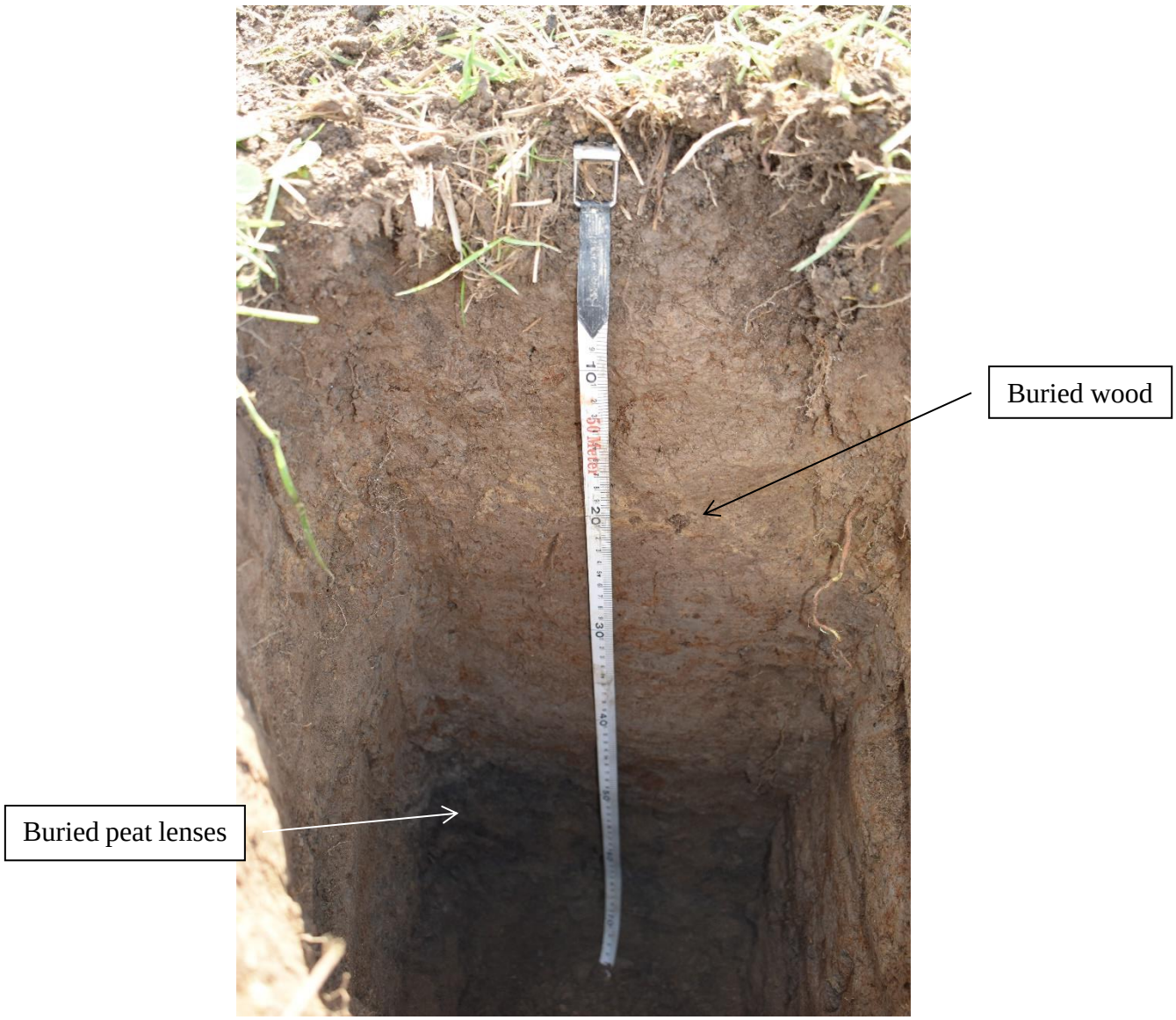

Figure 4.8: Example of a soil profile of a pit on Terrace 1. Samples of charcoal were sampled from these for ^{14}C dating to date the formation of Terrace 1. Note the pale grey low chroma colours (representing sustained reducing conditions near the land surface) and orange mottling and MnO_2 concretions indicative of redox reactions.

Figure 4.9: Awaroa Stream with the youngest terrace of the field area. The winding depression (dashed lines) in the landscape represents the most recent abandoned paleochannel. Two sampling locations are labelled.

Samples were submitted for ^{14}C dating at the Rafter Laboratory of GNS Science. The calibrated ages obtained ranged from 766 ± 18 cal yr BP (41761/2) to 170 ± 19 cal yr BP (41761/3) (Table 4.2). The oldest date, 766 ± 18 cal yr BP, equivalent to 1184 ± 18 AD, is about 100 years prior to the currently accepted date for early Polynesian arrival in New Zealand, likely around 1250 to 1275 AD in North Island (Hogg et al., 2003; Wilmshurst et al., 2008; Perry et al., 2014; Bunbury et al., 2022). The others postdate early Polynesian arrival and were likely the result of anthropogenic burning of forest in the area. The two dates of 280 ± 19 cal yr BP (41761/1) and 277 ± 19 cal yr BP (41761/4) coincide with dates obtained from sites elsewhere in the Hamilton Basin that indicate that this was a period of increased burning and gardening activities in the region (Gumbley et al., 2004; Gumbley, 2017). The charcoal and wood deposits (which I had sampled) were buried by between 30 cm to 55 cm of alluvium from the Awaroa and Mangakahika streams.

Table 4.2: Radiocarbon dates of the four samples at Quine Road.

Sample name	**Rafter lab ID**	**Calibrated age** (95% probability range) *
QuRd_NS_01	41761/1	277 ± 19 cal yr BP
QuRd_NS_03	41761/2	766 ± 18 cal yr BP
QuRd_SS_03	41761/3	170 ± 19 cal yr BP
QuRd_SS_04	41761/4	280 ± 19 cal yr BP

*Based on atmospheric curves of Hogg et al. (2020) and calibration using Oxcal v.4.4.4

Before soil pits were dug, auger holes were obtained to check if there was suitable material to date. While the soil pits were only useful for collecting samples and observation until I reached the water table (c. 50 cm depth during the field work in Autumn 2022), the augers provided more stratigraphy. Gravel-sized greywacke clasts were found at 1 m depth in the gully bottoms by auger. This is likely alluvium from the Hangawera Hills to the west of the site, deposited by a similar drainage system or paleo-channel of the current streams.

4.4 Discussion

4.4.1 Number of events on the Quine Rd scarp

When comparing the offsets of the different terraces calculated from the parallel transects, the older terraces (Terraces 4–8) have the largest vertical offsets, from 2.5 ± 0.15 m in Terrace 5 to 2.8 ± 0.15 m in Terrace 7, after adjusting for the slope of the Hinuera Surface to the east. Terrace 3 has an adjusted offset of 1.0 m, while Terrace 2 and Terrace 1 have no offset (Table 4.1). The offsets of the Assuming that each earthquake causes surface rupturing and that only one earthquake occurred between the formation of the subsequent terraces with different displacements, two earthquakes occurred on this strand of the fault in the past c. 24 ka cal yr BP (Chapter 3.3). The earliest (penultimate) rupture event must have occurred between the formation of Terraces 4 and 3, and the later event between Terraces 3 and 2. The most recent earthquake can be inferred to have caused a surface rupture of 1.0 ± 0.15 m, whereas the older earthquake produced an offset of between 1.45 m, and 1.75 m after subtracting the most recent displacement from the offsets of Terraces 4–8.

The oldest of the ^{14}C dates obtained for the youngest terrace is used for this section. The oldest terrace (on the Hinuera C Surface) was estimated at c. 24 ka cal yr BP as noted previously.

4.4.2 Incision rates of the streams and dating the earthquakes

The general mode of landscape development at Quine Rd after the abandonment of the Hinuera C surface c. 24,000 cal yr BP was erosion. As this abandonment occurred during the LGM, there is a possibility of aeolian erosion occurring. However, the patterns of stream networks seen in the DEM (Figure 4.2) indicate that the majority of erosion was likely fluvial, and eroded sediments would end up in the Piako River and subsequently in the ocean well to the north of the Firth of Thames because the coastline was c. 120 m below that of the present (see Figure 3.2C). To determine likely ages for the two events at the Quine Rd study site, estimates of the ages of the terraces were needed. Figure 4.10 plots the terrace heights of the Quine Rd scarp (Figure 4.4), against terrace age. For this graph two known ages are plotted: that for Terrace 1 (766 ± 18 cal yr BP), and for Terrace 8 (24 ka cal yr BP years), as described above.

Two different river incision models were used for estimating ages for the intermediary undated terraces: (1) assuming a linear relationship between terrace age and terrace height; and (2) by scaling the incision curve modelled for the Waihou River (Villamor et al., 2016) to the measured terrace heights. The first approach assumes a linear rate of erosion over the time frame of concern by joining the two known points; the second assumes a period of rapid erosion between approximately 20 cal ka BP and 16 cal ka BP with slower rates after this time as described by Persaud et al. (2016) for the Waihou River. While not the same catchment, the Persaud et al. (2016) study was immediately adjacent in the Hauraki Plains, and the main factors controlling incision rates (climate, vegetation cover, geology, base level) would be very similar (e.g., Schofield, 1965; Manville and Wilson, 2004). Hence the incision rate of the Waihou River could be a fair approximation of the incision rate of the stream in this catchment of the Piako River (Chapter 2.4.1). Using these two approaches, ages for each terrace were estimated by interpolating the position of the points based on terrace height.

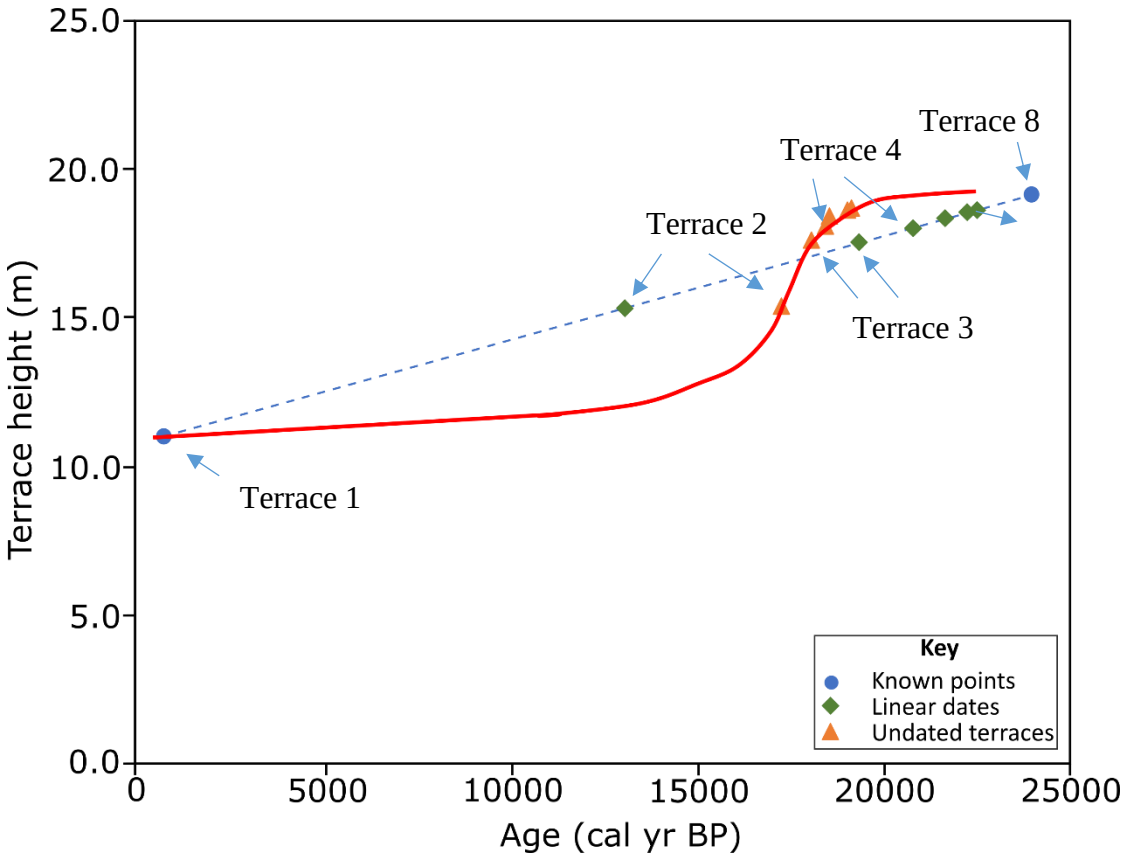

Figure 4.10: Plot of terrace height versus terrace age. The blue circles mark Terrace 1, which was aged at 766 ± 18 cal yr BP (Table 4.2), and Terrace 8, which was dated at c. 24 cal ka BP (based on geomorphology). The other terraces (green diamonds), without dates, were plotted along a trend line assuming a linear rate of erosion and terrace formation. Each terrace has a corresponding orange triangle at the same height that assumes an incision rate similar to that of the Waihou River (Persaud et al., 2016).

Table 4.3: Modelled ages of the terraces at Quine Road formed by incision of streams. Different rates of incision were modelled assuming a linear and a curved rate between two points with known ages (Figure 4.9). The average age assumes a range between the two ages from the terrace.

Terrace number	**Terrace height (m)**	**Displacement (m)**	**Age, assuming a linear rate of incision (cal yr BP)**	**Age, assuming a curved rate of incision (cal yr BP)**	**Average age of both modelled incision rates (cal yr BP)**
1	11	0.0	766 ± 18 *	766 ± 18 *	766 ± 18 *
2	15.3	0.0	13100 ± 500	16900 ± 500	15000 ± 1900
3	17.5	1.0	19411 ± 500	17700 ± 500	18600 ± 900
4	18	2.6	20845 ± 500	18100 ± 500	19500 ± 1400
5	18.3	2.5	21705 ± 500	18200 ± 500	20000 ± 1800
6	18.5	2.7	22279 ± 500	18700 ± 500	20500 ± 1800
7	18.6	2.8	22566 ± 500	18800 ± 500	20700 ± 1900
8	19.1	2.6	24000¶	24000¶	24000¶

* Age from ^{14}C dates obtained from charcoal samples from the terrace (± 2σ).

¶ Age from assumption that this surface is a remnant of the original Hinuera C surface.

The scarp heights of each of the terraces (Table 4.1) were plotted against the inferred ages of the terraces (Figure 4.11). The differences of the ages from the linear and curved incision models were used for the ranges and the average of the two values for the points. From the differences of the scarp heights, at least two earthquakes large enough to rupture the surface are likely to have occurred on the Quine Road trace, as the measured fault scarp heights fall into two distinct displacement groups. The penultimate displacement all terraces older and including Terrace 4 and the most recent rupture displaced all terrace including Terrace 3. Therefore, the two earthquakes occurred between the formation of Terraces 4 and 3 and of Terraces 3 and 2. The modelled ages would then put the ages of the penultimate earthquake between 19,500 ± 1,400 cal yr BP (Terrace 4) and 18,600 ± 600 cal yr BP (Terrace 3) and the most recent rupture between 18,600 ± 600 cal yr BP (Terrace 3) and 15,000 ± 1,900 cal yr BP (Terrace 2). The lack of offset in Terraces 1 and 2 suggests that there have not been any earthquakes on the Quine Road trace in the last

15,000 ± 1,900 cal yrs, after the second earthquake occurred. Due to the uncertainty of the age of the formation of Terrace 3, the uncertainties in the ages of the penultimate and most recent earthquakes overlap. The penultimate earthquake, with a displacement of 1.6 m, must have occurred before the formation of Terrace 3 due to the differences in the scarp heights of Terraces 4–8 and Terrace 3. And then the second earthquake, with a displacement of 1.0 m, occurred after the formation of Terrace 3, due to the differences in the scarp height between Terrace 3 and Terraces 1 and 2.

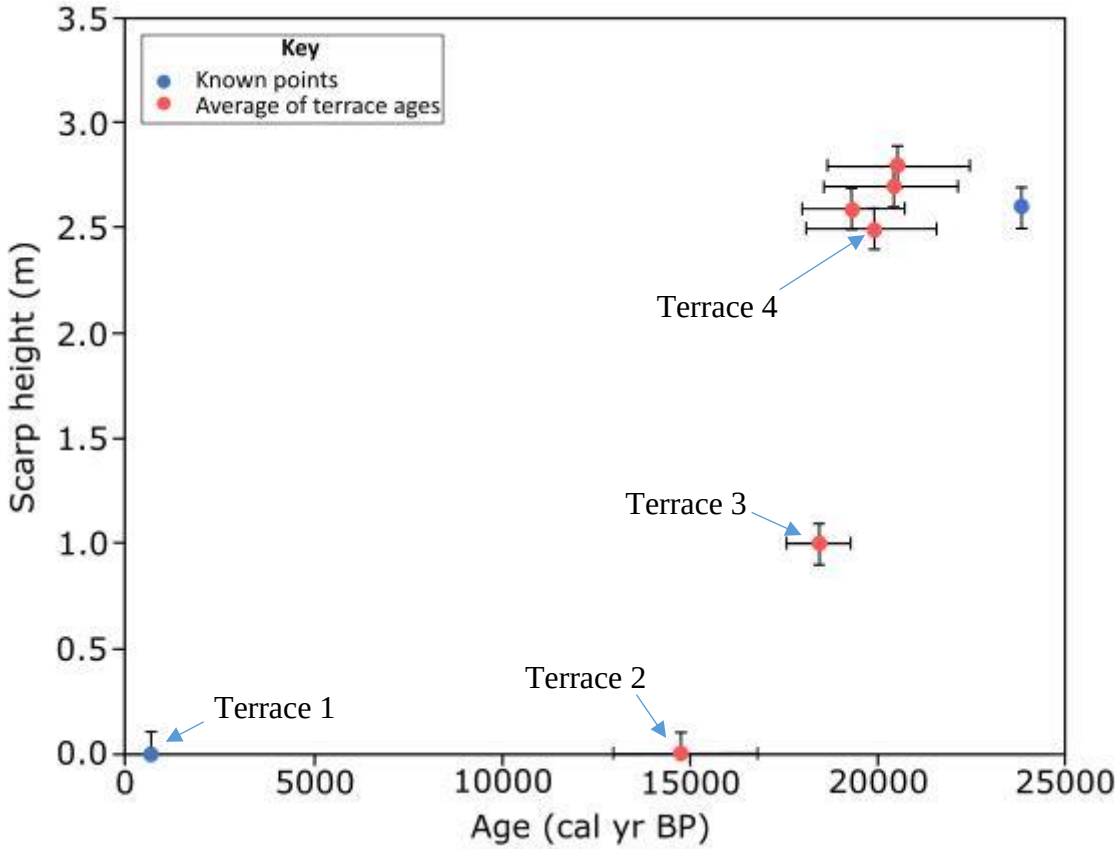

Figure 4.11: Scarp height plotted against the age of terraces. The ages used are the averages of Terraces 1 and 8 (blue circles), which remain constant because of ^{14}C dating and geomorphological assumptions. Terraces 2–7 are plotted as the average of the linear and curved ages, and the range represented is the difference between the two ages (Table 4.1).

4.4.3 Calculation of slip rate from terrace ages and displacement

Using the displacement of the terraces and the ages of them, the slip rate of this fault trace can be found. The slip rate can then be used for calculating seismic hazard. The average vertical displacement of Terraces 4–8 is 2.64 ± 0.15 m, which, due to differences in

displacements between terraces of different ages, occurred over two events as just described (section 4.4.2). The average age of the youngest terrace displaced by two events has been calculated to be 19,500 ± 1400 cal yr BP. By dividing the average displacement of Terraces 4–8 by the average age of Terrace 4, the calculated vertical slip rate would be 0.135 ± 0.01 mm/yr. This is compatible with the slip rate of 0.16 mm/yr (range 0.1–0.3 mm/yr) of the preliminary characterisation of the Te Puninga Fault for the Community Fault Model (Seebeck et al., 2023). However, the Te Puninga Fault is comprised of at least nine parallel fault strands at the latitude of Quine Road (Figure 4.1). Therefore, one would expect that the Quine Road slip rate would only be a small proportion of the total value as the net vertical displacement should be distributed across all these fault strands. From the rates derived in my study, it seems that the Community Fault Model value is underestimated.

4.5 Summary

The fault trace at Quine Road lies on the edge of the Hinuera Formation near the western margin of the Hauraki Plains. A geomorphological study of this scarp was undertaken using a DEM and hillshade model on ArcGIS Pro and ArcMap, supported with mapping at the site. The scarp is approximately perpendicular to two streams, the Awaroa and Mangakahika streams. These streams have produced terraced surfaces as they have cut into the landscape in the past c. 24 cal ka BP since the final deposition of unit Hinuera C of the Hinuera Formation. The scarp is a normal fault, with the footwall to the east, dipping to the west. This is opposite to the general direction of the slope of the surface, dipping towards the east, and, thus, this progressive displacement produced terraces from the streams of different heights across the scarp, from 11 m to 21 m in elevation.

Geomorphological mapping of these terraces determined the different terrace heights of on the footwall and hanging wall of the scarp. As the terraces decrease in elevation, they get younger in age. These terraces were correlated across the scarp, and the differences in heights were recorded as offset due to fault displacement. The offsets were also adjusted for the slope of the terraces: 0.86° on Terraces 4–8, 0.57° on Terrace 3, and negligible on Terraces 1 and 2. The youngest terraces (Terraces 1 and 2) had no offset, indicating they were formed after the last earthquake. Terrace 3 had on offset of 1.0 m, after adjusting for the slope, indicting there was movement on the fault after the formation of the terrace. Terraces 4–8 had offsets of 2.5–2.8 ± 0.15 m after adjusting for the slope, from the difference in elevation from profiles drawn parallel to the scarp and between 1.7 m and 2.5 from profiles drawn perpendicular to the scarp.

From the differences in the scarp heights on terraces, dated at different heights, it is likely that two earthquakes caused the surface to rupture on the Quine Road trace in the past c. 24 cal ka. The two earthquakes occurred, firstly between the formation of Terraces 4 and 3, and the second between the formation of Terraces 3 and 2. By modelling the incision rates of the streams and the ages of the formation of the terraces, the first earthquake likely occurred between 19,500 ± 1,400 cal yr BP (Terrace 4) and 18,600 ± 600 cal yr BP (Terrace 3), and the second earthquake likely occurred between 18,600 ± 600 cal yr BP (Terrace 3) and 15,000 ± 1,900 cal yr BP (Terrace 2). Terraces 1 and 2 did not show any offset and, thus, no surface-rupturing earthquakes have occurred on the Quine Road trace since 15,000 ± 1,900 cal yr BP. Using the age of the youngest terrace

to rupture twice (Terrace 4), and the average displacement of Terraces 4–8, a slip rate of 0.135 ± 0.01 mm/yr was calculated. This slip rate is compatible with the published Community Fault Model slip rate estimate of 0.16 ± 0.3 mm/yr. However, this estimation for Quine Rd is only one strand of nine at this latitude in the Te Puninga Fault, and so it is possible that the Community Fault Model understates the slip rate.

Chapter 5

Ground penetrating radar analysis of the Quine Road scarp and the paleoseismic trench locations

5.1 Introduction

Ground penetrating radar (GPR) is a non-destructive geophysical technique of imaging subsurface units. While it cannot give as much information as paleoseismic trenching, it is cheaper, and less time consuming, and does not interfere with the operations of a farm to the same extent as trenching (time the paddock is out of operation and having to resow the pasture). In particular, for faults expressed as numerous fault traces at the surface, such as the Te Puninga fault, paleoseismic trenching would be very costly to implement at every trace. GPR can be used to transfer some of the knowledge gained in the trenches to other traces in a cost-effective way. GPR surveys can also be undertaken prior to trenching for site selection as they may help distinguish whether a geomorphic scarp is a fault trace or an alluvial terrace riser. Also, they may help assess whether the tectonic deformation that formed the fault scarp is a fold or a fault (a fault would be preferred for siting a trench). GPR has been successfully used in paleoseismic studies in New Zealand before (Tronicke et al., 2005; McClymont et al., 2009; Villamor et al., 2022).

GPR uses pulses of electromagnetic waves, typically in the magnitude of MHz, and measures the elapsed time between its pulses. The elapsed time is distorted by the conductive and dielectric properties of the subsurface material. Seismic reflectors are the product of changes of these dielectric properties. Further background information about GPR is presented in Chapter 2.5.

5.2 Methods

5.3 Field methods

GPR analyses were chosen along traces of the Te Puninga Fault. GPR surveys across the two paleoseismic trench sites (Figure 5.1, images 2–3) enabled me to assess how well GPR can be correlated with the layers exposed in the trenches. A third survey at the Quine Rd site (Figure 5.1A and image 1) provides information to evaluate whether a future paleoseismic trench at the site would be useful. Lines adjacent to the two paleoseismic

trench locations from February 2021 were chosen, since the units had been extensively studied and trench logs produced, which could likely be correlated to the GPR profiles. The 3rd site chosen was in the Quine Road field area, which was the site of the extensive geomorphological study described in Chapter 4.

In all three locations, a total of six lines were surveyed. All of these were surveyed twice, with a 450 MHz and a 160 MHz instrument. The lower frequency allows for deeper penetration, at the expense of resolution in shallower layers. And vice versa for the higher frequency.

Real-time kinematic positioning (RTK) was used to measure elevation data along the line. These were taken at 20 cm intervals.

5.3.1 Data processing

Once collected, the raw GPR data were processed using Reflex2D. Processing steps included applying a linear gain to traces observed in the subsoil to amplify their signal, and a background removal of "noise" from the data, including subtracting the mean using a "dewow" filter. A static correction was applied to align the first data arrival. Lastly, elevation data from the RTK were applied to the profile and the data were graphed.

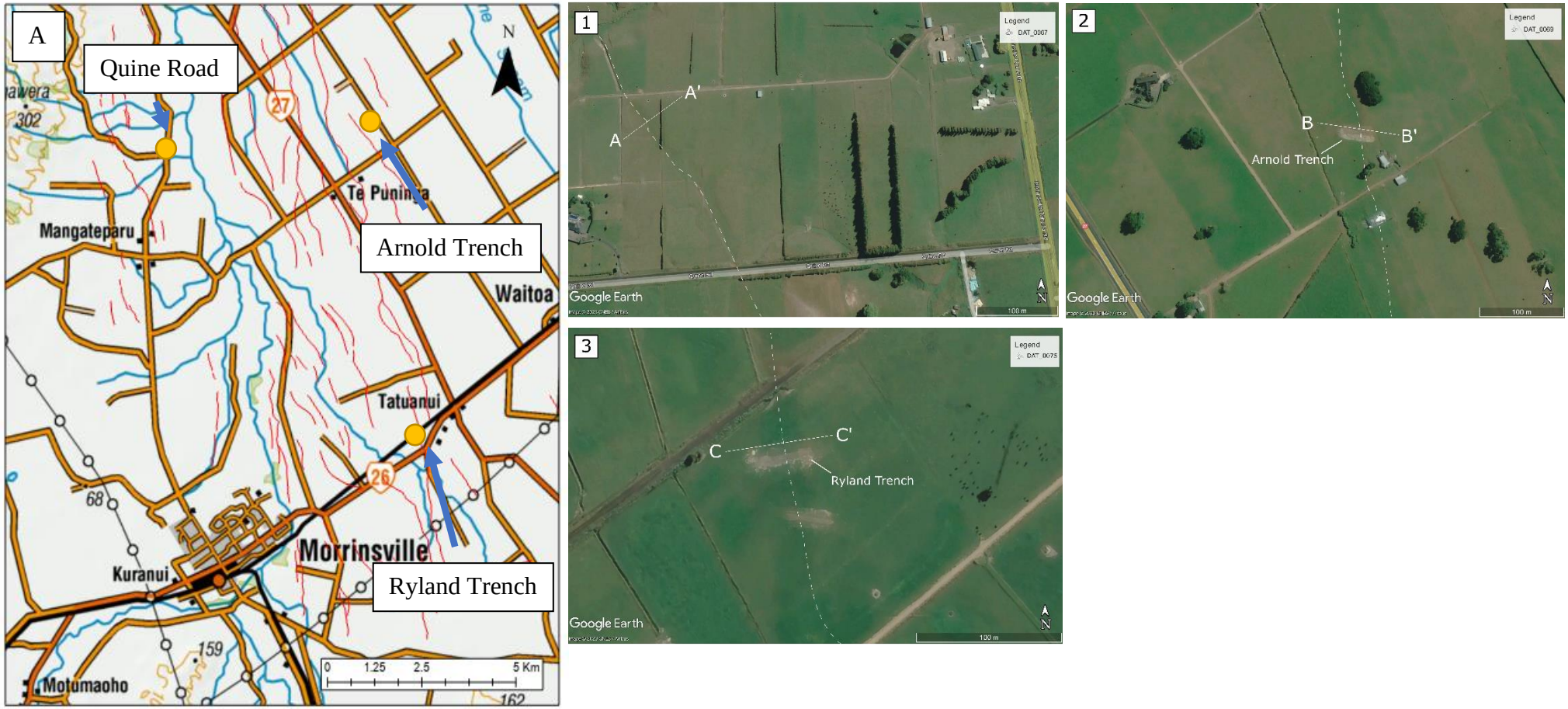

Figure 5.1: A: Location of the three GPR location across traces of the Te Puninga Fault. Map from NZ Map Series 260. B: Larger scale satellite (Google Earth) photographs of the labelled GPR profiles with paleoseismic trench locations shown where appropriate at 1) Quine Rd; 2) Arnold Trench; and 3) Ryland Trench.

5.4 Results

Three profiles of the scarps (DAT_0067, DAT_0069 and DAT_0074), using the 160 MHz antenna, are displayed (Figure 5.2). The distance (metres) along the transect was plotted on the x axis against time (nanoseconds) of the reflection of the pulse on the y axis. On a secondary axis, the depth was plotted as a function of time. The relationship between time of the reflection time and depth depends on the dielectric constant of the materials. The constant is difficult to approximate in sediments with variable grainsize, such as the Hinuera Formation. The approximation was made that the materials were silts and sands and hence 0.15 m/ns was used. This value was employed for a recent GPR study in the nearby Hamilton Basin (Melchert, 2022; R. Melchert, personal communication, 2023) and falls within the acceptable values for dry sand as used by Reynold (1997).

Once the depth was plotted on a secondary axis, profiles were superimposed with a simple stratigraphy and unit description, with the intention of possible correlating the lithological units with the main reflectors.

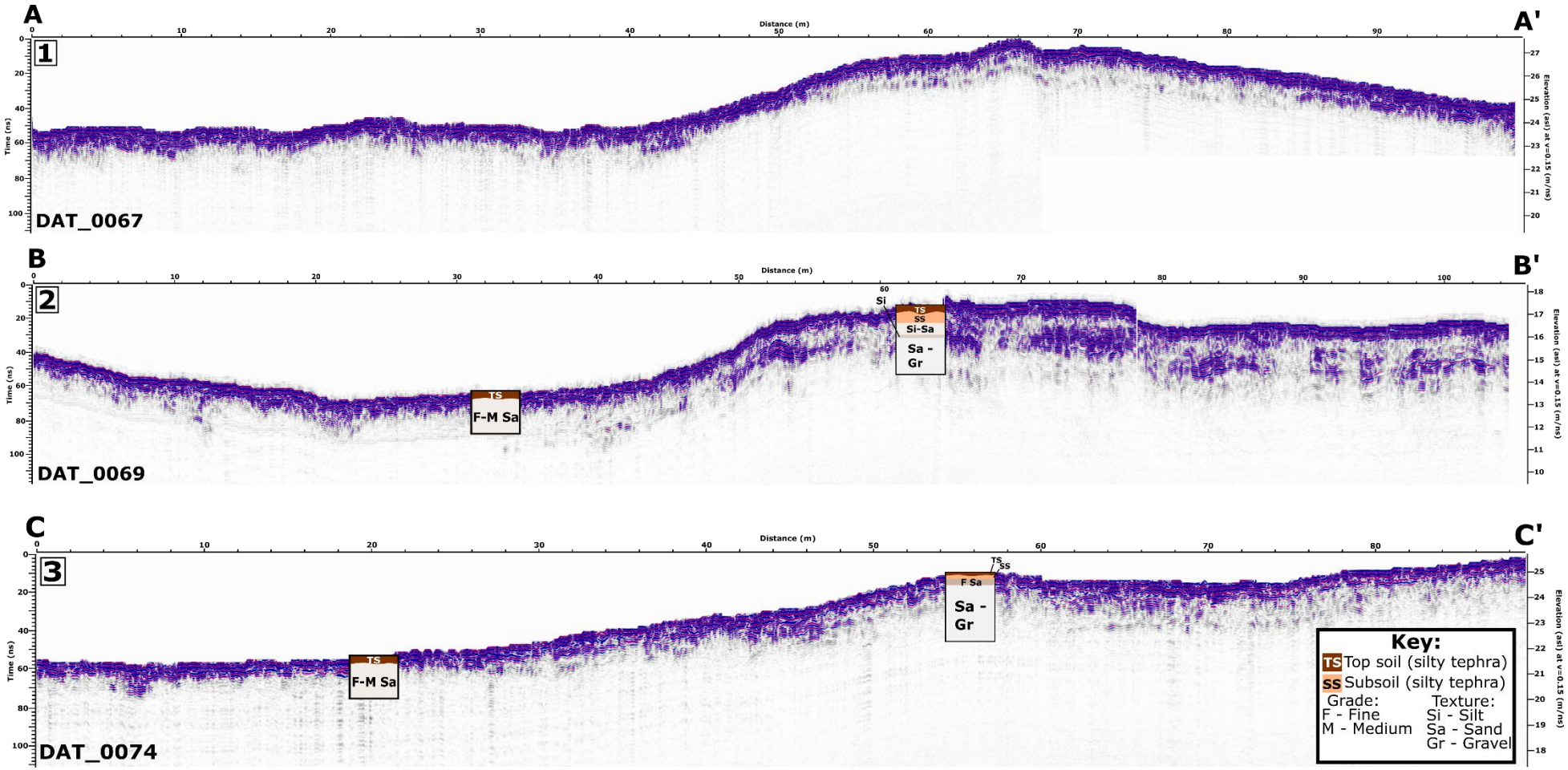

Figure 5.2: GPR profiles (A-A', B-B', C-C') of three scarps on the Te Puninga Fault: 1. Quine Road, 2. Arnold Farm, 3. Ryland Farm. Data processed on Reflex2D software. Stratigraphic columns from the trenches are overlaid on the lines adjacent to trenches so that stratigraphy could be compared.

5.5 Discussion

The GPR survey was experimental, as discussed earlier in the chapter. However, I have three main findings: a) The profiles show enough data to be of use for future paleoseismic investigations on the Hauraki Plains; b) the landforms at all three sites are the result of seismic deformation rather than fluvially-formed terraces; c) there is a possibility that sediments were faulted rather than folded at Quine Road.

Assuming the depths on Figure 5.2 are correct, then between 1.5–2.5 deep m profiles were recorded by the GPR. This depth range is comparable with the depth of stratigraphy that would be exposed in a paleoseismic trench (see Chapter 3). A deeper section would be more useful as often deeper layers show more prominent displacement than shallow layers, which are optimal to identify faulting and locate fault plane more precisely. The GPR could therefore be used to potentially predict the units that would be exposed in a trench, at least, and hence determine whether it would be worth trenching that site. While the upper units in the footwall of the Te Puninga Fault were relatively well imaged, the finer grained (high clay content) layers in the hanging wall were waterlogged (high water table) and were not imaged, that is, GPR penetrated less in the lower area as water content affects the signal (Ulriksen, 1980; Lowe, 1985).

In all three profiles, the main trend of the reflectors curves is parallel to the surface, suggesting the scarp is indeed a tectonic rather than an alluvial feature. These sediments would have been deposited more or less horizontally as a result of deposition as (very) low-angle alluvial fans. And if these slopes in the landscape were formed by degradational river terraces, material would have been eroded away by fluvial action, and the remaining sediments would still be horizontal (Figure 5.3). However, as the reflectors curve parallel with the land surface, then the surface was folded as a result of faulting. This feature was observed in both the Arnold and Ryland paleoseismic trenches, where the exposed sediments appeared to fold rather than produce a clear fault as a result to deformation.

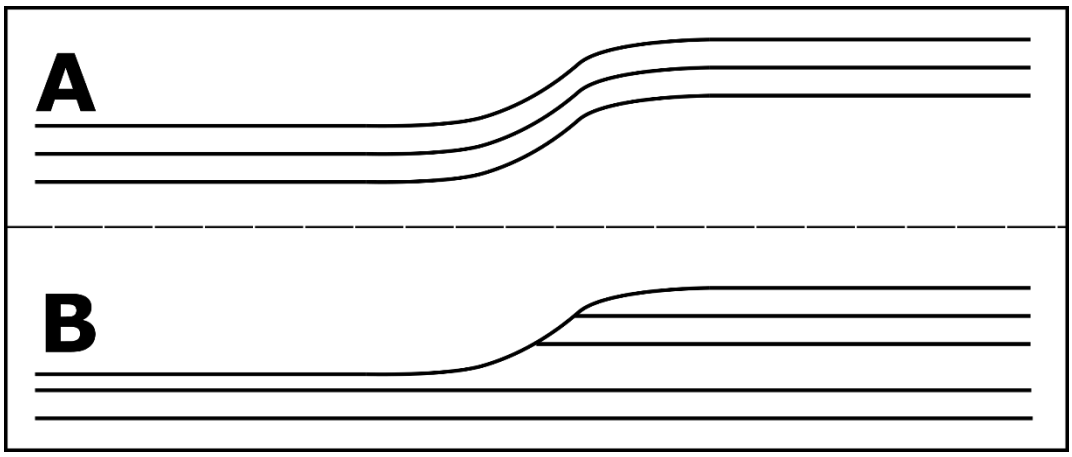

Figure 5.3: Simplified diagram comparing the GPR reflector trends of a tectonic fold (A) and terrace riser (B). All three GPR lines for this study showed evidence of tectonic folding.

The profile that was not adjacent to a paleoseismic trench at Quine Road (profile A-A', Figure 5.2) was acquired to assess whether trenching at that site would be useful. This site could be of interest for possible future paleoseismic trench to better constrain the seismic record at the site. Even more information can be gained from the trench if a clear fault rather than a fold (as was found in the Ryland and Arnold trenches) is exposed in the trench. The general shape of the layers in the Quine GPR profile suggests that there is tectonic folding (layers follow the surface geomorphology and there is no clear erosion). However, due to breaks in the reflectors, there are two parts of the profile that may be locations of faulting (Figure 5.4A and B). Hence these sites would be preferred places to locate a trench. The GPR profile also suggests that there is either overthickening of, or additional lithological units, on the downthrown part of the scarp (Figure 5.4C and D). This is potentially another interesting feature to be observed in a trench in case it provides information for the timing of the last or penultimate events discussed in Chapter 4.

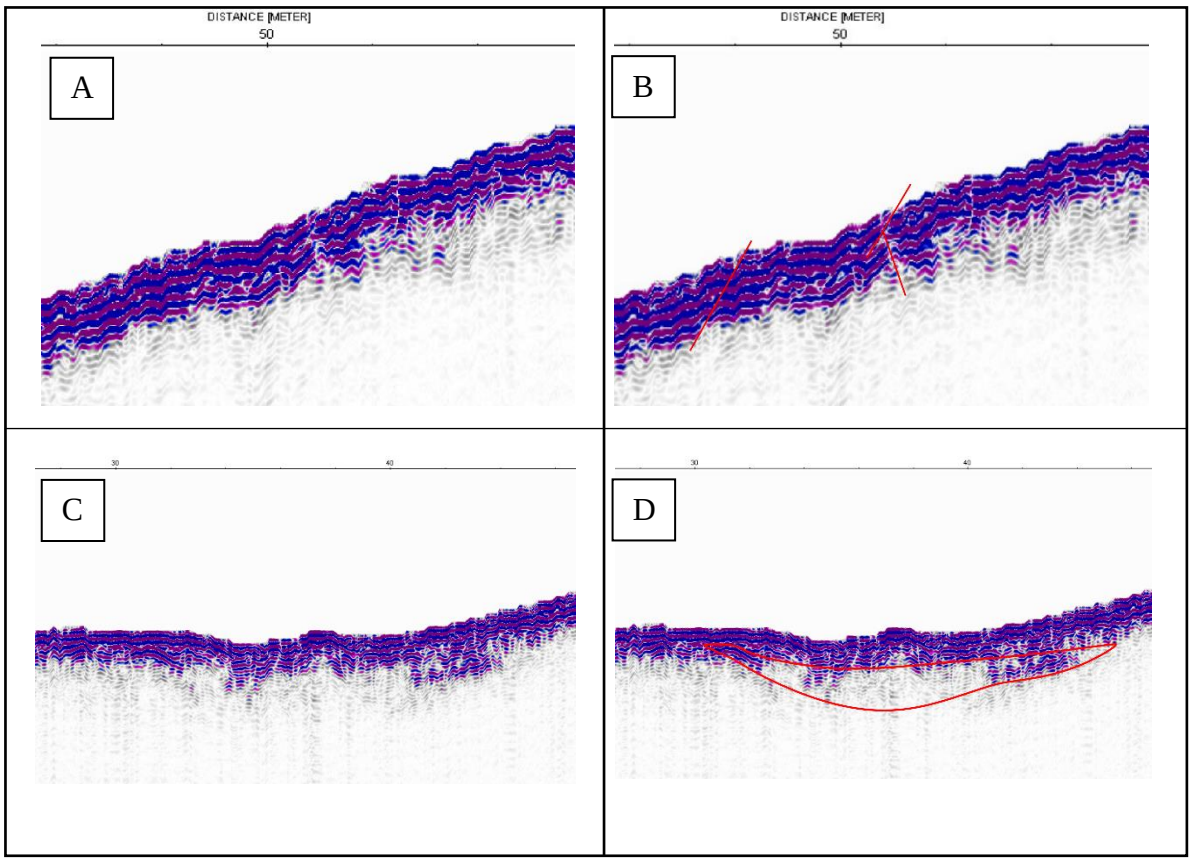

Figure 5.4: GPR profile showing possible evidence of faulting at the Quine Road scarp, with original trace (A and C) and potential faulting indicated by red lines (B and D).

5.6 Conclusion

Although it does not provide as much information of the subsurface as paleoseismic trenching, GPR is non-destructive, is less disruptive to farm acivities, and is cheaper. Because of this, GPR has been used in paleoseismic studies before in New Zealand.

In my study, GPR was used to map the three scarps studied and reported in Chapters 3 and 4. Two transects were positioned adjacent to each of the Arnold and Ryland trenches so that the profiles could be compared with the reflectors and the known stratigraphy from the trench logs. The other transect analysed was at the Quine Road area, which, as a consequence of the estimated ages of displacement found in Chapter 4, could be a potential site for further paleoseismic trenching. In the study using GPR, I found a) that a suitable depth of stratigraphy (<2.5 m) was obtained in all the sites, but deeper penetration would have been even more useful; b) the displaced surfaces were all formed by faulting, rather than fluvial erosion surfaces; c) there is a possibility that, unlike the

Arnold and Ryland trenches, some of the sediments at Quine Road may have been faulted rather than folded.

Chapter 6
Conclusions

The Te Puninga Fault was discovered in 2016 from high resolution LiDAR on the western margin of the Hauraki Plains as part of a project investigating the Kerepehi Fault (Persaud et al., 2016). As the fault has offset the Hinuera Surface (on unit Hinuera C of Manville and Wilson 2004), it was determined that the fault was active (ruptured in the past 125,000 years), and preliminary evidence indicted a Mw>6.8. The fault presents a hazard and risk to the region, which previously had been designated as having a low to moderate seismic risk, based on the historic record of seismicity and limited number of active faults. Until recently, it was believed the Kerepehi Fault, in the middle to eastern Hauraki Plains, was the only active fault in the region. Consequently, understanding the seismicity of the Te Puninga fault is important for revaluating the seismic hazard and risk to the Hauraki Plains and the adjacent Hamilton Basin.

This study aimed to provide a chronology and assessment of past seismicity for earthquakes on the Te Puninga Fault during the late Quaternary. To achieve this aim, three objectives were identified. For this conclusion chapter, I have re-iterated the objectives (from Chapter 1.1.1) and I then summarise the findings from them to meet the aim.

Objective (a)

Establish a stratigraphy and chronology for deposits exposed in two paleoseismic trenches athwart the Te Puninga Fault using ^{14}C dating and tephrochronology to set up the chronostratigraphic framework for paleoseismic studies on the fault (Chapter 3).

In both paleoseismic trenches (Arnold and Ryland trenches), the oldest lithological unit exposed was the Late Pleistocene volcanogenic alluvium of the Hinuera Formation, specifically comprising Hinuera C deposits as defined by Manville and Wilson (2004). The surface of the Hinuera C sediments was estimated at both sites using ^{14}C dates from the trenches to be approximately 24,000 cal yr BP. In the footwall of the Ryland trench, ^{14}C dates of a peat lens of 11,000 cal yr BP indicated a thickness of <1.5 m of post-

Hinuera alluvium. This Holocene alluvium was correlated with the Waitoa Formation of Houghton and Cuthbertson (1989).

In both trenches the alluvium was overlaid by a coverbed of composite, mostly rhyolitic, tephra deposits, that have been slightly weathered and modified into soil horizons, forming pedogenic soils classed as Allophanic Soils (on well or moderately well drained sites) or Gley Soils (on poorly drained sites) in the NZSC of Hewitt (2010). EPMA analysis of glass shards isolated from samples taken from the basal tephra deposits showed them to be either Okareka (c. 23,500 cal yr BP) or Rerewhakaaitu (c. 17,600 cal yr BP), or both. The probable presence of Okareka tephra supports the age attributed to the Hinuera Surface of c. 24.0 cal ka BP. Thin visible tephras layers of Taupo (1718 ± 10 cal yr BP) and Kaharoa (636 ± 12 cal yr BP) tephras were also observed in the upper parts of both trenches as visible, discontinuous deposits.

Objective (b)

Use LiDAR to closely measure how a scarp that dips in the opposite direction to the land surface interacts with offset stream terraces straddling a segment of the fault in a geomorphological case study at Quine Rd. This LiDAR-based case study can provide further evidence of surface displacement and help model ages of earthquakes on the segment (Chapter 4).

Geomorphological mapping of the Quine Road scarp using a DEM and hillshade model enabled eight terraces, from 11 m to 21 m asl in elevation, to be mapped. These were primarily identified by elevation profile transects parallel to the fault scarp. Offsets of these terraces due to faulting were calculated from the differences in heights from the parallel elevation profiles and elevation profile transects crossing the scarp perpendicularly.

The terraces were numbered 1 to 8 with the youngest Terrace 1, dated at 766 ± 18 cal yr BP on the basis of ^{14}C dates of buried charcoal, and Terraced 8, the oldest, aged at 24,000 cal yr BP, as the landscape position and geomorphology suggests this was the original Hinuera C surface. The ages of the other terraces were estimated from two models of incision by the streams. One model assuming a linear incision rate between the two known ages and the other assuming a curved incision rate, assuming an increase of incision relating to climate changes after the LGM.

The scarp height changed significantly between Terrace 4 (2.6 ± 0.15 m) and Terrace 3 (1.0 ± 0.15 m) and them again by Terrace 2 (0 m). Therefore, is it probable two earthquakes occurred after 24,000 cal yr BP. It is likely that the penultimate earthquake that generated the displacement occurred between the formation of Terrace 4 (19,500 ± 1,400 cal yr BP) and Terrace 3 (18,600 ± 600 cal yr BP), and the most recent earthquake occurred between the formation of Terrace 3 (18,600 ± 600 cal yr BP) and Terrace 2 (15,000 ± 1,900 cal yr BP). Using the age of the youngest terrace that was displaced in two events (19,500 cal yr BP), and the average displacement of the other terraces displaced twice (2.64 ± 0.15 m), a slip rate of 0.135 ± 0.01 mm/yr was calculated. As this is one of at least nine strands of the Te Puninga Fault at this latitude, is a possible the published slip rate of 0.160 ± 0.03 mm/yr by Persaud et al. (2016) is understated.

Objective (c)

A trial study of the application of ground penetrating radar (GPR) on the Te Puninga Fault to assist with future paleoseismic studies (Chapter 5).

GPR was undertaken on the three scarps that were previously studied as part of this thesis. Two transects were positioned next to each of the Arnold and Ryland trenches so that comparisons could be made between the reflectors and the known stratigraphic units, and one transect was analysed at Quine Road, a potential site for further paleoseismic trenching in the future. In this GPR study, I reached the following conclusions: a) that a suitable depth of stratigraphy (<2.5 m) was obtained in all the sites, although it would be ideal to have greater depth; b) the displaced surfaces were all formed by faulting, rather than by fluvial erosion; and c) there is a possibility that, unlike the Arnold and Ryland trenches, some of the sediments at Quine Road were faulted rather than folded

References

Adams, R.D., Muir, M.G., Kean, R.J. 1972. Te Aroha earthquake 9 January 1972. *Bulletin of the New Zealand Society for Earthquake Engineering.* 5:54–58.

Annan, A.P. 2002. GPR—History, trends, and future developments. *Subsurface Sensing Technologies and Applications* 3, 253–270. https://doi.org/10.1023/A:1020657129590

Balance, P. 2017. New Zealand geology: an illustrated guide. *GSNZ Miscellaneous Publication* 148, 397 pp, version 2

Barrell, D.J.A., Almond, P.C., Vandergoes, M.J., Lowe, D.J., Newnham, R.M., NZ-INTIMATE members. 2013. A composite pollen-based stratotype for inter-regional evaluation of climatic events in New Zealand over the past 30,000 years (NZ-INTIMATE project). *Quaternary Science Reviews* 74, 4–20.

Brathwaite, R.L., Christie, A.B. 1996. Geology of the Waihi area 1:50,000: part sheets T13 and U13. Lower Hutt: Institute of Geological and Nuclear Sciences. 1 sheet + 64p.

Busby, J.P., Cuss, R.J., Raines, M.G., Beamish D. 2004. Application of ground penetrating radar to geological investigations. *British Geological Survey Internal Report*, IR/04/21. 33pp.

Chick, L.M., de Lange, W.P., Healy, T.R. 2001. Potential tsunami hazard associated with the Kerepehi Fault, Firth of Thames, New Zealand. *Natural Hazards* 24(3), 309–318. doi: 10.1023/A:1012210314609

Churchman, G.J., Lowe, D.J. 2012. Alteration, formation, and occurrence of minerals in soils. In: Huang, P.M., Li, Y., Sumner, M.E. (eds) *"Handbook of Soil Sciences. 2nd edition. Vol. 1: Properties and Processes"*. CRC Press, Boca Raton, FL, pp.20.1-20.72.

Clayden, B., Hewitt, A.E. 1989. Horizon notation for New Zealand soils. Manaaki Whenua Press, Lincoln. 30 pp.

Clement, A.J.H., Sloss, C.R., Fuller, I.C. 2010. Late Quaternary geomorphology of the Manawatu coastal plain, North Island, New Zealand. *Quaternary International* 221, 36–45.

Clement, A.J.H, Whitehouse, P.L., Sloss C.R. 2016. An examination of spatial variability in the timing and magnitude of Holocene relative sea-level changes in the New Zealand archipelago. *Quaternary Science Reviews* 131, 73–101.

Cuthbertson, A.S. 1981. *The Hinuera Formation in the southern Hauraki Lowland, Central North Island.* [MSc thesis, University of Waikato, Hamilton].

Dempsey, D., Eccles, J.D., Huang, J., Jeong, S., Nicolin, E., Stolte, A., Wotherspoon, L., and Bradley B.A. 2021. Ground motion simulation of hypothetical earthquakes in the upper North Island of New Zealand. *New Zealand Journal of Geology and Geophysics* 64, 570-588. https://doi.org/10.1080/00288306.2020.1842469

Di Capua, A., De Rosa, R., Kereszturi, G., Le Pera, E., Rosi, M., Watt, S. 2022. Volcanically derived deposits and sequences: a unified terminological scheme for application in modern and ancient environments. *Geological Society, London, Special Publications* 520, 11–27.

Downes, G.L. 2005. Earthquakes. Pp. 56-58 In: Edbrooke, S.W. (compiler). Geology of the Waikato area. Institute of Geological and Nuclear Sciences 1:250,000 Geological Map 4. 1 sheet and 68p. IGNS, Lower Hutt,

Edbrooke, S.W. 2005. Geology of the Waikato area. Institute of Geological and Nuclear Sciences 1:250,000 Geological Map 4. Lower Hutt, GNS Science; 1 sheet + 68p.

Froggatt, P.C. 1992. Standardization of the chemical analysis of tephra deposits. Report of the ICCT working group. *Quaternary International* 13-14, 93-96.

Froggatt, P.C., Gosson, G.J. 1982. Techniques for the preparation of tephra samples for mineral or chemical analysis and radiometric dating. *Geology Department, Victoria University of Wellington Publication* 23, 1-12.

Gehrels, M. 2009. *An enhanced 1800-year record of recent volcanic ash-fall events for northern New Zealand from the analysis of cryptotephra*. PhD thesis, The University of Plymouth, UK.

Geonet, 2023. Te Aroha's shaky start to the year. Retrieved from https://www.geonet.org.nz/news/7Cu7546jqFr8BppNeyzl8G"

Grant-Taylor, T.L, Rafter, T.A. 1963. New Zealand natural radiocarbon measurements I–IV. *Radiocarbon* 5, 118–162.

Hewitt, A.E. 2010. New Zealand Soil Classification 3rd ed. *Landcare Research Science Series* 1. Manaaki Whenua Press. 133 pp.

Hewitt, A.E., Balks, M.R., Lowe, D.J. 2021. *The Soils of Aotearoa New Zealand*. Springer, Cham, 332pp.

Hochstein, M.P. and Nixon, I.M. 1979. Geophysical study of the Hauraki Depression, North Island, New Zealand. *New Zealand Journal of Geology and Geophysics*. 22(1), 1-19.

Hogg, A.G, Lowe, D.J, Hendy, C.H. 1987. University of Waikato radiocarbon dates I. *Radiocarbon* 29, 263–301.

Hogg, A.G, Higham T.F.G., Lowe D.J., Palmer J., Reimer P., Newnham RM. 2003. A wiggle-match date for Polynesian settlement of New Zealand. *Antiquity* 77, 116–125.

Hogg, A.G., Lowe, J., Palmer, J.G., Boswijk, G., Bronk Ramsey, C.J. 2012. Revised calendar date for the Taupo eruption derived by ^{14}C wiggle-matching using a New Zealand kauri ^{14}C calibration data set. *The Holocene* 22, 439–449.

Hogg, A.G., Wilson, C.J.N., Lowe, D.J., Turney, C.S.M., White, P., Lorrey, A.M., Manning, S.W., Palmer, J.G., Bury, S., Brown, J., Southon, J., Petchey, F. 2019. Wiggle-match radiocarbon dating of the Taupo eruption. *Nature Communications* 10, 4669.

Hogg, A.G., Heaton T.J., Hua Q, Palmer JG, Turney CSM, Southon J, Bayliss A, Blackwell PG, Boswijk G, Bronk Ramsey C, Pearson C, Petchey F, Reimer P, Reimer R, Wacker L. 2020. SHCal20 Southern Hemisphere calibration, 0–55,000 years cal BP. *Radiocarbon* 62, 759–778.

Hopkins, J.L, Lowe, D.J, Horrocks J.H. 2021a. Tephrochronology in Aotearoa New Zealand. *New Zealand Journal of Geology and Geophysics* 64, 153–200.

Hopkins, J. L., Bidmead, J. E., Lowe, D. J., Wysoczanski, R. J., Pillans, B. J., Ashworth, L., Rees, A.B.H., Tuckett, F. 2021b. TephraNZ: a major- and trace-element reference dataset for glass-shard analyses from prominent Quaternary rhyolitic tephras in New Zealand and implications for correlation. *Geochronology* 3, 465–504. https://doi.org/10.5194/gchron-3-465-2021

Houghton, B.F., Cuthbertson, A.S. 1989. Sheet T14 BD: Kaimai. Geological map of New Zealand 1:50,000. New Zealand Geological Survey, New Zealand Department of Scientific and Industrial Research, Wellington; 1 sheet + 35p.

Hughes, J.W., Lowe, D.J., Villamor, P., Moon, V.G., Clark, K.J., Morris, P., McQuillan, G.R., Medialdea, A., Coffey, G., Berryman, K., Langridge, R., Hogg, A.G., Alloway, B.V., Shalla, Y., Mark, O. 2022. Stratigraphy and age of volcano-fluvial

and tephra deposits associated with the Te Puninga Fault, Morrinsville, Hauraki Basin. *In*: Zernack A.V., Palmer, J., editors. Geoscience Society of New Zealand Annual Conference 2021: Programme and Abstracts Volume. *Geoscience Society of New Zealand Miscellanenous Publication* 158A, p.124

Hume, T.M., Sherwood, A.M., Nelson, C.S. 1975. Alluvial sedimentology of the Upper Pleistocene Hinuera Formation, Hamilton Basin, New Zealand. *Journal of the Royal Society of New Zealand* 5, 421-462.

Jarosewich, E., Nelen, J.A., Norberg, J.A. 1980. Reference samples for electron microprobe analysis. *Geostand Newsletter* 4, 43–47. https://doi.org/10.1111/j.1751-908X.1980.tb00273.x

Jochum, K.P., Stoll, B., Herwig, K., Willbold, M., Hofmann, A.W., Amini, M., Aarburg, S.,Abouchami, W., Hellebrand, E., Mocek, B., Raczek, I., Stracke, A., Alard, O., Bouman,C., Becker, S., Dücking, M., Brätz, H., Klemd, R., de Bruin, D., Canil, D., Cornell, D., de Hoog, C., Dalpé, C., Danyushevsky, L., Eisenhauer, A., Gao, Y., Snow, J.E., Groschopf, N., Günther, D., Latkoczy, C., Guillong, M., Hauri, E.H., Höfer, H.E., Lahaye, Y., Horz, K., Jacob, D.E., Kasemann, S.A., Kent, A.J.R., Ludwig, T., Zack, T., Mason, P.R.D., Meixner, A., Rosner, M., Misawa, K., Nash, B.P., Pfänder, J., Premo, W.R., Sun, W.D., Tiepolo, M., Vannucci, R., Vennemann, T., Wayne, D., Woodhead, J.D. 2006. MPI-DING reference glasses for in situ microanalysis: new reference values for element concentrations and isotope ratios. *Geochemistry, Geophysics, Geosystems* 7, 1–44. https://doi.org/10.1029/2005GC001060.

Kear, D.S., Schofield, J.C. 1978. Geology of the Ngaruawahia Subdivision. *New Zealand Geological Survey Bulletin* 88.

Kluger, M.O., Lowe, D.J., Moon, V.G., Chaneva, J., Johnston, R., Villamor, P., Ilanko, T., Melchert, R., Orense, R.P., Loame, R.C., Ross, N. 2023. Seismically-induced down sagging structures in tephra layers (tephra-seismites) preserved in lakes since 17.5 cal ka, Hamilton lowlands, New Zealand. *Sedimentary Geology* 445, 106327.

Knight, R., Endres, A., 1990, A new concept in modeling the dielectric response of sandstones: defining a wetted rock and bulk water system. *Geophysics* 55 (5), 586–594.

Langridge, R.M., Ries, W.F., Litchfield, N.J., Villamor, P., Van Dissen, R.J., Barrell, D.J.A., Rattenbury, M.S., Heron, D.W., Haubrock, S., Townsend, D.B., Lee, J.M.

2016. The New Zealand active faults database. *New Zealand Journal of Geology and Geophysics* 59, 86-96.

Le Maitre, R.W., Streckeisen, A., Zanettin, B., Le Bas, M.J., Bonin, B., Bateman, P., Bellieni, G., Dudek, A., Efremova, A., Keller, J. 2002. *Igneous rocks. A classification and glossary of terms. Recommendations of the IUGS Subcommission on the Systematics of Igneous Rocks*. Cambridge University Press, Cambridge.

Litchfield, N.J., R Van Dissen, R., Sutherland, R., Barnes, P.M., Cox, SC., Norris, R., Beavan, R.J., Langridge, R., Villamor, P., Berryman, K., Stirling, M., Nicol, A., Nodder, S., Lamarche, G., Barrell, D.J.A., Pettinga, J.R., Little, T., Pondard, N., Mountjoy J.J. and K Clark, K. 2014. A model of active faulting in New Zealand. *New Zealand Journal of Geology and Geophysics* 57, 32-56. DOI: 10.1080/00288306.2013.854256

Leonard, G.S., Begg, J.G., Wilson, C.J.N. (compilers) 2010. Geology of the Rotorua area: scale 1:250,000. Institute of Geological and Nuclear Sciences 1: 250,000 geological map 5. 1 sheet and 99 pp. Institute of Geological and Nuclear Sciences, Lower Hutt.

Loame, R.C., Villamor, P., Lowe, D.J., Milicich, S.D., Pittari, A., Barker, S.L.L., Rae, A., Gomez-Vasconcelos, M.G., Martinez-Martos, M., Ries, W.F. 2019. Using paleoseismology and tephrochronology to reconstruct fault rupturing and hydrothermal activity since c. 40 ka in Taupo Rift, New Zealand. *Quaternary International* 500, 52-70.

Lowe, D.J. 1985. Application of impulse radar to continuous profiling of tephra-bearing lake sediments and peats: an initial evaluation. *New Zealand Journal of Geology and Geophysics* 28, 667-674.

Lowe, D.J. 1986. Controls on the rates of weathering and clay mineral genesis in airfall tephras: a review and New Zealand case study. *In:* Colman, S.M., Dethier, D.P. (eds) *Rates of Chemical Weathering of Rocks and Minerals.* Orlando, Academic Press, pp. 265-330.

Lowe, D.J. 1988. Stratigraphy, age, composition, and correlation of late Quaternary tephras interbedded with organic sediments in Waikato lakes, North Island, New Zealand. *New Zealand Journal of Geology and Geophysics* 31, 125-165.

Lowe, D.J. (editor/compiler) 2006. Guidebook for 'Land and Lakes' field trip, New Zealand Society of Soil Science Biennial Conference, Rotorua. New Zealand Society of Soil Science, Lincoln. 63pp.

Lowe, D.J. 2011. Tephrochronology and its application: a review. Q*uaternary Geochronology* 6(2), 107–153.

Lowe, D.J. 2019a. Using soil stratigraphy and tephrochronology to understand the origin, age, and classification of a unique Late Quaternary tephra-derived Ultisol in Aotearoa New Zealand. *Quaternary* 2 (1), 9 (https://doi.org/10.3390/quat2010009).

Lowe, D.J. 2019b. Origin and classification of the Kainui silt loam: update on the leopard that changed its spots. *New Zealand Soil News* 67 (1), 75-85.

Lowe DJ. 2023. Landscapes and soils of the Hamilton Basin and South Waikato area – introductory notes updated. Earth Sciences group, School of Science, University of Waikato, Hamilton. 51 pp. https://www.researchgate.net/publication/369998946_Soils_and_landscapes_of_the_Hamilton_Basin_and_part_South_Waikato_area_-_a_summary

Lowe, D.J., Green, J.D. 2023. Origins and ages of Waikato lakes. In: Özkundakci, D., Grainger, N., Dean-Speirs, T. (editors), *Hidden gems of the Waikato – the history, ecology and management of Waikato lakes.* Waikato Regional Council, Hamilton (in press)

Lowe, D.J., Hunt, J.B. 2001. A summary of terminology used in tephra-related studies. *Les Dossiers de l'Archeo-Logis* 1, 17-22.

Lowe, D.J., Shane, P.A., Alloway, B.V., Newnham, R.M., 2008. Fingerprints and age models for widespread New Zealand tephra marker beds erupted since 30,000 years ago: a framework for NZ-INTIMATE. *Quaternary Science Reviews* 27, 95-126.

Lowe, D.J., Blaauw, M., Hogg, A.G., Newnham, R.M. 2013. Ages of 24 widespread tephras erupted since 30,000 years ago in New Zealand, with re-evaluation of the timing and palaeoclimatic implications of the late-glacial cool episode recorded at Kaipo bog. *Quaternary Science Reviews* 74, 170-194.

Lowe, D.J., Pearc,, N.J., Jorgensen, M.A., Kuehn, S.C., Tryon, C.A., Hayward, C.L. 2017. Correlating tephras and cryptotephras using glass compositional analyses and numerical and statistical methods: review and evaluation. *Quaternary Science Reviews* 175, 1–44.

Manville, V. 2001. Environmental impacts of large-scale explosive rhyolitic eruptions in the central North Island. *In*: Smith, R.T., editor. Fieldtrip Guides, Geological Society of New Zealand Annual Conference, Hamilton. *Geological Society of New Zealand Miscellaneous Publication* 110B, 19p.

Manville, V., Wilson, C.J.N. 2004. The 26.5 ka Oruanui eruption, New Zealand: a review of the roles of volcanism and climate in the post-eruptive sedimentary response. *New Zealand Journal of Geology and Geophysics* 47, 525-547.

Martinez, A., Byrnes, A.P. 2001. Modeling dielectric-constant values of geologic materials: an aid to ground-penetrating radar data collection and interpretation. *Current Research in Earth Sciences Bulletin* 247, 1-16.

McGlone, M.S., Nelson, C.S., Hume, T.M. 1978. Palynology, age and environmental significance of some peat beds in the Upper Pleistocene Hinuera Formation, South Auckland, New Zealand. *Journal of the Royal Society of New Zealand* 8(4), 385-393.

McGlone, M.S., Nelson, C.S, Todd, A.J. 1984. Vegetation history and environmental significance of pre-peat and surficial peat deposits at Ohinewai, Lower Waikato lowland. *Journal of the Royal Society of New Zealand* 14, 233–244.

McGlone, M.S. 1988. New Zealand. *In*: Huntley, B., Webb, III T., editors. *Handbook of vegetation science*, Vol. 7: *Vegetation history*. Kluwer Academic Publishers, The Hague, p.558–599.

Melchert, R.A. 2022. Sedimentology and characterisation of soft-sediment deformation structures within lacustrine successions in 20,400-yr-old Lake Rotoroa, Hamilton, northern New Zealand [unpublished MSc dissertation]. University of Waikato, Hamilton.

Milne, D., Clayden, B., Singleton, P., Wilson, A.N. 1995. *Soil Description Handbook*. Revised edition. Manaaki Whenua Press. 157 pp

Newnham, R.M., de Lange, P.J., Lowe, D.J. 1995. Holocene vegetation, climate and history of a raised bog complex, northern New Zealand based on palynology, plant macrofossils and tephrochronology. *The Holocene 5*, 267–282. https://doi.org/10.1177/095968369500500302

Newnham, R.M., Lowe, D.J., Williams, P.W. 1999. Quaternary environmental change in New Zealand: a review. *Progress in Physical Geography* 23, 567-610.

Newnham, R.M., Eden, D.N., Lowe, D.J., Hendy, C.H. 2003. Rerewhakaaitu Tephra, a land-sea marker for the Last Termination in New Zealand, with implications for global climate change. *Quaternary Science Reviews* 22, 289-308.

Newnham, R.M., McGlone, M.S., Moar, N., Wilmshurst, J.M., Vandergoes, M.J. 2013. The vegetation cover of New Zealand at the Last Glacial Maximum. *Quaternary Science Reviews* 74, 202–214.

Nicolin, E., Dempsey, D., Kah, J., Wotherspoon, L. 2019. What should Auckland expect from a Magnitude 7 Hauraki Rift earthquake? QuakeCoRE: Posters https://ir.canterbury.ac.nz/handle/10092/17206

Parfitt, R.L., Saigusa, M., Cowie, J.D. 1984. Allophane and halloysite formation in a volcanic ash bed under different moisture conditions. *Soil Science* 138(5), 360-364.

Persaud, M., Villamor, P., Berryman, K.P., Ries, W., Cousins, J., Litchfield N., Alloway B.V. 2016. The Kerepehi Fault, Hauraki Rift, North Island, New Zealand: active fault characterisation and hazard, *New Zealand Journal of Geology and Geophysics* 59(1), 117-135. DOI: 10.1080/00288306.2015.1127826

Peti, L., Hopkins, J.L., Augustinus, P. 2021. Revised tephrochronology for key tephras in the 130-ka Ōrākei Basin maar core, Auckland Volcanic Field, New Zealand: implications for the timing of climatic changes, New Zealand. *New Zealand Journal of Geology and Geophysics* 64, 235–249.

Reynolds, J.M. 2011. *An introduction to applied and environmental geophysics – 2nd ed.* John Wiley and Sons, Chicester.

Schofield, J.C. 1965. The Hinuera Formation and associated Quaternary events (with an appendix on experimental alluviation). *New Zealand Journal of Geology and Geophysics* 8, 772–791.

Seebeck, H., Van Dissen, R., Litchfield, N., Barnes, P.M., Nicol, A., Langridge, R., Barrell, D.J.A.,Villamor, P., Ellis, S., Rattenbury, M., Bannister, S., Gerstenberger, M., Ghisetti, F., Sutherland, R., Hirschberg, H., Fraser, J., Nodder, S.D., Stirling, M., Humphrey, J., Bland, K.J., Howell, A., Mountjoy, J., Moon, V., Stahl, T., Spinardi, F., Townsend, D., Clark, K., Hamling, I., Cox, S., de Lange, W., Wopereis, P., Johnston, M., Morgenstern, R., Coffey, G., Eccles, J.D., Little, T., Fry, B., Griffin, J., Townend, J., Mortimer, N., Alcaraz, S., Massiot, C., Rowland, J.V., Muirhead, J., Upton, P., Lee, J. 2023. The New Zealand Community Fault Model – version 1.0: an improved geological foundation for seismic hazard modelling. *New Zealand Journal of Geology and Geophysics*, DOI: 10.1080/00288306.2023.2181362

Shane, P.A.R. 2000. Tephrochronology: a New Zealand case study. *Earth-science Reviews* 49, 223-259.

Shane, P.A.R., Smith, V., Nairn, I.A., 2003. Biotite composition as a tool for the identification of Quaternary tephra beds. *Quaternary Research* 59, 262–270.

Singleton, P.L., Mcleod, M., Percival, H.J. 1989. Allophane and halloysite content and soil solution silicon in soils from rhyolitic volcanic material, New Zealand. *Australian Journal of Soil Research* 27, 67–77.

Smith, V.C., Shane, P.A.R., Nairn, I.A., 2005. Trends in rhyolite geochemistry, mineralogy, and magma storage during the last 50 kyr at Okataina and Taupo volcanic centres, Taupo Volcanic Zone, New Zealand. *Journal of Volcanology and Geothermal Research* 148, 372-406.

Stirling, M., McVerry, G., Gerstenberger, M., Litchfield, N., Van Dissen, R., Berryman, K., Barnes, P., Wallace, L., Villamor, P., Langridge, R. 2012. National seismic hazard model for New Zealand: 2010 update. *Bulletin of the Seismological Society of America* 102, 1514–1542. https://doi.org/10.1785/0120110170" https://doi.org/10.1785/0120110170.

Ulriksen, C.P. 1980. Investigation of peat thickness with radar. *Proceedings of the 6th International Peat Congress*, p.126-129.

Vandergoes, M.J., Hogg, A.G., Lowe, D.J., Newnham, R.M., Denton, G.H., Southon, J., Barrell, D.J.A., Wilson, C.J.N., McGlone, M.S., Allan, A.S.R., Almond, P.C., Petchey, F., Dalbell, K., Dieffenbacher-Krall, A.C., Blaauw, M. 2013. A revised age for the Kawakawa/Oruanui tephra, a key marker for the Last Glacial Maximum in New Zealand. *Quaternary Science Reviews* 74, 195-201

Villamor, P. 2022. Paleoseismology of the newly discovered Te Puninga Fault, Hauraki Plains. EQC project number 20790 (GNS-EQC00036). Final Report BIG 012 2020, 31 December 2022. Lower Hutt: GNS Science.

Villamor, P., Litchfield, N. J., Gómez-Ortiz, D., Martin-González, F., Alloway, B. V., Berryman, K. R., Clark, K. J., Ries, W. F., Howell, A., Ansell, I. A. 2022. Fault ruptures triggered by large rhyolitic eruptions at the boundary between tectonic and magmatic rift segments: the Manawahe Fault, Taupō Rift. *New Zealand. Journal of Volcanology and Geothermal Research* 427, 107478.

Villamor, P., Clark, K., Coffey, G., Hughes, J.W., Lowe, D.J., Hogg, A.G., Moon, V.G., Moratalla, J, Thingbaijam, K. 2023. Seismic characterization of the Te Puninga Fault, Hauraki Plains, New Zealand. *New Zealand Journal of Geology and Geophysics* (in preparation).

White, P.A., Raiber, M., Tschritter, C. 2018. Geological model and water budget of the Hauraki Plains, Waikato region. Wairakei (NZ): GNS Science. 63 p. (*GNS Science consultancy report*; 2015/232).

Williams, P.W. 2017. *New Zealand landscape – behind the scene*. Elsevier, Amsterdam, 470p.

Wilson, A.N. 1980. Soils of the Piako County. *New Zealand Soil Survey report* 39.

Wilson, C.J.N. 2001. The 26.5 ka Oruanui eruption, New Zealand: an introduction and overview. *Journal of Volcanology and Geothermal Research* 112, 133–174.

Appendices

Appendix 1.1: Ryland – north wall

***Ap** 0-17 cm. Silty sand; dark brownish black; friable, weakly pedal, brittle peds; abundant roots; moderately allophanic (NaF test); distinct wavy boundary.

Bw 17-30 cm. Silt; yellowish brown; friable, apedal earthy; many roots, some large root channels; strongly allophanic; indistinct smooth boundary.

¶**H_A** 30-58 cm. Fine to medium sand; blocky to prismatic; >90 % low chroma colours, ~5% MnO_2 concretions; strong peds; few roots, few large root channels ~3 cm; smooth diffuse boundary.

H_{B1} 58-90 cm. Fine to medium sand with some fine pumice lapilli; less coherent than H_A; a few deep root channels containing Ap horizon material; ~40% orange mottles, 60% low chroma colours; indistinct smooth boundary.

H_{B2} 90-160 cm. Medium sand with coarse sand and medium pumice lapilli lenses; redox segregations, ~75% orange and ~25% low chroma, <5% MnO_2 concretions; strongly reduced (positive Childs' test); indistinct smooth boundary.

H_{B3} 160-225 cm. Medium sand with coarse sand and lenses of medium pumice lapilli; thin horizontal heavy mineral (designated mafic hereafter) beds; 50% orange staining and 10% MnO_2 concretions in the upper 30 cm; strongly reduced; indistinct smooth boundary.

H_C 225-260 cm. Coarse sand with 3-5 cm thick fine to medium lapilli pumice beds; mafic mineral crossbeds (1-2 mm thick) present; strongly reduced.

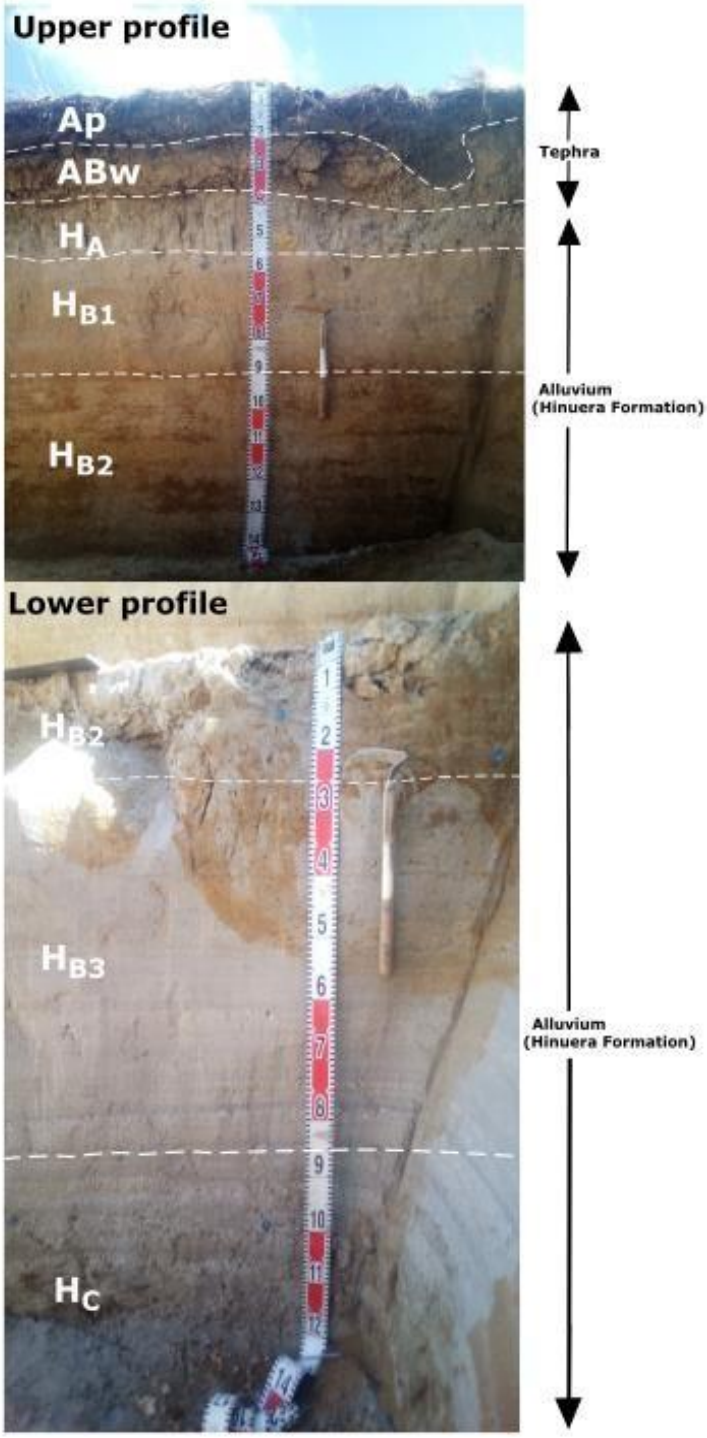

Notes

* Ap and Bw are soil horizon designations from Clayden and Hewitt (1989); textural and other terms follow Milne et al. (1995). Upper landscape soils at Arnold and Ryland sites are representatives of the Waihou and Te Puninga series (Wilson 1980), respectively, and are Orthic Allophanic Soils (Arnold) and Impeded Allophanic Soils (Ryland) (Hewitt 2010); lower landscape soils are representatives of the Waitoa series (Wilson 1980), and are Orthic Gley Soils (Hewitt 2010) at both trench sites.

¶ H-notations refer to units defined in this study (not soil horizon designations). Stratigraphy is based on field

observations and Hume et al. (1975), Wilson (1980), Lowe (1988, 2023), Manville and Wilson (2004), Leonard et al. (2010), and Persaud et al. (2016).

Appendix 1.2: Ryland - south wall

East profile

Ap1 0-37 cm. Sandy loam; dark greyish brown; many strong polyhedral peds; common roots; indistinct wavy boundary.

Ap2 37-50 cm. Sandy loam; dark olive brown; Many strong polyhedral peds; common roots with brown mottles; below 46 cm, orangebrown silty mottles occur; abrupt wavy boundary.

50-61 cm. Medium sand; grey with brown mottles; intermittent orange-grey silt (Kaharoa tephra, Ka)[1] overlying a white discontinuous pumice lapilli layer <5 mm thick (Taupo tephra, Tp); abrupt wavy boundary.

61-85 cm. Fine white sand with some fine pumice lapilli, fining upwards; 5% mafic minerals; distinct smooth boundary.

85-150 cm. Coarse sand with <5% fine pumice lapilli; <5% orange mottles; ~1 mm-thick beds of mafic minerals; coarse sand and pumice lapilli beds dipping steeply westward; thin peat layer at depth of 140 cm.

[1]Tephra correlations are provisional and based on field properties and stratigraphic position.

West profile

Ap1 0-37 cm. Sandy loam; dark greyish brown; many strong polyhedral peds; common roots; indistinct wavy boundary.

Ap2 37-50 cm. Sandy loam; dark olive brown; many strong peds; common roots with brown mottles; below 46 cm, orange-brown silty mottles occur; abrupt wavy boundary.

50-61 cm. Medium sand; grey with brown mottles; intermittent orange-grey silt (Ka) overlying a white discontinuous pumice lapilli layer <5 mm thick (Tp); abrupt wavy boundary.

61-85 cm. Fine white sand with 5% mafic minerals and some pumice lapilli, fining upwards; distinct smooth boundary.

H_{A1} 85-115 cm. Fine sandy loam; 10% orange mottles, 90% low chroma colours; massive; contains wood (roots); diffuse boundary.

H_{A2} 115-150 cm. Fine sandy loam; 30% orange mottles, 70% low chroma colours; massive; contains wood (roots)

Appendix 1.3: Arnold - north wall

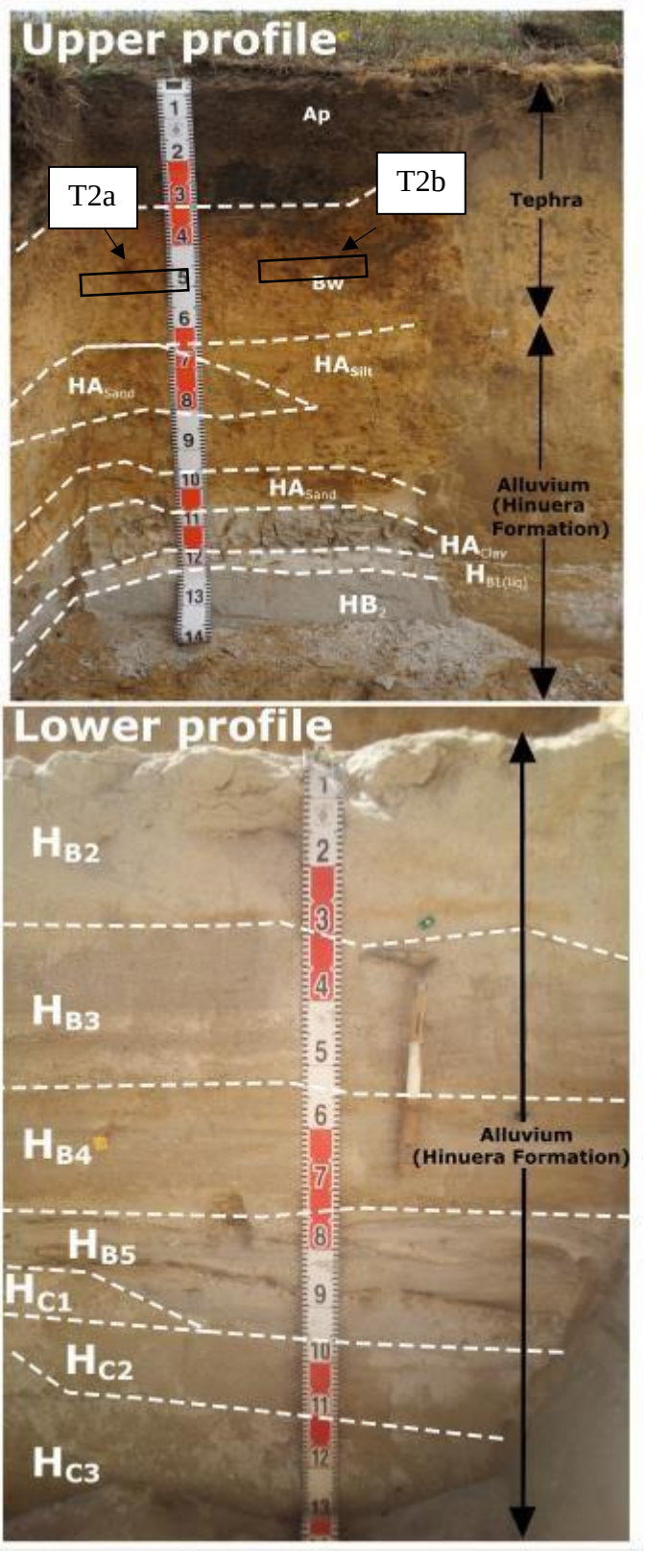

Ap 0-30 cm. Silt loam; grey yellowish brown (10YR 4/2†); apedal, earthy; basal part mixed brownish-black, potentially from ploughing; weakly allophanic; distinct wavy boundary.

Bw 35-65 cm. Silty sand; yellowish brown, <5% orange mottles; friable; strongly allophanic; diffuse smooth boundary. Samples T2a and T2b were sampled at base of this unit.

HA$_{Sand}$ 65-85 cm and 95-107 cm. Coarse sand and pumice lapilli; yellowish brown, ~20% orange mottles; spatially variable – occurs as both a lens in profile and as a horizontal layer.

HA$_{Silt}$ 65-95 cm. Silty sand with rare pumice lapilli; 40% orange mottles, 30-40% low chroma colours; indistinct boundary to lower HA$_{Sand}$ layer (see photo).

HA$_{Clay}$ 107-115 cm. Clayey silt; 80% low chroma colours; blocky; abrupt smooth boundary.

H$_{B1(liq)}$ 115-120 cm. White, fine sand-silt layer; possible liquefaction (liq) or sand blow; abrupt smooth boundary.

H$_{B2}$ 120-186 cm. Medium to coarse sand with coarse sand and fine pumice lapilli beds; pale grey with ~5% orange staining; indistinct wavy boundary.

H$_{B3}$ 186-197 cm. Medium sand with fine mafic mineral beds; pumice lapilli lenses <4 mm thick; grey with 10% orange staining and 20% MnO_2 concretions; smooth indistinct boundary.

H$_{B4}$ 197-216 cm. Fine to medium sand with 30% mafic minerals; fine, rhyolitic sand lens pinching out; coarse grained interbeds; grey with 40% orange staining, distinct horizontal pattern; smooth indistinct boundary.

H_{B5} 216-236 cm. Fine sand with some pumice lapilli clasts (~3 mm) and fine mafic sand crossbedding; Medium pumice lapilli lenses; grey with <5% mottles; smooth distinct boundary.

H_{C1} Pinching out on left of photo. Coarse sand to gravel with medium pumice lapilli; grey; abrupt smooth boundary.

H_{C2} 236-250 cm. Coarse sand; dark grey; 30% mafic minerals; well sorted matrix with lenses of larger, medium pumice lapilli clasts; strongly reduced; distinct wavy boundary.

H_{C3} 250 cm. Fine to coarse sand, poorly sorted, contains fine to medium pumice lapilli; dark grey; variable mafic mineral concentrations; strongly reduced.

---

†Munsell colour notation

Appendix 1.4: Arnold - south wall

(Bowl)

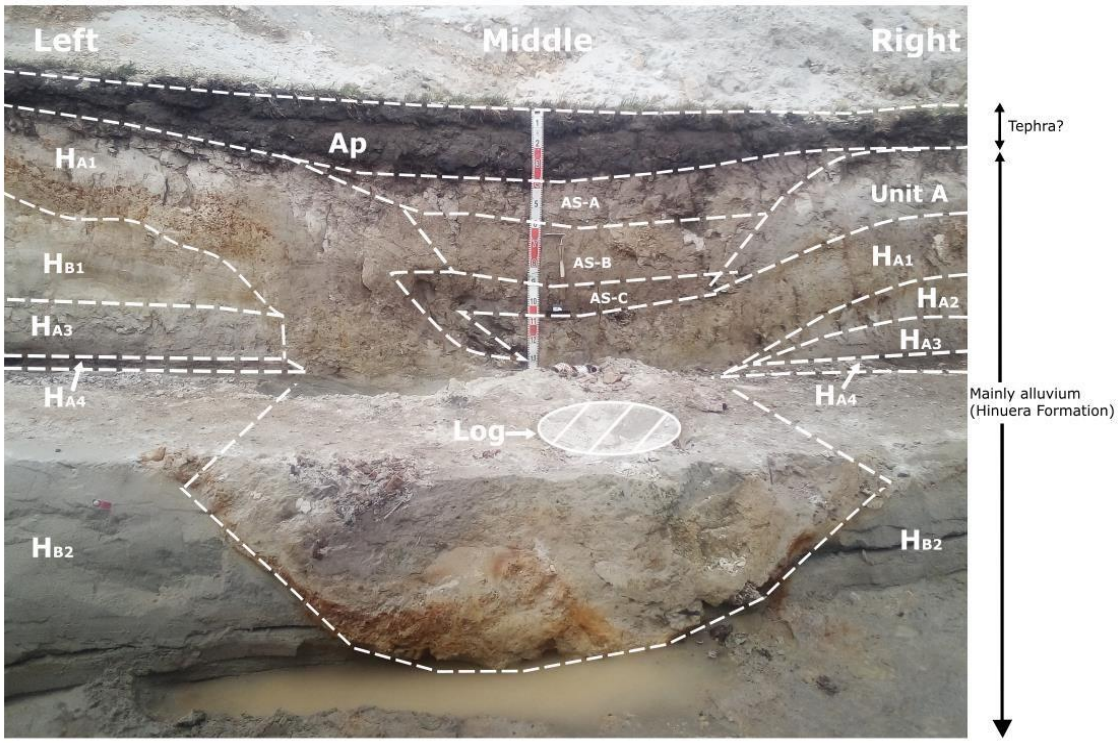

Ap 0-37 cm. Silt loam; greyish yellow brown (10YR 4/2); fine pumice lapilli at 25 cm depth; moderate pedality, strong polyhedral peds, many roots; contains lenses of greyish orange silt (Ka?); distinct wavy boundary.

Left

H_{A1} 33-55 cm. Fine sand; dull yellow orange (10YR 7/2) with 20% bright yellowish brown (10 YR 6/6) mottles and distinctive dark greenish grey (5BG 4/1) to greenish grey (5BG 5/1) and dark bluish grey (5BG 3/1) mottles (probably fougerite, also known informally as 'green rust)' oxidising to greyish olive (7.5Y 5/3) and then olive brown (2.5Y 4/4) over time; indistinct wavy boundary.

H_{B1} 55-105 cm. Fine to medium sand; massive; 75% low chroma colours, dull yellow orange (10YR 7/2), 5% yellow orange mottles (10YR 7/8); green fougerite mottles present, as above.

H_{A3} 105-135 cm. Right: 88-135 cm; fine sand, fining downwards to clay; 95% low chroma colours, dull yellow orange (10YR 7/2), with 5% yellow orange (10YR 7/8) mottles.

H_{A4} 135-139 cm. Peaty organic layer; laminated with leaf remnants; dull yellowish brown (10YR 5/3).

H_{B2} 139 cm+. Coarse sand with pumice lapilli bedding; greyish yellow brown (10YR 6/2) with 5% orange mottles; 15% mafic minerals.

Right

Unit A 15-40 cm. Fine sand; low chroma colours, dull yellow orange (10YR 7/2); blocky; smooth wavy boundary.

H_{A1} 40-58 cm. See above.

H_{A2} 58-88 cm. Fine sand; pale grey (10YR 7/2) with 20% orange mottles and greenish grey mottles of fougerite (green rust) in upper profile; massive; large root channels (<10 cm); smooth wavy boundary.

H_{A3} 88-132 cm. See above.

H_{A4} 132-135 cm Peaty organic layer; laminated with leaf remnants; dull yellowish brown (10YR 5/3).

H_{B2} 135 cm+. See above.

Middle: *Units only observed in this profile.*

AS.A 35-55 cm. Fine silty sand with lenses of fine pumice lapilli (Tp); brownish grey (10YR 6/1); blocky.

AS.B 55-90 cm. Fine silty sand; dull yellow orange (10YR 7/2) with 40% low chroma colours, 30% orange mottles; massive; contains fine ~1 mm-thick layers of leaf material.

AS.C 90-105 cm. Fine sand with mixed dark brown-orange material.

Arnold - south wall at marker A7

Ap 0-27 cm. Silty sand; greyish yellow brown (10YR 4/2); fine pumice lapilli at 25 cm depth; moderate pedality, strong peds; many roots; distinct wavy boundary.

Unit A 27-40 cm. (But due to irregular boundary, extends to 60 cm depth in other locations.) Fine sand; low chroma colours (10YR 7/2); blocky; distinct irregular boundary.

H_{A1} 40-65 cm. Fine sand; dull yellow orange (10YR 7/2), 20% bright yellowish brown (10 YR 6/6) mottles; abrupt smooth boundary.

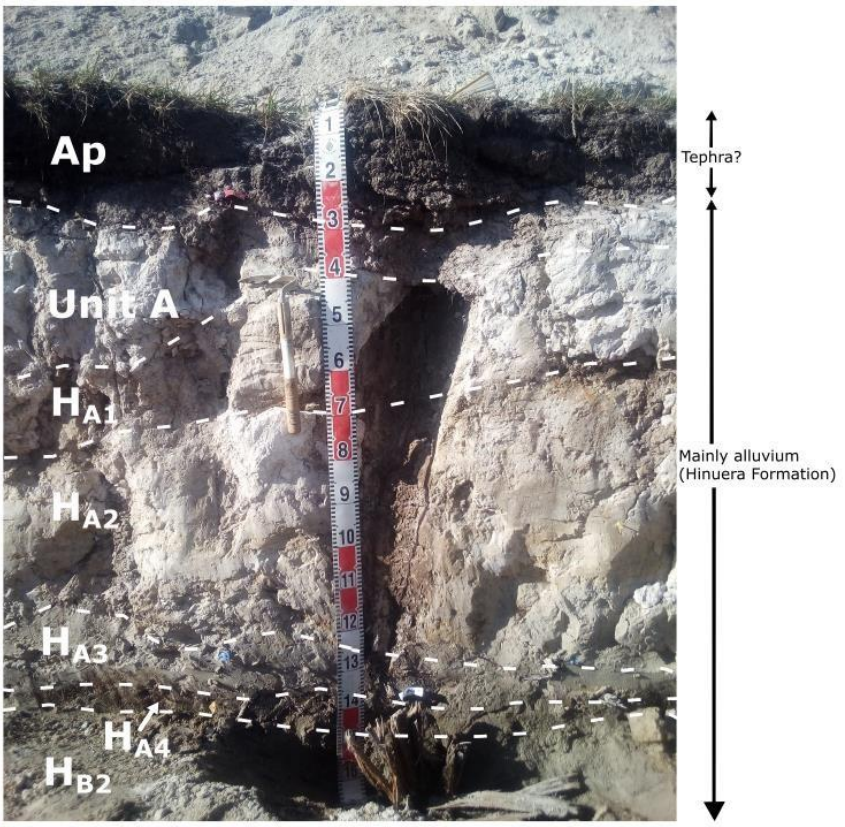

H_{A2} 75-125 cm. Fine sand; light grey (10YR 7/1), 20% orange staining and mottles; massive; large root channels (<10 cm); abrupt wavy boundary

H_{A3} 125-140 cm. Fine sand, fining downwards to clay; low chroma colours predominate, dull yellow orange (10YR 7/2) with 15% yellow-orange mottles (10YR 7/8); abrupt smooth boundary.

H_{A4} 140-143 cm**.** Peaty organic layer; laminated, leaf remnants; dull yellowish brown (10YR 5/3); abrupt smooth boundary.

H_{B2} 143-160+ cm. Coarse sand with fine pumice lapilli bedding; greyish yellow brown (10YR 6/2), 5% orange mottles; 15% mafic minerals.

Appendix 5: Four radiocarbon ages obtained from Arnold's and Ryland's paleoseismic trenches on the Te Puninga Fault, and three from Hinuera Formation near Matamata. Other ages obtained on deposits in the trenches (from the Waikato lab) are given in Figures 3.3 and 3.4 (Chapter 3)

Waikato Radiocarbon Laboratory number (Wk)	**Material dated and pre-treatment[2]**	**Conventional radiocarbon age** (^{14}C yr BP ± 1 sd)	**Calibrated ^{14}C age[3]** (cal yr BP, 95.4% probability range)	**δ^{13}C[4]** (‰)	**Location[5] and geological unit[6]**	**Reference**
Wk52561 (R1N-28 = Ryland peat-1)[1]	Twigs and plant material	10,071 ± 20	11,690 ± 30 11.5% 11,485 ± 165 84.0%		Ryland's Trench, lower extension's north wall (WF)[5]	This study
Wk52552 (Arnold peat-1)[1]	Peat	19,773 ± 46	23,795 ± 75 88.3% 23,485 ± 55 7.1%		Arnold's Trench, south wall, base of trench (HF-Hin C)[5]	
Wk52554 (Arnold peat-3)[1]	Peat	19,963 ± 47	23,970 ± 170 95.4%		Arnold's Trench, south wall, base of trench (HF-Hin C)[5]	
Wk52555 (Arnold peat-4)[1]	Leaf in peat	20,705 ± 50	24,900 ± 220 95.4%		Arnold's Trench, south wall, base of trench (HF-Hin C)[5]	
Wk216	Peat	19,400 ± 200	23,781 ± 200 95.4%	-28.2	Quarry near Matamata c. 2.5 m depth (HF-Hin C)[5]	Hogg et al. (1987); Houghton and Cuthbertson (1989)
Wk217	Peat	18,400 ± 200	22,863 ± 200 95.4%	-26.8	Cutting near Matamata c. 6.2 to 7.0 m depth (HF-Hin C)[5]	
Wk218	Peat	23,900 ± 400	28,904 ± 200 95.4%	-25.9	Bore 37 near Matamata c. 28.1 m depth (HF-Hin A)[5]	

[1] Field sample number in parentheses (Chapter 3)

[2] Pretreatment: Visible contaminants removed, sample washed in hot HCl, rinsed and treated with multiple hot NaOH washes. The NaOH insoluble fraction was treated with hot HCl, filtered, rinsed, and dried. Dated via AMS.

[3] Calibrated using OxCal v.4.4.4 (https://c14.arch.ox.ac.uk/oxcal/OxCal.html) (based on Bronk Ramsey 2001, 2009) and SHCal20 (atmospheric curve) (Hogg et al. 2020)

[4] The $\delta^{13}C$ value was measured on prepared graphite using an AMS spectrometer. The radiocarbon date has therefore been corrected for isotopic fractionation. However, the AMS-measured $\delta^{13}C$ value can differ from the $\delta^{13}C$ of the original material and it is therefore not shown.

[5] Specific sampling locations are shown in Chapter 3

[6] WF: Waitoa Formation of Houghton and Cuthbertson (1989) and Brathwaite and Christie (1996); HF-Hin C: Hinuera Formation, unit Hinuera C of Manville and Wilson (2004); HF-Hin A: Hinuera Formation, unit Hinuera A of Manville and Wilson (2004)

Appendix 6a: Raw EPMA-derived glass data (not normalised) of the Arnold and Ryland Trenches.

No.	SiO_2	TiO_2	Al_2O_3	FeO*	MnO	MgO	CaO	Na_2O	K_2O	Cl	Total	Comment
1	76.55	0.07	12.06	1.28	0.00	0.04	0.43	4.02	5.06	0.11	99.52	VG568-01
2	77.51	0.11	12.21	1.20	0.02	0.03	0.48	3.97	4.88	0.11	100.42	VG568-02
3	76.19	0.08	12.08	1.30	0.02	0.03	0.49	4.11	4.62	0.14	98.92	VG568-03
6	73.79	0.14	11.86	1.42	0.04	0.12	0.94	4.05	3.62	0.21	95.98	R1-2_03
7	74.41	0.12	11.71	0.16	0.03	0.08	0.59	4.22	3.65	0.19	94.98	R1-2_04
8	73.99	0.23	12.92	1.98	0.03	0.18	1.50	4.34	2.89	0.15	98.08	R1-2_05
9	75.91	0.14	12.15	0.13	0.06	0.13	1.08	4.11	2.86	0.07	96.58	R1-2_06
10	74.45	0.14	11.73	0.19	0.03	0.08	0.62	4.25	3.81	0.22	95.29	R1-2_07
11	74.74	0.11	11.91	1.37	1.37	0.09	0.96	4.06	3.17	0.19	97.78	R1-2_08
12	75.44	0.16	12.20	0.98	0.02	0.13	0.93	4.17	3.18	0.16	97.20	R1-2_09
13	74.14	1.16	11.69	1.39	0.17	0.06	0.62	0.47	3.75	0.18	93.44	R1-2_10
14	76.04	0.15	11.81	1.22	0.04	0.04	0.00	4.45	3.67	0.01	97.42	R1-2_11
15	76.11	0.00	12.02	1.29	0.04	0.05	0.00	4.54	3.79	0.19	97.83	R1-2_12
16	77.02	0.12	12.24	1.12	0.06	0.09	0.00	4.29	3.74	0.16	98.69	R1-2_13
17	77.13	0.13	12.16	1.12	0.00	0.10	1.11	3.75	3.78	0.17	99.29	R1-2_14
18	73.15	0.96	11.74	1.16	0.03	0.12	0.97	4.00	3.35	0.19	95.49	R1-2_15
19	77.45	0.13	12.38	0.98	0.04	0.13	0.77	4.57	3.67	0.13	100.11	R1-2_16
20	74.86	0.13	11.89	1.34	0.04	0.12	1.13	0.05	3.39	0.20	92.96	R1-2_17
21	73.93	0.11	11.95	1.35	0.05	0.09	1.09	3.75	3.34	0.19	95.66	R1-2_18
22	73.30	0.11	11.47	1.30	0.08	0.08	0.64	0.05	4.36	0.19	91.38	R1-2_19
23	72.76	0.15	11.61	1.24	0.03	0.10	0.83	0.05	3.60	0.17	90.37	R1-2_20
24	75.76	0.12	12.18	0.75	0.03	0.07	0.75	4.04	3.59	0.14	97.29	R1-2_21
25	72.91	0.11	11.93	1.30	0.04	0.12	1.01	4.21	3.06	0.19	94.70	R1-2_22
26	77.06	0.13	12.27	0.82	0.04	0.08	0.74	4.13	3.34	0.16	98.60	R1-2_23
27	76.20	0.95	11.99	1.34	0.05	0.08	0.70	0.47	3.81	0.02	95.61	R1-2_24

28	73.90	0.10	11.57	1.12	0.03	0.00	0.79	3.68	3.73	0.20	94.90	R1-2_25
29	77.43	0.07	12.44	1.04	0.00	0.04	0.48	4.36	4.96	0.01	100.81	VG568-04
30	74.82	0.27	13.26	2.08	0.06	0.00	1.55	4.67	2.96	0.01	99.68	R1-1_01
31	74.05	0.30	13.31	2.21	0.08	0.00	1.47	4.77	2.85	0.18	99.04	R1-1_02
36	73.93	0.29	14.59	2.30	0.06	0.25	2.11	4.89	2.62	0.19	101.03	R1-1_07
37	60.82	0.00	26.02	0.42	0.00	0.03	7.96	8.05	0.29	0.00	103.60	R1-1_08
38	61.55	0.24	11.54	1.40	0.04	0.24	1.11	4.00	2.00	0.14	82.12	R1-1_09
39	51.73	0.17	0.63	42.46	1.52	17.03	1.40	0.09	0.01	0.01	115.04	R1-1_10
40	75.65	2.01	13.11	1.78	0.07	0.00	1.18	3.61	5.08	0.15	102.48	R1-1_11
41	58.86	0.02	26.28	0.36	0.05	0.02	8.72	7.35	0.26	0.01	101.92	R1-1_12
42	74.34	0.33	13.32	2.17	0.04	0.25	1.54	4.27	3.01	0.17	99.27	R1-1_13
43	77.42	0.55	8.01	1.30	0.02	0.05	0.35	0.03	3.06	0.01	90.79	R1-1_14
44	51.71	0.17	0.64	42.00	1.60	16.91	1.42	0.00	0.00	0.00	114.44	R1-1_15
47	60.77	0.00	25.54	0.39	0.00	0.02	7.22	8.33	0.41	0.01	102.68	R1-1_18
48	61.18	0.28	11.56	1.83	0.08	0.26	1.32	0.05	2.32	0.18	78.88	R1-1_19
49	65.90	2.74	7.22	1.42	0.02	0.18	0.71	2.02	1.85	0.13	82.05	R1-1_20
50	71.49	0.30	12.87	2.70	0.04	0.23	1.48	4.71	2.57	0.15	96.40	R1-1_21
51	66.97	0.30	11.64	0.28	0.02	0.20	1.51	0.04	2.84	0.15	83.82	R1-1_22
52	69.13	0.29	12.14	2.16	0.07	0.23	1.38	4.17	2.56	0.17	92.12	R1-1_23
55	76.60	0.07	12.02	0.13	0.02	0.04	0.45	0.05	4.98	0.10	94.37	VG568-05
56	76.39	0.07	12.16	1.10	0.02	0.03	0.61	4.07	5.01	0.13	99.47	VG568-06
57	76.92	0.05	11.94	1.07	0.00	0.02	0.47	0.05	4.82	0.01	95.34	VG568-07
58	76.67	0.08	12.27	0.96	0.05	0.07	0.82	4.09	4.17	0.18	99.18	T2a_02
63	73.21	0.08	11.66	1.12	0.05	0.10	1.00	3.84	3.20	0.19	94.26	T2a_08
64	74.01	0.15	11.84	1.28	0.05	0.11	0.86	4.16	3.64	0.17	96.09	T2a_09
65	72.12	0.11	11.71	1.21	0.06	0.00	1.06	0.05	3.37	0.21	89.69	T2a_10
66	75.46	0.92	12.13	1.65	0.02	0.00	1.12	4.17	3.49	0.21	98.97	T2a_11
67	74.47	1.06	11.97	1.33	0.03	0.00	1.17	4.17	3.11	0.19	97.31	T2a_12

68	77.33	1.29	12.57	1.47	0.08	0.00	0.78	4.59	3.52	0.13	101.63	T2a_13
69	73.61	0.12	11.65	1.38	0.02	0.11	1.18	4.10	3.11	0.19	95.28	T2a_14
70	74.67	0.13	12.19	1.60	0.07	0.13	1.09	4.25	3.16	0.20	97.28	T2a_15
71	73.98	0.10	11.90	1.36	0.06	0.10	0.00	3.98	3.26	0.20	94.75	T2a_16
72	73.67	0.11	11.92	1.42	0.03	0.12	0.00	3.89	3.60	0.19	94.76	T2a_17
73	74.33	0.14	11.99	1.46	0.02	0.12	0.00	4.09	3.42	0.19	95.56	T2a_18
74	74.39	0.11	12.11	1.29	0.90	0.13	0.00	3.96	3.47	0.19	96.36	T2a_19
75	74.44	0.13	11.88	1.48	0.06	0.11	1.09	0.05	3.47	0.20	92.69	T2a_20
76	76.77	0.08	12.38	0.15	0.07	0.08	0.80	3.93	4.24	0.19	98.50	T2a_21
77	74.22	0.17	11.97	1.44	0.04	0.13	1.14	4.18	3.29	0.21	96.58	T2a_22
78	74.23	0.14	11.88	1.29	0.03	0.11	1.03	4.40	3.03	0.21	96.15	T2a_23
79	74.17	0.11	11.80	1.24	0.06	0.11	1.01	0.06	3.32	0.21	91.88	T2a_24
80	73.32	0.13	11.88	0.17	0.06	0.13	1.00	4.05	3.12	0.22	93.85	T2a_25
81	66.36	0.11	10.54	0.15	0.05	0.09	1.12	2.73	3.25	0.22	84.40	T2a_26
82	77.67	0.12	12.42	0.98	0.02	0.07	0.81	4.62	3.56	0.16	100.28	T2a_27
83	75.67	0.11	12.36	1.49	0.04	0.11	1.07	4.29	3.30	0.19	98.43	T2a_28
84	73.43	0.15	11.92	1.46	0.01	0.11	1.11	3.75	3.19	0.20	95.13	T2a_29
85	74.96	0.12	12.21	1.39	0.04	0.12	1.18	4.28	3.25	0.19	97.54	T2a_30
86	74.72	0.11	12.12	1.30	0.04	0.11	1.06	4.04	3.26	0.20	96.76	T2a_31
87	73.32	0.11	11.79	1.49	0.02	0.10	0.98	4.04	3.17	0.20	95.02	T2a_32
88	75.03	0.13	12.14	1.42	0.04	0.11	1.06	4.18	3.01	0.21	97.12	T2a_33
90	69.07	0.10	0.00	0.00	0.07	0.06	0.63	4.00	3.78	0.24	77.70	T2a_35
91	74.51	1.35	12.09	1.43	0.00	0.00	1.04	4.31	2.82	0.19	97.53	T2a_36
92	76.83	0.06	12.39	0.91	0.03	0.07	0.75	4.21	4.44	0.19	99.70	T2a_37
93	74.01	0.11	11.99	1.27	0.06	0.09	1.00	3.98	3.56	0.21	96.08	T2a_38
94	74.63	1.51	12.00	1.12	0.05	0.00	0.98	4.31	3.24	0.18	97.83	T2a_39
95	77.96	0.15	12.57	0.93	0.05	0.08	0.00	4.22	4.31	0.15	100.26	T2a_40
96	76.98	0.08	12.32	1.28	0.00	0.03	0.00	4.14	4.93	0.11	99.77	VG568-08

97	77.14	0.11	12.16	0.18	0.01	0.03	0.50	4.19	5.24	0.11	99.57	VG568-09
98	75.63	0.11	12.23	1.22	0.05	0.14	1.08	4.20	3.60	0.19	98.25	T2b_01
99	75.03	0.15	12.08	1.11	0.06	0.10	0.90	3.84	3.89	0.15	97.17	T2b_02
100	72.95	0.13	11.80	1.29	0.05	0.10	1.06	0.05	3.22	0.20	90.65	T2b_03
101	73.16	0.13	11.82	0.18	0.02	0.13	1.05	3.95	3.21	0.19	93.65	T2b_04
102	73.06	0.13	11.60	0.19	0.06	0.06	1.02	0.05	3.09	0.20	89.28	T2b_05
103	73.48	0.14	11.71	1.26	0.05	0.03	0.56	3.78	3.90	0.22	94.90	T2b_06
104	72.85	0.11	11.48	0.18	0.03	0.11	0.98	0.05	3.27	0.19	89.06	T2b_07
105	73.91	0.13	12.14	1.69	0.04	0.07	0.87	4.37	3.79	0.20	97.00	T2b_08
106	73.46	0.13	11.70	0.16	0.04	0.09	1.04	0.05	3.19	0.18	89.86	T2b_09
107	74.78	0.13	11.93	1.26	0.03	0.10	1.04	4.22	3.30	0.20	96.79	T2b_10
108	74.48	0.15	12.06	1.70	0.04	0.11	1.14	4.18	3.32	0.20	97.17	T2b_11
109	75.80	0.16	12.17	1.00	0.03	0.10	0.83	4.38	3.24	0.18	97.70	T2b_12
110	73.28	0.14	11.94	1.24	0.06	0.12	1.12	4.09	2.95	0.18	94.95	T2b_13
111	76.55	0.10	12.69	1.26	0.04	0.10	0.87	4.41	3.91	0.15	99.92	T2b_14
112	73.76	0.13	11.95	1.24	0.04	0.10	1.00	4.12	3.28	0.19	95.60	T2b_15
113	73.93	0.12	11.60	1.32	0.05	0.05	0.67	4.30	3.83	0.21	95.87	T2b_16
114	75.80	0.12	12.16	1.28	0.04	0.10	1.02	4.42	3.28	0.20	98.21	T2b_17
115	74.23	0.16	11.73	1.32	0.04	0.07	0.87	4.08	3.47	0.19	95.97	T2b_18
116	75.81	0.13	12.11	1.34	0.03	0.12	1.03	4.30	3.20	0.20	98.07	T2b_19
117	75.58	0.12	11.90	1.34	0.01	0.10	0.98	4.27	3.25	0.22	97.55	T2b_20
118	77.12	0.10	12.20	1.25	0.02	0.05	0.46	3.27	5.03	0.11	99.51	VG568-10
119	76.81	0.05	12.01	1.41	0.03	0.01	0.51	4.12	5.05	0.11	100.00	VG568-11

*Total Fe expressed as FeO

Appendix 6b: Glass sample names used in Appendix 6a

Sample name	**Geological unit**
Ka	Kaharoa Tephra[+]
Tp	Taupo Tephra[+]
T2a	Basal composite tephra sample[+]
T2b	Basal composite tephra sample[+]
VG568	Secondary rhyolitic glass sample (Jarosewich et al., 1980)

[+] Described and identified in the field from stratigraphic positions and field properties (Chapter 1.3)